Supporting information

"Catalyzing Singlet Fission by Transition Metals: Second versus Third Row Effects"

Yuxuan Hou,[a,‡] Ilias Papadopoulos,[b,‡,†] Yifan Bo,[b,] Anna-Sophie Wollny,[b] Michael J. Ferguson,[a] Lukas A. Mai,[b] Rik R. Tykwinski,[a,*] and Dirk M. Guldi[b,*]

[a]Department of Chemistry, University of Alberta, 11227 Saskatchewan Drive, Edmonton, Alberta, Canada T6G 2G2.

Correspondence to: rik.tykwinski@ualberta.ca

[b]Department of Chemistry and Pharmacy & Interdisciplinary Center for Molecular Materials (ICMM), Friedrich-Alexander-University Erlangen-Nuremberg, Egerlandstraße 3, 91058 Erlangen, Germany.

Correspondence to: dirk.guldi@fau.de

(‡ These authors contributed equally)

[†]Present address: Department of Applied Chemistry, Graduate School of Engineering, Center for Molecular Systems (CMS), Kyushu University, 744 Moto-oka, Nishi-ku, Fukuoka 819-0395, Japan.

Table of Contents

Synthesis and Experimental Data

Hazards. No unexpected or unusually high safety hazards were encountered during the course of this research.

Reagents were purchased reagent grade from commercial suppliers and used without further purification. Dry tetrahydrofuran (THF), CH_2Cl_2, and toluene (Tol) were obtained from a commercial solvent purification system (LC Technology Solutions INC). $MgSO_4$ was used as the drying reagent after aqueous work-up. ^1H and ^{13}C NMR spectra were recorded on an Agilent/Varian DD2 MR two-channel 400 MHz spectrometer (^1H: 400 MHz), an Agilent/Varian Inova four-channel 500 MHz spectrometer (^1H: 498 MHz), an Agilent VNMRS four-channel, dual receiver 700 MHz spectrometer (^{13}C: 176 MHz), or an Agilent/Varian VNMRS two-channel 500 MHz spectrometer equipped with a $^{13}C/^1H$ dual cold probe (^1H: 498 MHz, ^{13}C: 126 MHz). NMR spectra were recorded at ambient probe temperature and referenced to the residual solvent signal (^1H: $CDCl_3$: 7.26 ppm, ^{13}C: $CDCl_3$: 77.06 ppm). The coupling constants of protons in ^1H spectra have been reported as pseudo first-order when possible, even though they can be higher-order (ABC, ABX, AA'BB') spin systems; coupling constants are reported as observed. Routine, steady-state UV-vis measurements were carried out on a Cary-400 spectrophotometer at room temperature. High resolution mass spectra were obtained from an Agilent Technologies 6220 oaTOF instrument (ESI) or a Bruker 9.4T Apex-Qe FTICR instrument (MALDI). IR spectra were recorded on a Thermo Nicolet 8700 FTIR spectrometer and continuum FTIR microscope as films. Differential scanning calorimetry (DSC) measurements were made on a Mettler Toledo DSC or Perkin Elmer Pyris 1 DSC. All DSC measurements were carried out under a flow of nitrogen with a heating rate of 10 °C/min. Melting points were measured with 6406-K Thomas-Hoover melting point apparatus with periscopic thermometer reader. Thin layer chromatography (TLC) analyses were carried out on TLC glass plates from Merck KGaA and visualized via UV-light (254/364 nm). Column chromatography used SiliaFlash® P60 (SiliCycle). Size exclusion column chromatography was performed using Bio-Beads™ SX3 Support (Bio-Rad). Preparative GPC was carried out on a Shimadzu recycling GPC system equipped with a LC-20AR pump, SPD-M20A UV detector and a set of PSS SDV (20 × 300 mm) columns in chloroform as eluent at a flow rate of 6.25 mL/min. $\mathbf{L_{pc}}$, $\mathbf{L_{ref}}$, [1] $Pt(PhCN)_2Cl_2$, [2] and $Pd(PhCN)_2Cl_2$ [3] were synthesized as previously reported.

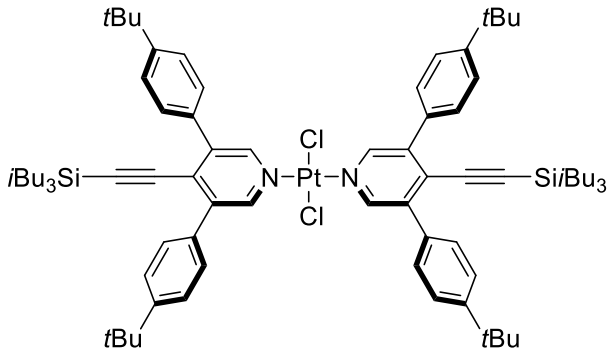

Compound Pt(L_{ref})$_2$Cl$_2$. A mixture of **L_{ref}** (25 mg, 0.044 mmol) and Pt(PhCN)$_2$Cl$_2$ (10 mg, 0.021 mmol) in dry Tol (10 mL) was stirred at 80 °C for 16 h under an atmosphere of argon. The reaction mixture was cooled to rt, and the solvent was then removed under reduced pressure. The residue was purified by column chromatography (silica gel, CH_2Cl_2/hexanes 1:4). Solvent was removed, and the residue was dissolved in CH_2Cl_2 (2 mL) followed by the addition of MeOH (15 mL). The resulting suspension was filtered, and the residue was washed with MeOH (3 × 2 mL), affording **Pt(L_{ref})$_2$Cl$_2$** as a pale yellow crystal (28 mg, 93%). Mp 276 °C (decomp). R_f = 0.66 (EtOAc/hexanes 1:6). UV-vis (CH_2Cl_2) λ_{max} (ε) 265 (60700), 323 nm (36700). IR (CH_2Cl_2, cast) 3089 (w), 3032 (w), 2954 (s), 2927 (m), 2902 (m), 2867 (m), 2155 (m), 1595 (w), 1462 (m) cm^{-1}. ^{1}H NMR (500 MHz, $CDCl_3$) δ 8.78 (s, 4H), 7.53 (d, J = 8.5 Hz, 8H), 7.45 (d, J = 8.5 Hz, 8H), 1.58 (nonet, J = 6.6 Hz, 6H), 1.37 (s, 36H), 0.76 (d, J = 6.5 Hz, 36H), 0.46 (d, J = 7.0 Hz, 12H). ^{13}C NMR (125 MHz, $CDCl_3$) δ 151.7, 151.4, 140.7, 132.5, 130.4, 129.3, 125.3, 110.4, 101.4, 34.7, 31.4, 26.2, 24.8, 24.3. ESI HRMS calcd for $C_{78}H_{110}{}^{35}Cl_2N_2Na^{195}PtSi_2$ ([M + Na]$^+$) 1418.7125, found 1418.7151. DSC: Decomposition, 283 °C (onset), 285 °C (peak).

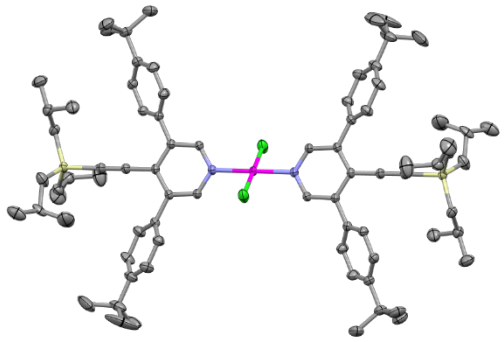

A crystal of **Pt(L_{ref})$_2$Cl$_2$** suitable for crystallographic analysis has been grown at rt by slow evaporation of a CH_2Cl_2 solution layered with MeOH. X-ray data for **Pt(L_{ref})$_2$Cl$_2$** ($C_{78}H_{110}Cl_2N_2PtSi_2$), F_w = 1397.84; crystal dimensions 0.29 × 0.23 × 0.21 mm, monoclinic crystal system; space group $C2/c$ (No. 15); a = 23.7356(18) Å, b = 13.9543(10) Å, c = 24.4208(18) Å; β = 111.9341(10)°; V = 7503.0(10) Å^3; Z = 4; ρ_{calcd} = 1.237 g/cm^3; 2θ_{max} = 66.84°; μ = 2.014 mm^{-1}; T = 173 K; total data collected = 145582; R_1 = 0.0216 [11655 observed reflections with $F_o{}^2 \geq 2\sigma(F_o^2)$]; ωR_2 = 0.0566 for 14311 data, 426 variables, and 22 restraints; largest difference, peak and hole = 0.740 and –0.765 e Å^{-3}. The C39–C40A and C39–C40B distances were restrained to be approximately the same by use of the *SHELXL* **SADI**

instruction. Additionally, the anisotropic displacement parameters of the atoms within the disordered isobutyl group were restrained by the rigid-bond restraint **RIGU**. CCDC 2288684.

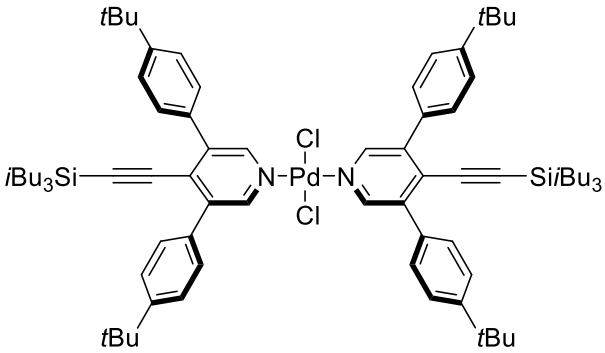

Compound Pd(L$_{ref}$)$_2$Cl$_2$. A mixture of **L$_{ref}$** (30 mg, 0.052 mmol) and Pd(PhCN)$_2$Cl$_2$ (10 mg, 0.026 mmol) in dry CH_2Cl_2 (5 mL) was stirred at rt for 15 h under an atmosphere of argon. The solvent was removed under reduced pressure and the residue was purified by column chromatography (silica gel, CH_2Cl_2/hexanes 1:1). Solvent was removed, and the residue was dissolved in CH_2Cl_2 (2 mL) followed by the addition of MeOH (15 mL). The resulting suspension was filtered, and the residue was washed with MeOH (3 × 2 mL), affording **Pd(L$_{ref}$)$_2$Cl$_2$** as a pale yellow crystal (31 mg, 91%). Mp 280 °C (decomp). R_f = 0.27 (CH_2Cl_2/hexanes 1:2). UV-vis (CH_2Cl_2) λ_{max} (ε) 266 (72400), 307 nm (sh, 26900). IR (CH_2Cl_2, cast) 3086 (w), 3032 (w), 2954 (s), 2902 (m), 2867 (m), 2158 (m), 1593 (m), 1463 (m) cm^{-1}. ^{1}H NMR (500 MHz, $CDCl_3$) δ 8.70 (s, 4H), 7.52 (d, J = 8.4 Hz, 8H), 7.44 (d, J = 8.4 Hz, 8H), 1.57 (nonet, J = 6.7 Hz, 6H), 1.37 (s, 36H), 0.76 (d, J = 6.5 Hz, 36H), 0.45 (d, J = 6.9 Hz, 12H). ^{13}C NMR (125 MHz, $CDCl_3$) δ 151.8, 151.1, 140.6, 132.6, 130.7, 129.3, 125.3, 110.3, 101.4, 34.8, 31.4, 26.2, 24.8, 24.4. ESI HRMS calcd for $C_{78}H_{110}{}^{35}Cl_2N_2Na^{106}PdSi_2$ ([M + Na]$^+$) 1329.6512, found 1329.6529. DSC: Decomposition, 300 °C (onset), 300 °C (peak).

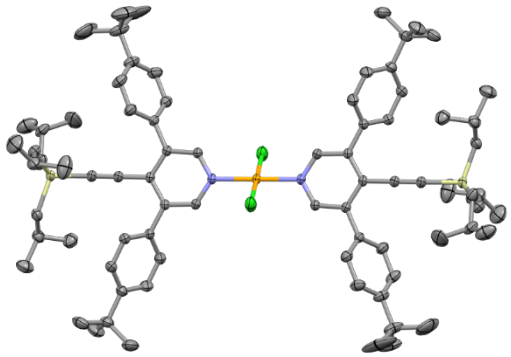

A crystal of **Pd(L$_{ref}$)$_2$Cl$_2$** suitable for crystallographic analysis has been grown at rt by slow evaporation of a CH_2Cl_2 solution layered with MeOH. X-ray data for **Pd(L$_{ref}$)$_2$Cl$_2$** ($C_{78}H_{110}Cl_2N_2PdSi_2$), F_w = 1309.15; crystal dimensions 0.39 × 0.21 × 0.14 mm, monoclinic crystal system; space group $C2/c$ (No. 15); a = 23.7115(11) Å, b = 13.9570(6) Å, c = 24.3980(11) Å; β = 111.7864(6)°; V = 7497.6(6) Å^3; Z = 4; ρ_{calcd} = 1.160 g/cm^3; 2θ_{max} =

63.18°; μ = 0.392 mm^{-1}; T = 173 K; total data collected = 137336; R_1 = 0.0310 [10516 observed reflections with $F_o^2 \geq 2\sigma(F_o^2)$]; ωR_2 = 0.0878 for 12572 data, 426 variables, and 1 restraint; largest difference, peak and hole = 0.455 and –0.364 e Å^{-3}. The C39–C40A and C39–C40B distances were restrained to be approximately the same by use of the *SHELXL* **SADI** instruction. CCDC: 2288685.

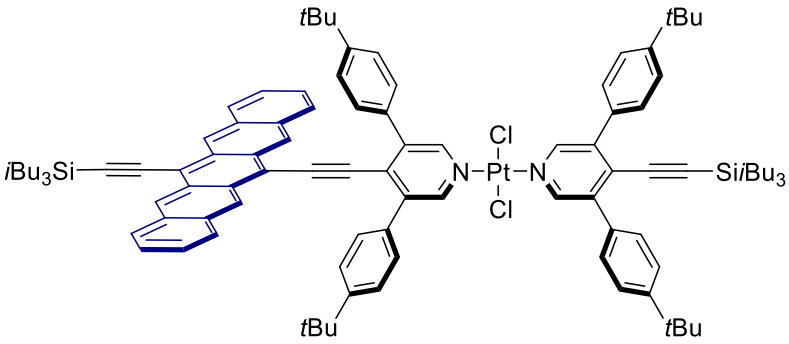

Compound Pt(L_{pc})(L_{ref})Cl_2. A solution of $Pt(PhCN)_2Cl_2$ (31 mg, 0.066 mmol) in dry Tol (2 mL) was stirred at 110 °C followed by adding a solution of **L_{ref}** (25 mg, 0.044 mmol) in dry Tol (7 mL) dropwise over 5 min. This reaction mixture was stirred at 110 °C for 20 min under an atmosphere of argon. The reaction mixture was cooled to rt, and the solvent was then removed under reduced pressure. Purification by column chromatography (silica gel, EtOAc/hexanes 1:4) afforded **Pt(L_{ref})(PhCN)Cl_2** as a pale yellow solid (40 mg, 97%). A solution of **Pt(L_{ref})(PhCN)Cl_2** (40 mg, 0.043 mmol) in dry Tol (3 mL) was stirred at 110 °C followed by adding a solution of **L_{pc}** (34 mg, 0.039 mmol) in dry Tol (10 mL) dropwise over 5 min. The reaction mixture was stirred at 110 °C for 14 h under an atmosphere of argon. The flask was wrapped in aluminum foil during the reaction to limit light exposure. The reaction mixture was cooled to rt, and the solvent was then removed under reduced pressure. The residue was purified by column chromatography (silica gel, EtOAc/hexanes 1:50) followed by size exclusion column chromatography (bio-beads SX3 support, Tol). Solvent was removed, and the residue was dissolved in CH_2Cl_2 (2 mL) followed by the addition of MeOH (20 mL). The resulting suspension was filtered, and the residue was washed with MeOH (3 × 2 mL), affording **Pt(L_{pc})(L_{ref})Cl_2** as a dark blue crystal (39 mg, 60%, 58% over 2 steps). Mp 270 °C (decomp). R_f = 0.59 (EtOAc/hexanes 1:6). UV-vis (CH_2Cl_2) λ_{max} (ε) 271 (85400), 306 (sh, 104000), 316 (265000), 344 (23400), 391 (sh, 14800), 406 (17000), 440 (660), 580 (sh, 5890), 626 (15800), 677 nm (27200). IR (CH_2Cl_2, cast) 3089 (w), 3051 (w), 2954 (s), 2902 (m), 2867 (m), 2175 (w), 2100 (w), 1592 (w), 1462 (m) cm^{-1}. ^{1}H NMR (500 MHz, $CDCl_3$) δ 9.18 (s, 2H), 8.97 (s, 2H), 8.85 (s, 2H), 8.35 (s, 2H), 7.91–7.85 (m,

6H), 7.59–7.55 (m, 4H), 7.53–7.45 (m, 10H), 7.41–7.32 (m, 4H), 2.18 (nonet, *J* = 6.6 Hz, 3H), 1.59 (nonet, *J* = 6.6 Hz, 3H), 1.38 (s, 18H), 1.18 (s, 18H), 1.18 (d, *J* = 6.6 Hz, 18H), 0.95 (d, *J* = 7.0 Hz, 6H), 0.78 (d, *J* = 6.6 Hz, 18H), 0.47 (d, *J* = 7.0 Hz, 6H). ^{13}C NMR (125 MHz, $CDCl_3$) 152.5, 151.9, 151.8, 151.5, 140.8, 140.1, 133.0, 132.6, 132.4, 132.3, 130.43, 130.40, 129.5, 129.3, 129.2, 128.4, 126.2, 126.1, 125.9, 125.7, 125.3, 120.3, 116.4, 111.1, 110.5, 104.5, 102.0, 101.5, 100.3, 34.77, 34.76, 31.4, 31.1, 26.6, 26.2, 25.5, 25.4, 24.9, 24.4 (three signals coincident or not observed). MALDI HRMS (DCTB) calcd for $C_{102}H_{122}{}^{35}Cl_2N_2{}^{195}PtSi_2$ (M^+) 1695.1866, found 1696.8143. DSC: Decomposition, 251°C (onset), 268 °C (peak).

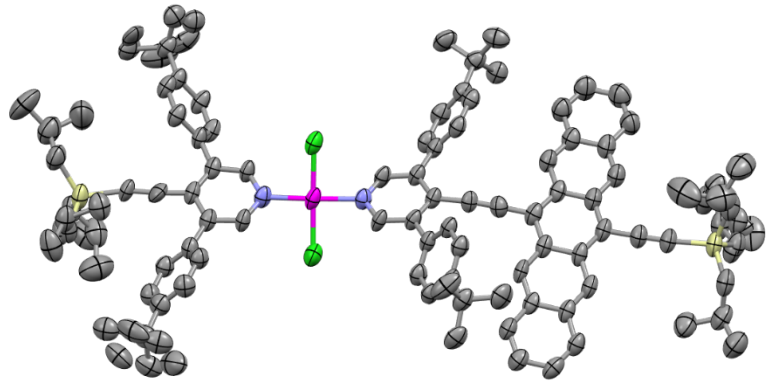

A crystal of **Pt(L$_{pc}$)(L$_{ref}$)Cl$_2$** suitable for crystallographic analysis has been grown at rt by slow evaporation of a CH_2Cl_2 solution layered with MeOH. X-ray data for **Pt(L$_{pc}$)(L$_{ref}$)Cl$_2$**•0.5CH_2Cl_2 ($C_{102.50}H_{123}Cl_3N_2PtSi_2$), F_w = 1740.64; crystal dimensions 0.22 × 0.10 × 0.02 mm, triclinic crystal system; space group $P\bar{1}$ (No. 2); a = 13.7003(4) Å, b = 16.5954(6) Å, c = 21.1156(9) Å; α= 91.722(3)°, β= 97.447(3)°, γ = 99.825(2)°; V = 4683.9(3) Å^3; Z = 2; ρ_{calcd} = 1.234 g/cm^3; $2\theta_{max}$ = 143.39°; μ = 4.172 mm^{-1}; T = 173 K; total data collected = 90605; R_1 = 0.0755 [12723 observed reflections with $F_o{}^2 \geq 2\sigma(F_o{}^2)$]; ωR_2 = 0.2031 for 17182 data, 1083 variables, and 91 restraints; largest difference, peak and hole = 2.884 and –1.296 e Å^{-3}. The C–C distances within the disordered *tert*-butyl groups were restrained by use of the *SHELXL* **SADI** instruction to be approximately the same. Likewise, the C–C and the C···C distances within the disordered isobutyl groups were also restrained. The Si2–C95 and Si2–C95A distances were restrained to be approximately the same. The rigid-bond restraint (**RIGU**) was applied to the following atoms to improve the quality of their anisotropic displacement parameters: C60 to C63A; C75, C76A to C78A; and C95 to C98. Finally, the following pairs of atoms were constrained to have equivalent anisotropic displacement parameters: C60 and C60A; C95 and C95A. CCDC: 2288686.

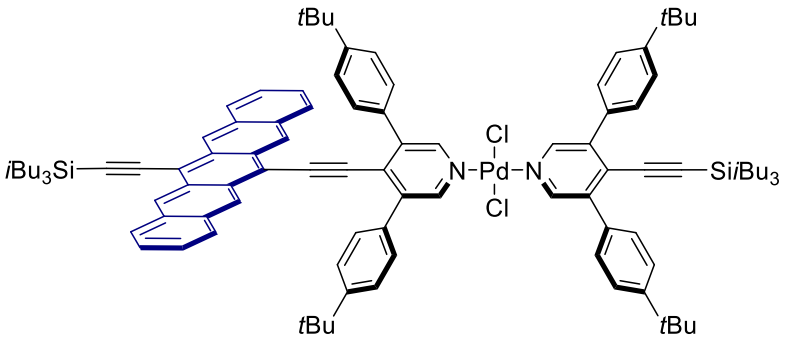

Compound Pd(L_{pc})(L_{ref})Cl_2. A solution of $Pd(PhCN)_2Cl_2$ (20 mg, 0.052 mmol) in dry CH_2Cl_2 (1 mL) was stirred at rt followed by dropwise addition (ca. 1 drop/s) of a solution of $\mathbf{L_{ref}}$ (35 mg, 0.062 mmol) in dry CH_2Cl_2 (2 mL) and then a solution of $\mathbf{L_{pc}}$ (45 mg, 0.052 mmol) in dry CH_2Cl_2 (2 mL) under an atmosphere of argon. The flask was wrapped in aluminum foil during the reaction to limit light exposure. After addition, the reaction mixture was plugged through a pad of alumina with CH_2Cl_2, and the solvent was then removed under reduced pressure. The residue was purified by recycling GPC ($CHCl_3$) followed by solvent removed under reduced pressure affording **Pd(L_{pc})(L_{ref})Cl_2** as a dark blue-green solid (30 mg, 36%). Mp 256 °C (decomp). R_f = 0.72 (CH_2Cl_2/hexanes 1:1). UV-vis (CH_2Cl_2) λ_{max} (ε) 270 (106000), 306 (sh, 115000), 315 (297000), 346 (sh, 20000), 401(15400), 442 (5890), 584 (sh, 5890), 625 (17000), 677 (30100). IR (CH_2Cl_2, cast) 3084 (w), 3050 (w), 2954 (s), 2903 (m), 2867 (m), 2175 (m), 2124 (w), 1589 (m), 1506 (w), 1462 (m) cm^{-1}. ^1H NMR (500 MHz, $CDCl_3$) δ 9.18 (s, 2H), 8.89 (s, 2H), 8.76 (s, 2H), 8.34 (s, 2H), 7.90–7.85 (m, 6H), 7.56–7.54 (m, 4H), 7.52–7.46 (m, 10H), 7.38–7.34 (m, 4H), 2.17 (nonet, J = 6.7 Hz, 3H), 1.59 (nonet, J = 6.7 Hz, 3H), 1.38 (s, 18H), 1.178 (s, 18H), 1.177 (d, J = 6.6 Hz, 18H), 0.95 (d, J = 6.9 Hz, 6H), 0.77 (d, J = 6.6 Hz, 18H), 0.47 (d, J = 6.6 Hz, 6H). ^{13}C NMR (125 MHz, $CDCl_3$) 152.5, 151.89, 151.5, 151.1, 140.6, 139.9, 133.1, 132.6, 132.4, 132.3, 130.74, 130.70, 130.5, 130.4, 129.5, 129.3, 129.2, 128.4, 126.2, 126.1, 125.9, 125.7, 125.3, 120.3, 116.2, 111.1, 110.4, 104.5, 101.9, 101.4, 100.2, 34.77, 34.76, 31.4, 31.1, 26.6, 26.2, 25.5, 25.4, 24.9, 24.4 (one signal coincident or not observed). MALDI HRMS (DCTB) calcd for $C_{102}H_{122}{}^{35}Cl_2N_2{}^{106}PdSi_2$ (M^+) 1606.7553, found 1606.7539.

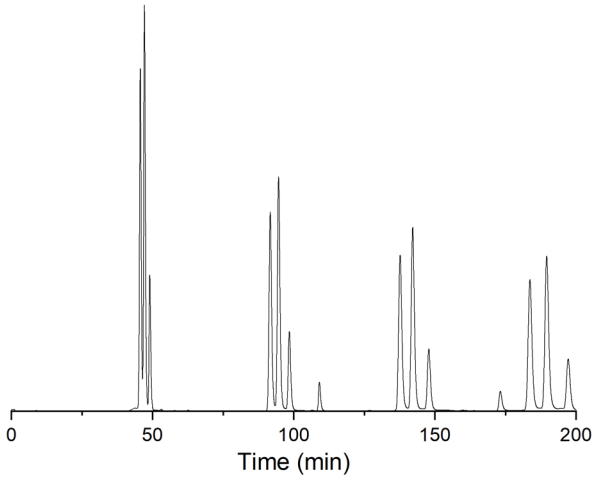

A typical recycling GPC trace of the residue for **Pd(L_{pc})(L_{ref})Cl_2** (eluting with $CHCl_3$, λ = 250 nm).

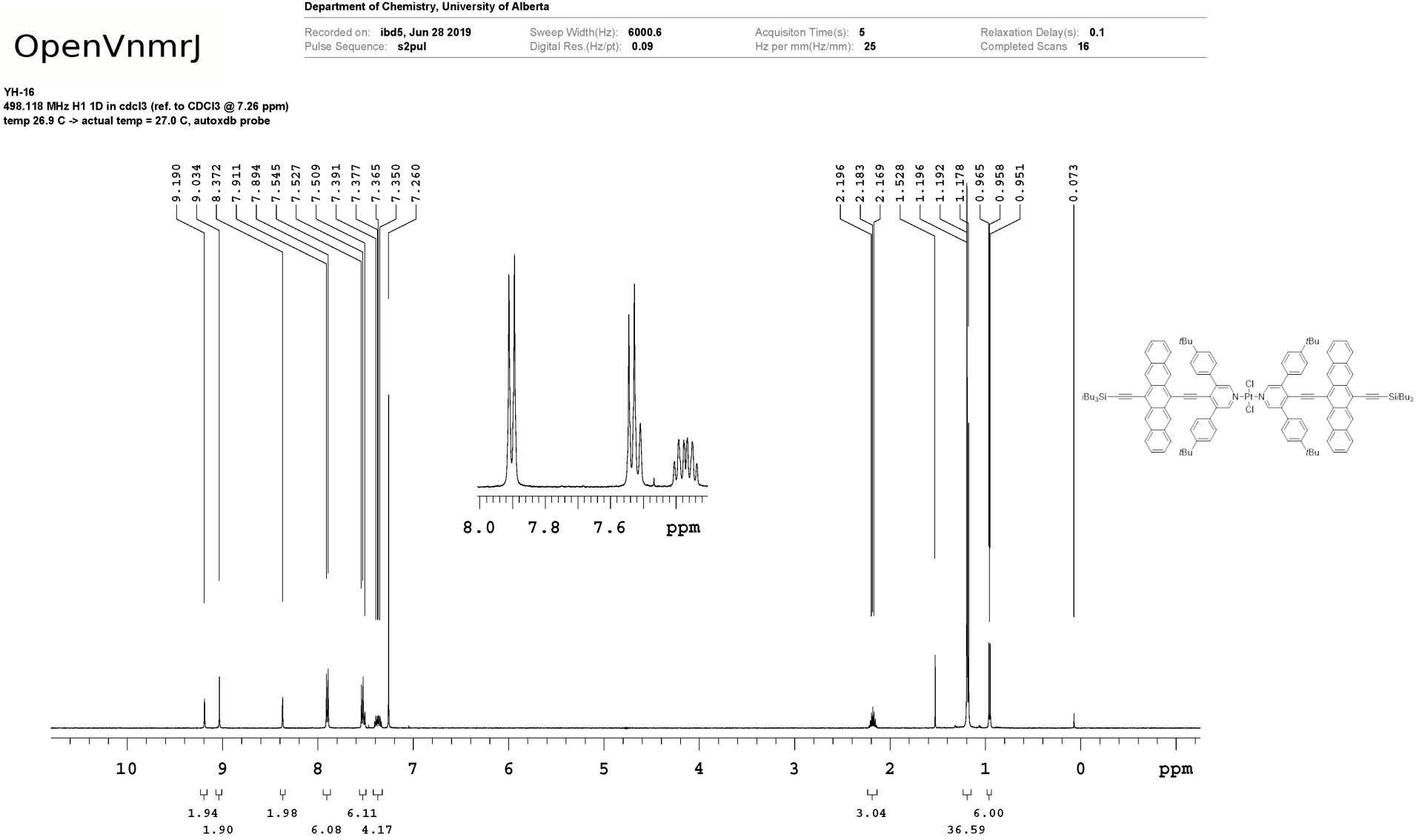

Figure S1. ^{1}H NMR spectrum (498 MHz) of compound **$Pt(L_{pc})_2Cl_2$** in $CDCl_3$.

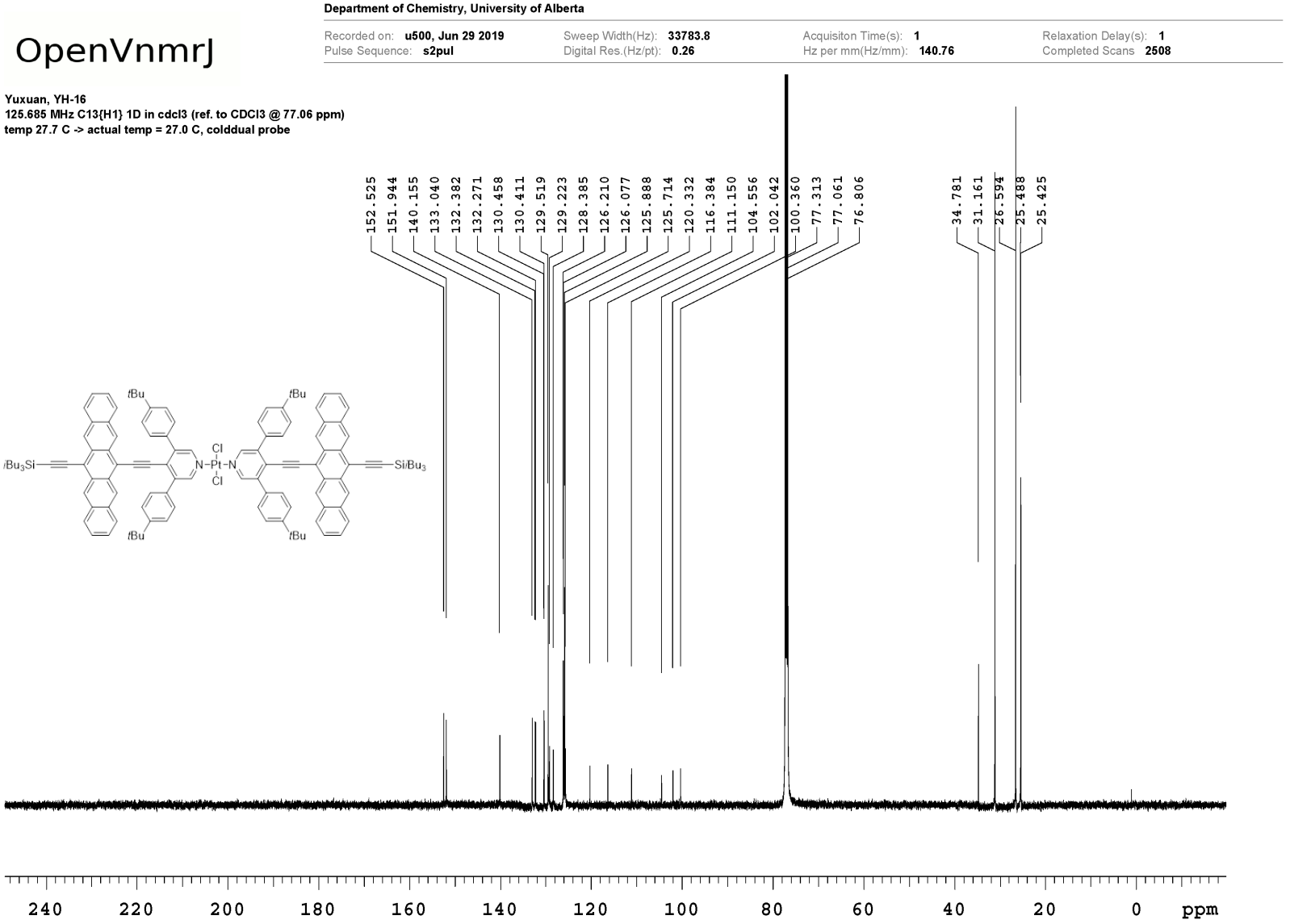

Figure S2. ^{13}C NMR spectrum (126 MHz) of compound **$Pt(L_{pc})_2Cl_2$** in $CDCl_3$.

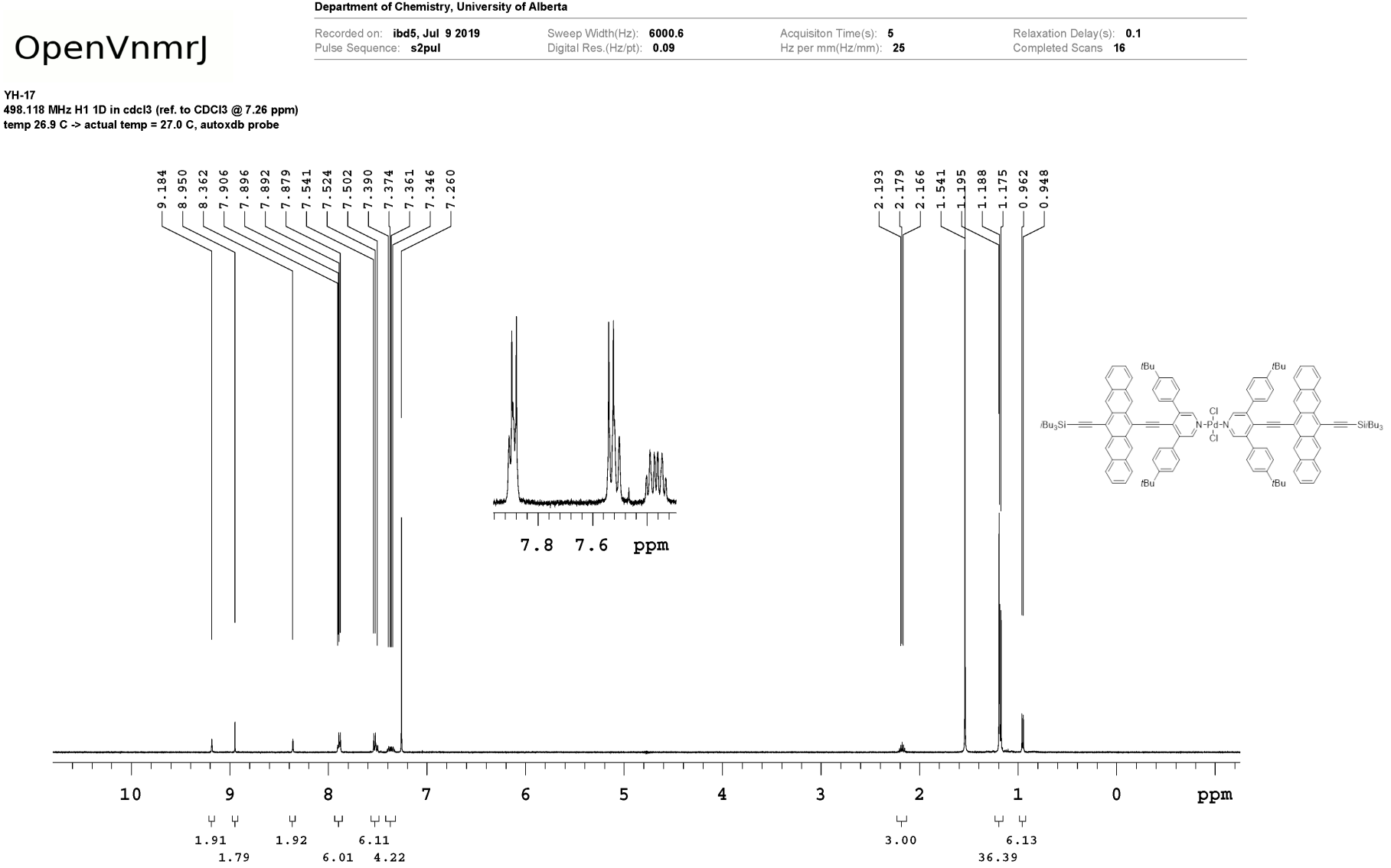

Figure S3. ^{1}H NMR spectrum (498 MHz) of compound **$Pd(L_{pc})_2Cl_2$** in $CDCl_3$.

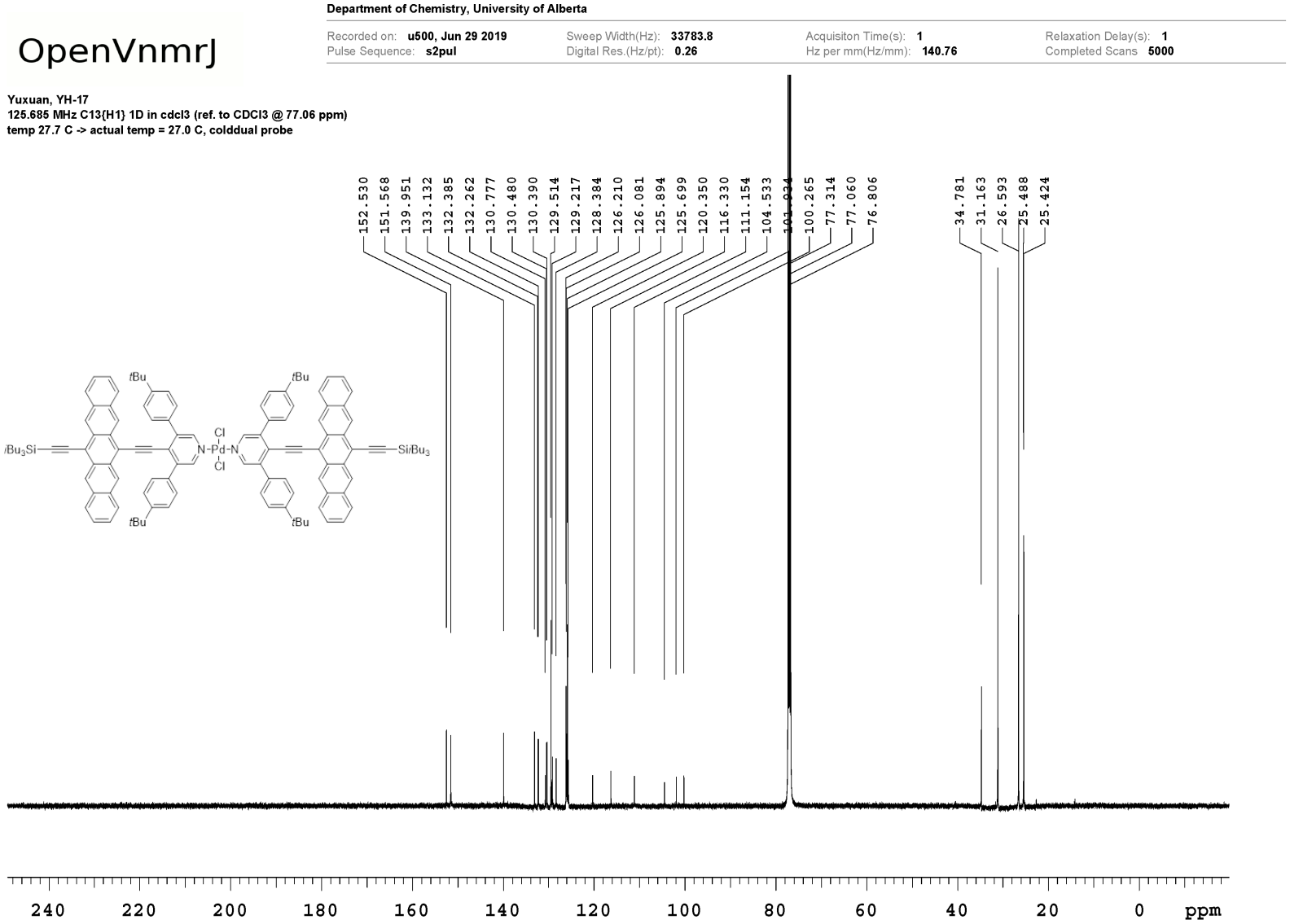

Figure S4. ^{13}C NMR spectrum (126 MHz) of compound **$Pd(L_{pc})_2Cl_2$** in $CDCl_3$.

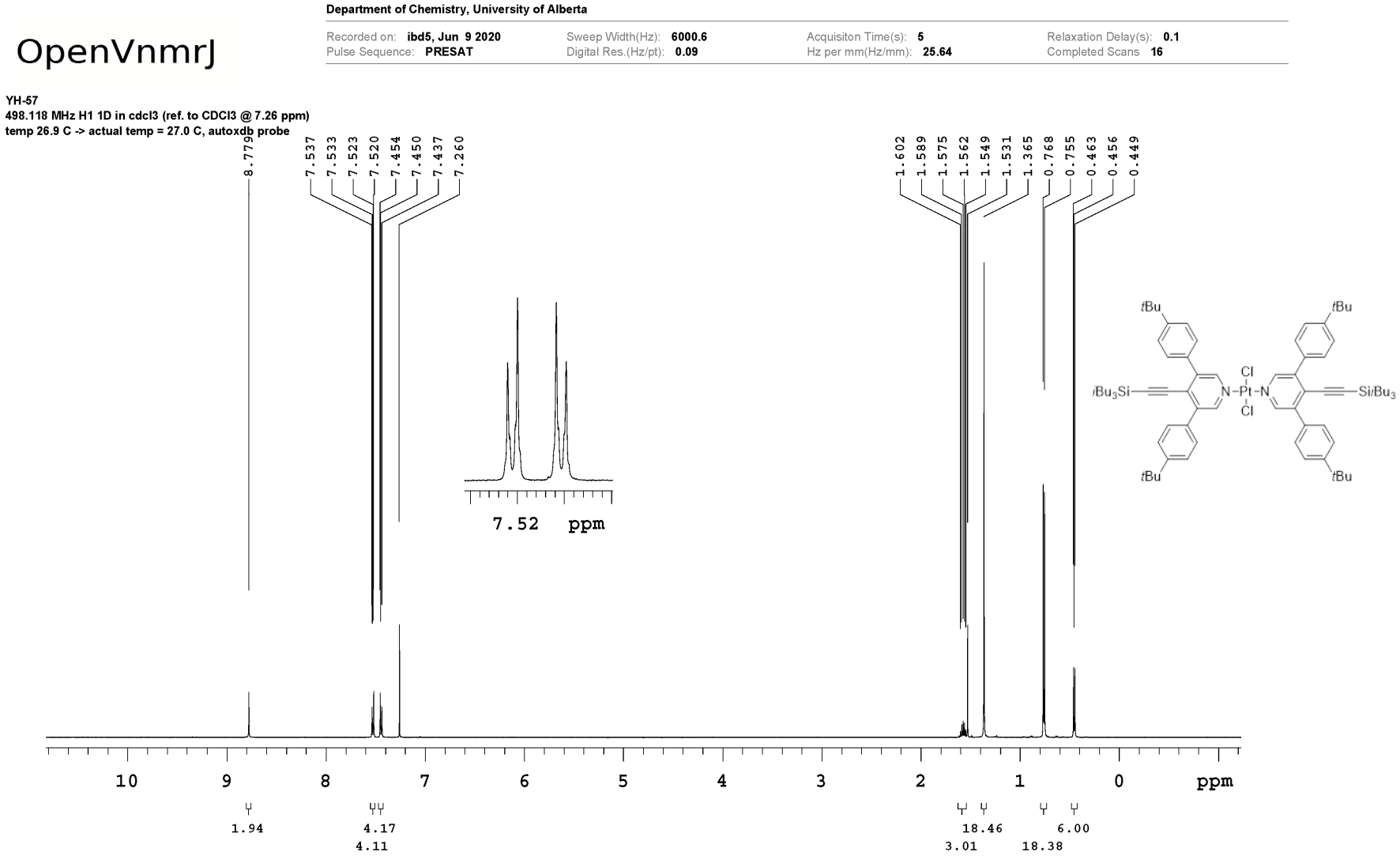

Figure S5. ^{1}H NMR spectrum (498 MHz) of compound **Pt(L_{ref})$_2$Cl$_2$** in $CDCl_3$.

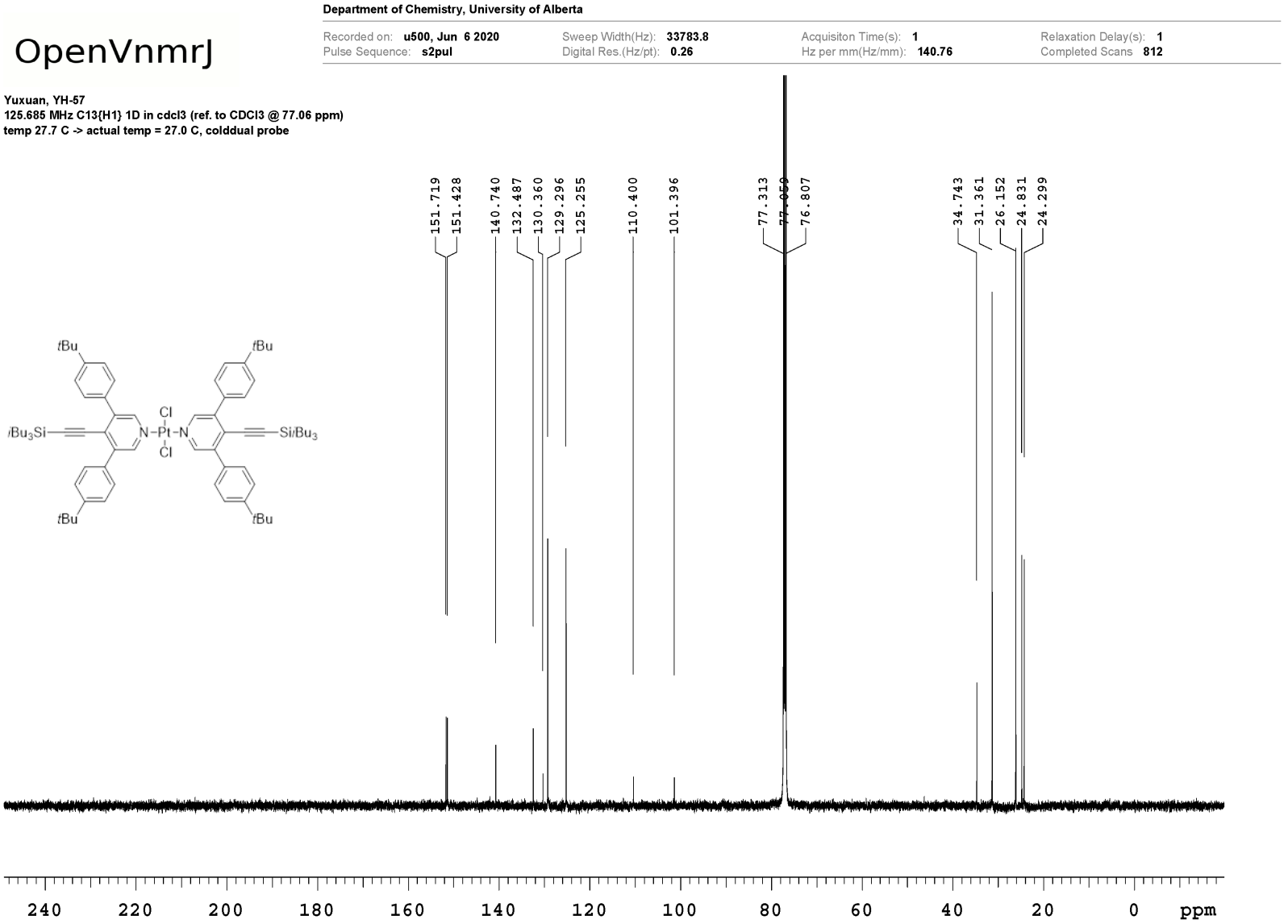

Figure S6. ^{13}C NMR spectrum (126 MHz) of compound **$Pt(L_{ref})_2Cl_2$** in $CDCl_3$.

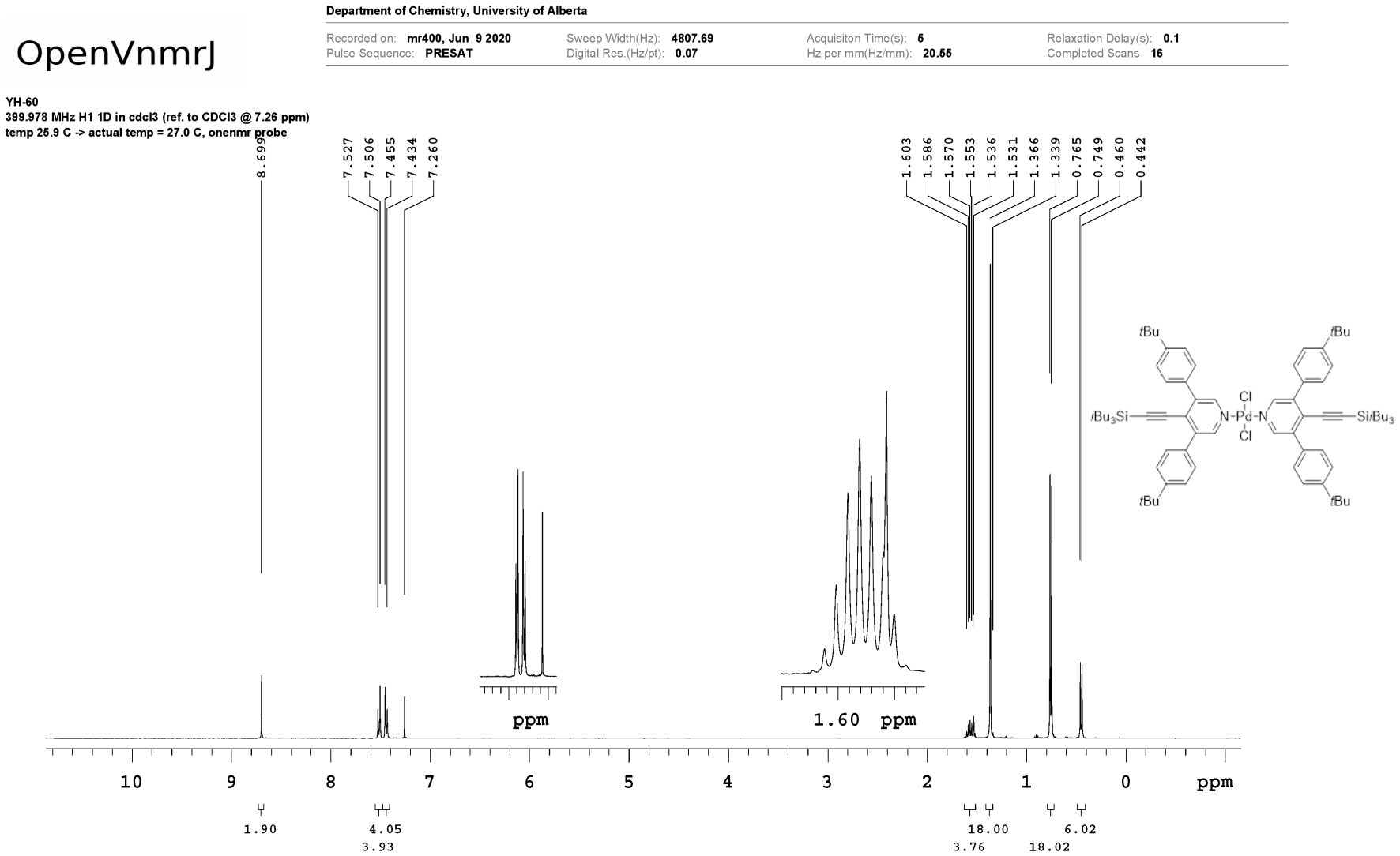

Figure S7. ^{1}H NMR spectrum (400 MHz) of compound **Pd(L$_{ref}$)$_2$Cl$_2$** in $CDCl_3$.

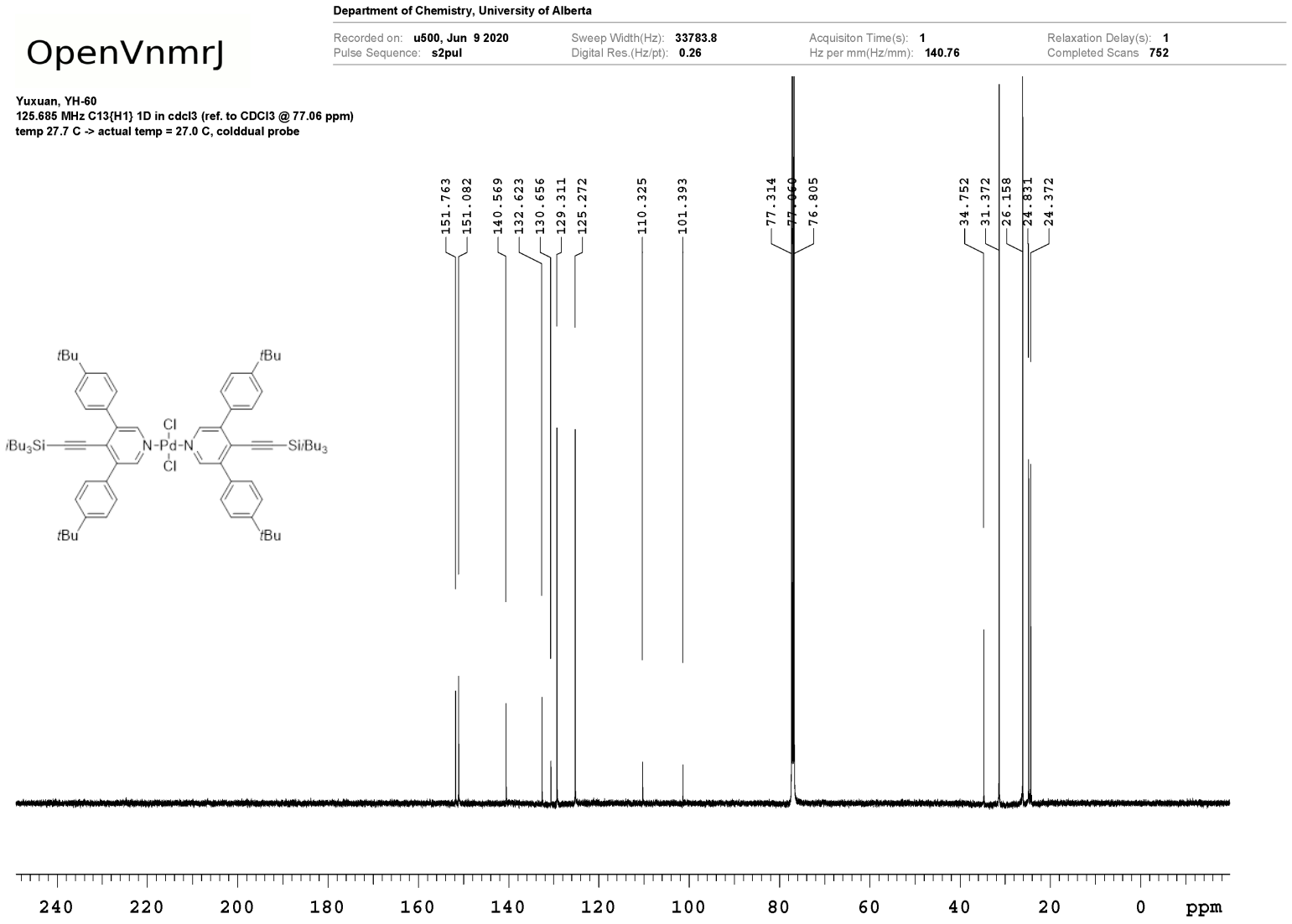

Figure S8. ^{13}C NMR spectrum (126 MHz) of compound **$Pd(L_{ref})_2Cl_2$** in $CDCl_3$.

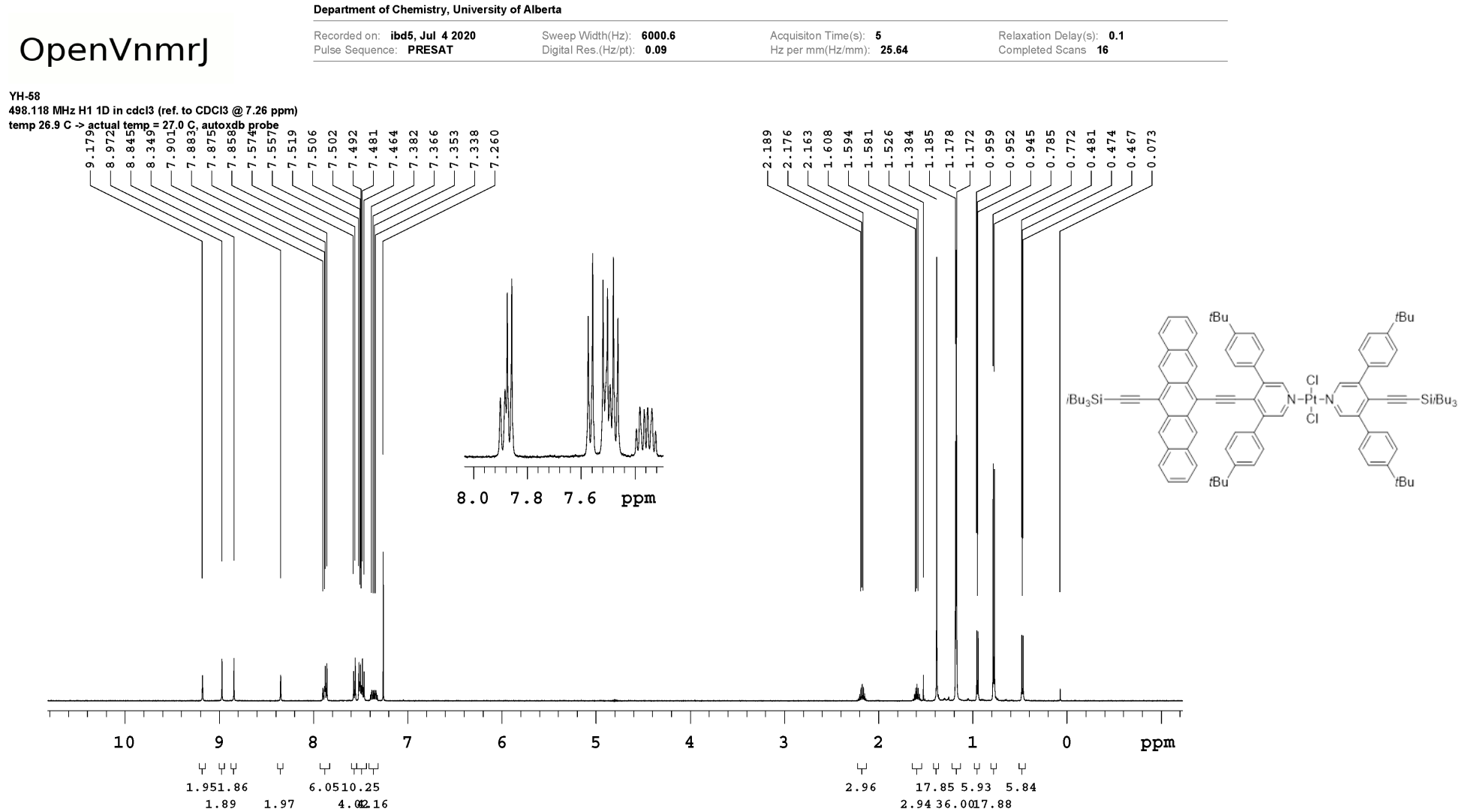

Figure S9. ^{1}H NMR spectrum (498 MHz) of compound **Pt(L_{pc})(L_{ref})Cl_2** in $CDCl_3$.

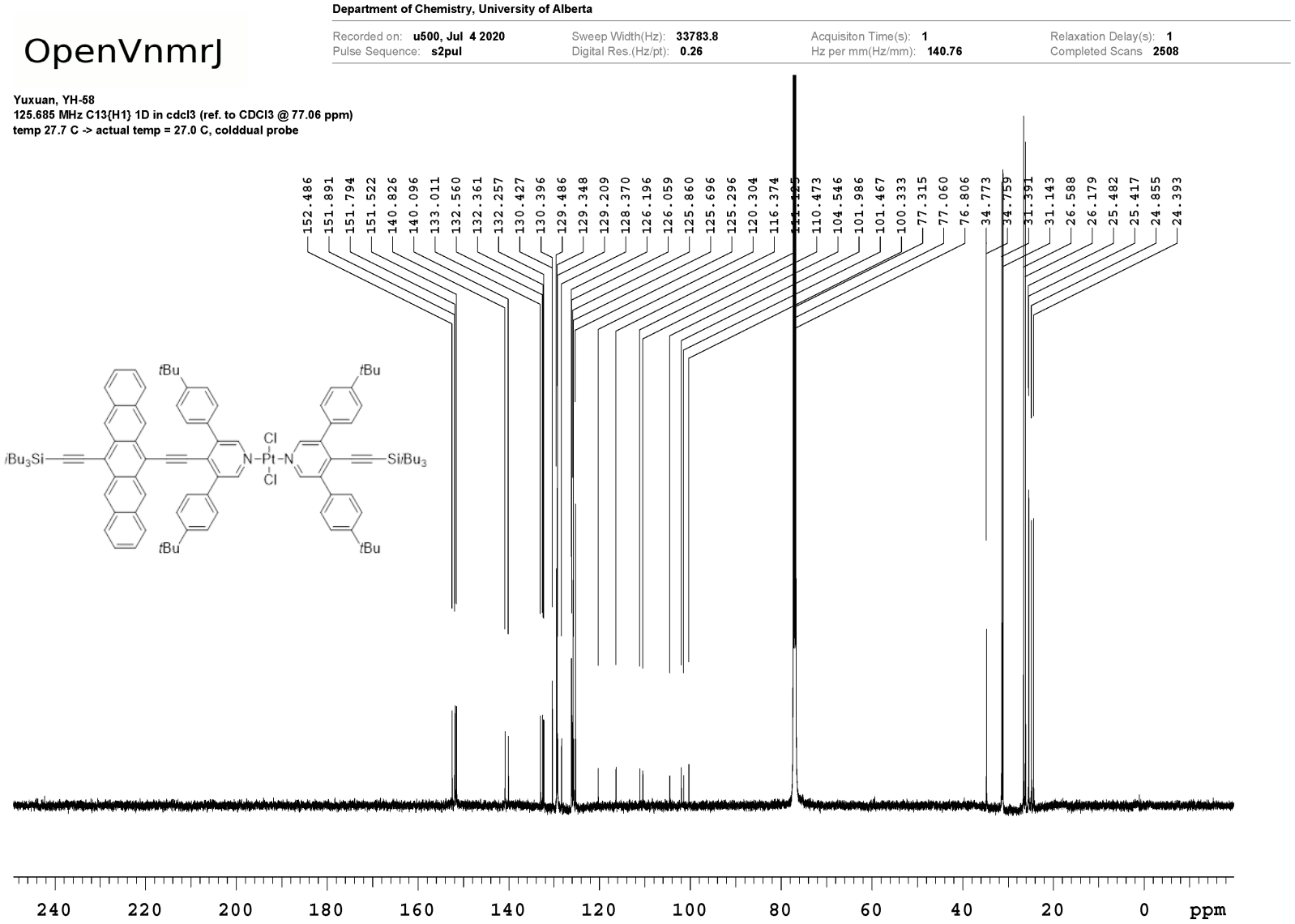

Figure S10. ^{13}C NMR spectrum (126 MHz) of compound **Pt(L_{pc})(L_{ref})Cl_2** in $CDCl_3$.

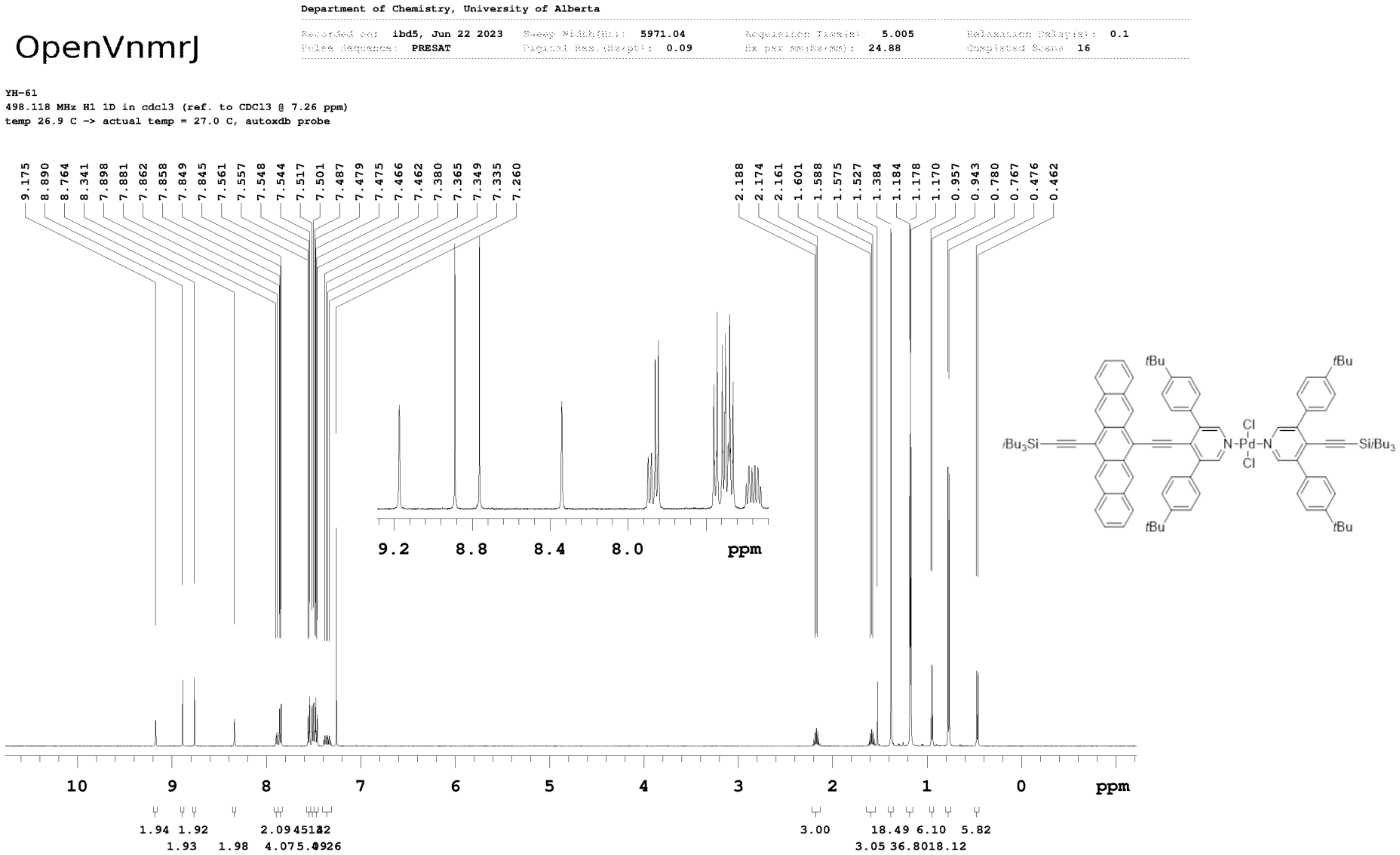

Figure S11. ^{1}H NMR spectrum (498 MHz) of compound **Pd(L_{pc})(L_{ref})Cl_2** in $CDCl_3$.

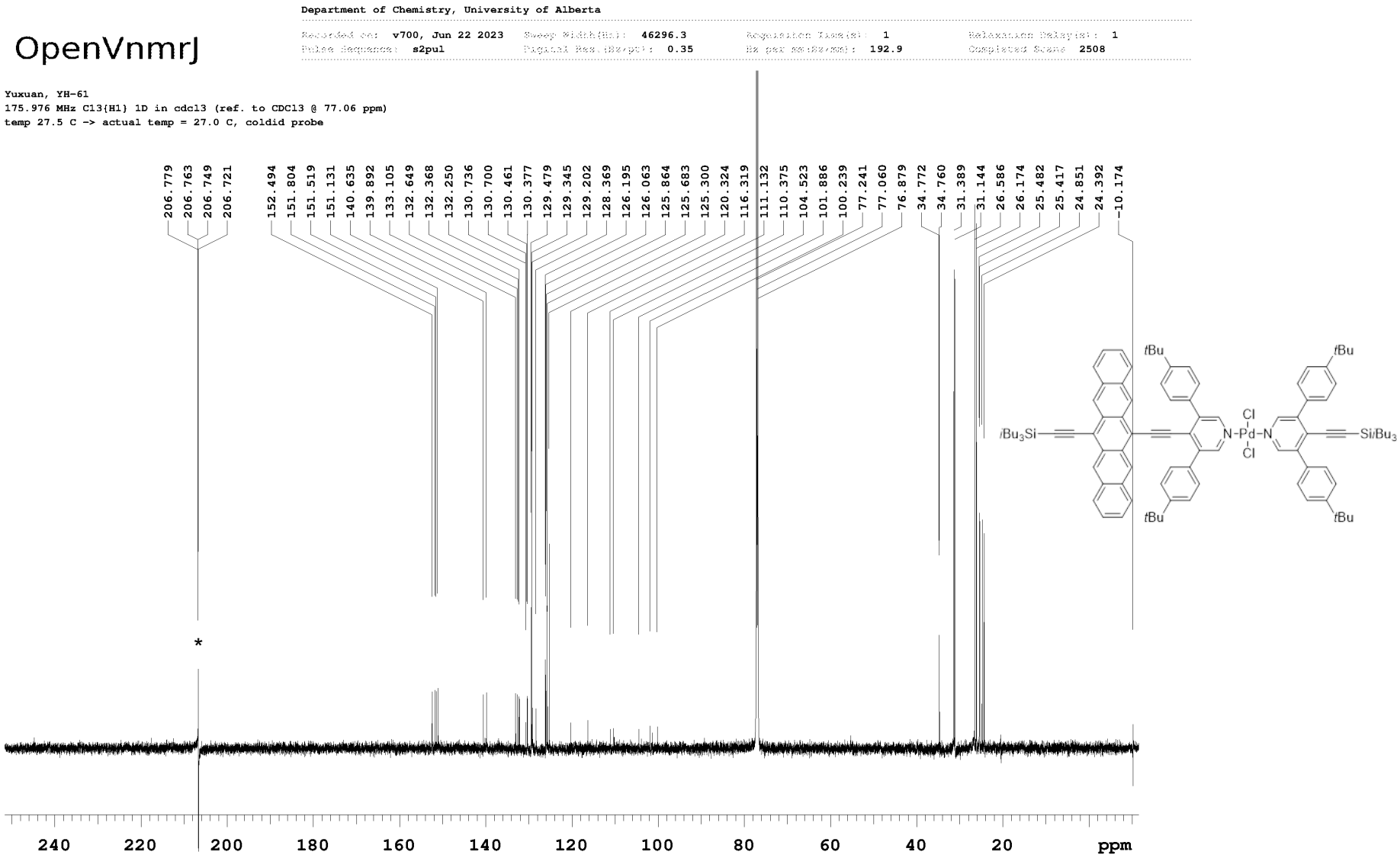

Figure S12. ^{13}C NMR spectrum (176 MHz) of compound **Pd(L_{pc})(L_{ref})Cl_2** in $CDCl_3$ (*artifact peak from the environment).

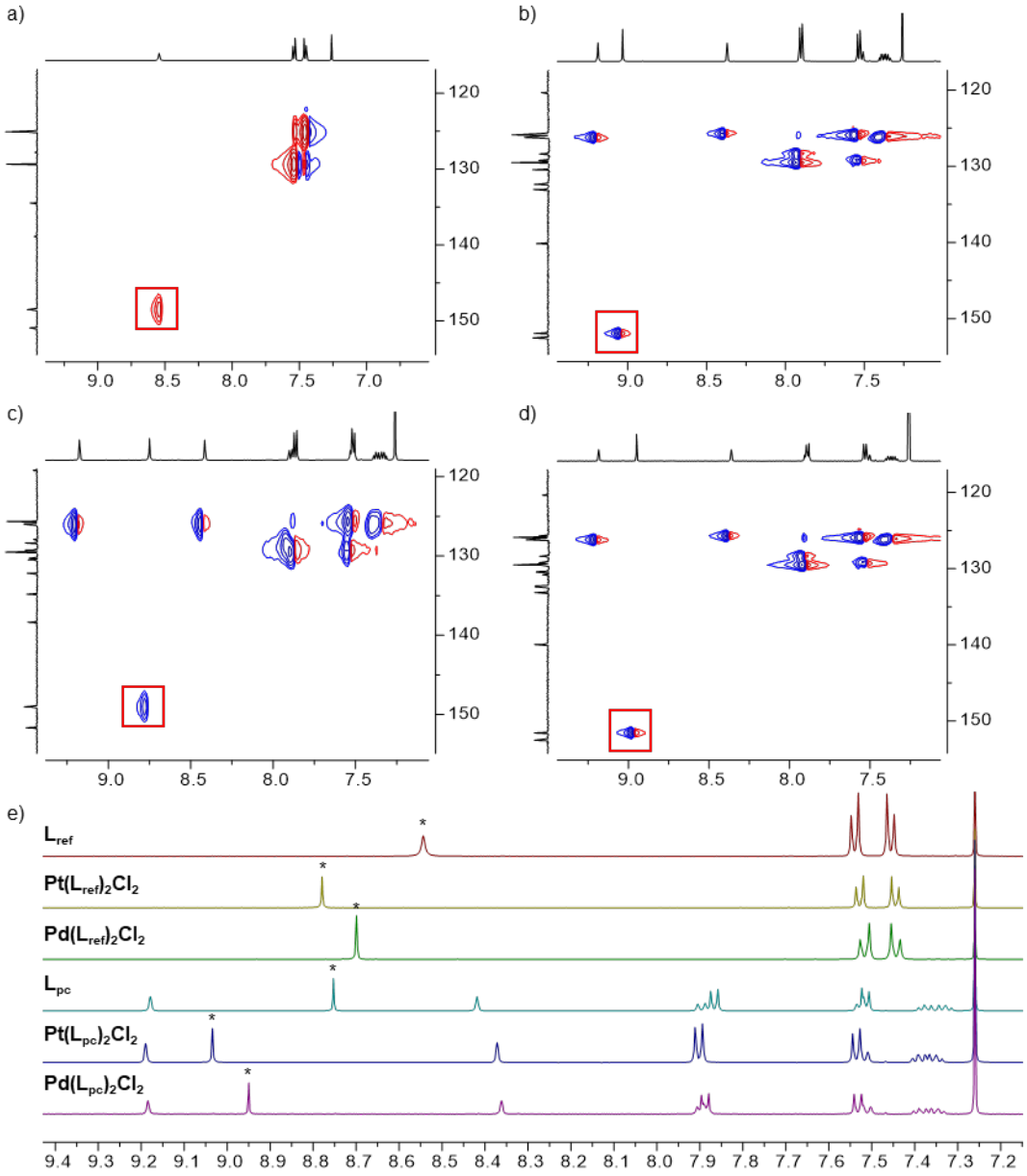

Figure S13. Aromatic region of $^{1}H–^{13}C$ HSQC spectra of a) $\mathbf{L_{ref}}$, b) $\mathbf{L_{pc}}$, c) $\mathbf{Pt(L_{pc})_2Cl_2}$, and d) $\mathbf{Pd(L_{pc})_2Cl_2}$ in $CDCl_3$; e) stacked plot of the aromatic region of ^{1}H NMR spectra (in $CDCl_3$) for compound $\mathbf{L_{ref}}$, $\mathbf{Pt(L_{ref})_2Cl_2}$, $\mathbf{Pd(L_{ref})_2Cl_2}$, $\mathbf{L_{pc}}$, $\mathbf{Pt(L_{pc})_2Cl_2}$, and $\mathbf{Pd(L_{pc})_2Cl_2}$. Signals for protons on pyridyl are labeled with *.

Mass Spectrometry Facility Department of Chemistry

Analysis Info

Analysis Name:	T:\Service\200622_0_E4_000002.d	Acquisition Date:	22/06/2020 2:12:37 PM
Method:	MALDI_DCTB_2k_new	Instrument:	apex-Qe
Sample Name:	YH-16-3	Operator:	
Comment:	Y. Hou, R. Tykwinski, DCTB as matrix, 9.4T FTICR MS		

Acquisition Parameter

Ionisation Mode: Positive MALDI Mode: n/a

Generate Molecular Formula Parameter

Formula, min.:	C95						
Formula, max.:	C126H134N2O0Cl2Si2Pt						
Measured m/z:	1995.91			Charge:	1	Tolerance: 2	ppm
Check Valence:	no	Min.:	0	Max.:	0		
Nitrogen Rule:	no						
Filter H/C Ratio:	no	Min.:	0	Max.:	3		
Estimate # of C:	yes					Electron Configuration:	both

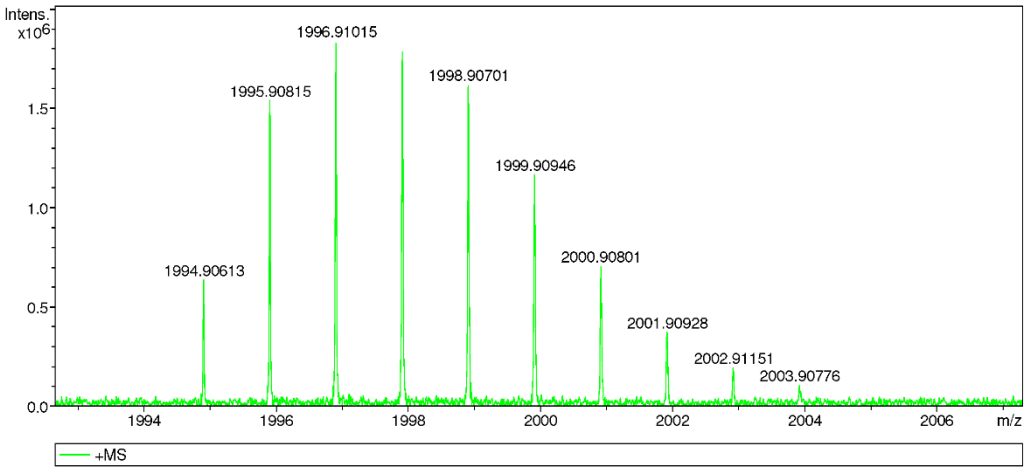

Sum Formula	Sigma	m/z	Err [ppm]	Mean Err [ppm]	Err [mDa]	rdb	N Rule	e⁻
C 126 H 134 Cl 2 N 2 Pt 1 Si 2	0.106	1995.91049	1.17	2.11	2.34	62.00	-	odd

Bruker Daltonics DataAnalysis 3.4 printed: 23/06/2020 9:09:20 AM Page 1 of 1

Figure S14. Expansion of HRMS for compound **$Pt(L_{pc})_2Cl_2$**

Mass Spectrometry Facility Department of Chemistry

Analysis Info

Analysis Name:	T:\Service\200622_0_E8_000001.d	Acquisition Date:	22/06/2020 2:01:32 PM
Method:	MALDI_DCTB_2k_new	Instrument:	apex-Qe
Sample Name:	YH-17-7	Operator:	
Comment:	Y. Hou, R. Tykwinski, DCTB as matrix, 9.4T FTICR MS		

Acquisition Parameter

Ionisation Mode:	Positive	MALDI Mode:	n/a

Generate Molecular Formula Parameter

Formula, min.:	C92						
Formula, max.:	C126H134N2O0Cl2Si2Pd						
Measured m/z:	1906.85			Charge:	1	Tolerance: 2	ppm
Check Valence:	no	Min.:	0	Max.:	0		
Nitrogen Rule:	no						
Filter H/C Ratio:	no	Min.:	0	Max.:	3		
Estimate # of C:	yes					Electron Configuration:	both

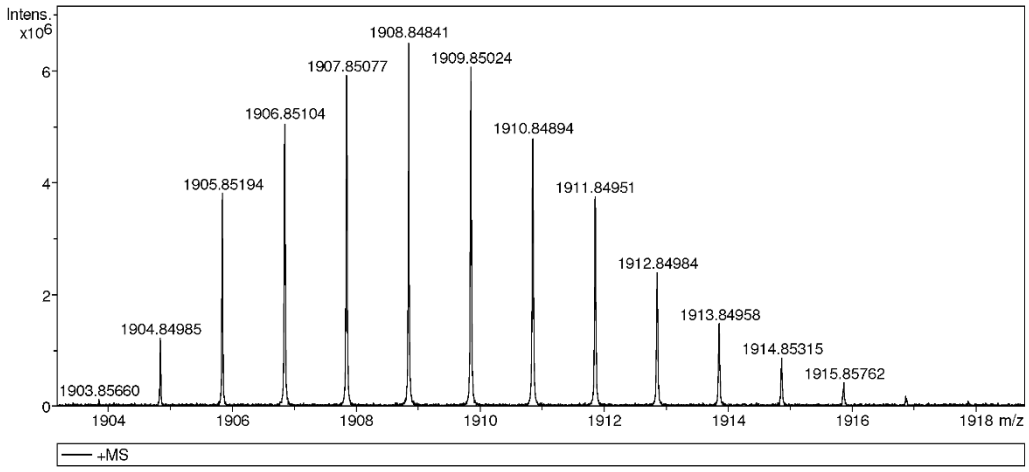

Sum Formula	Sigma	m/z	Err [ppm]	Mean Err [ppm]	Err [mDa]	rdb	N Rule	e⁻
C 126 H 134 Cl 2 N 2 Pd 1 Si 2	0.100	1906.84920	-0.97	1.30	-1.85	62.00	ok	odd

Bruker Daltonics DataAnalysis 3.4 printed: 23/06/2020 9:12:00 AM Page 1 of 1

Figure S15. Expansion of HRMS for compound **$Pd(L_{pc})_2Cl_2$**

Mass Spectrometry Facility Department of Chemistry

Analysis Info

Analysis Name:	T:\Service\200609_0_O4_000002.d	Acquisition Date:	09/06/2020 10:37:54 AM
Method:	MALDI_DCTB_1k_new	Instrument:	apex-Qe
Sample Name:	YH-57-1	Operator:	
Comment:	Y. Hou, R. Tykwinski, DCTB as matrix, 9.4T FTICR MS		

Acquisition Parameter

Ionisation Mode: Positive MALDI Mode: n/a

Generate Molecular Formula Parameter

Formula, min.:	C64						
Formula, max.:	C78H110N2O0Si2Cl2PtNa						
Measured m/z:	1418.71			Charge:	1	Tolerance: 2	ppm
Check Valence:	no	Min.:	0	Max.:	0		
Nitrogen Rule:	no						
Filter H/C Ratio:	no	Min.:	0	Max.:	3		
Estimate # of C:	yes					Electron Configuration:	both

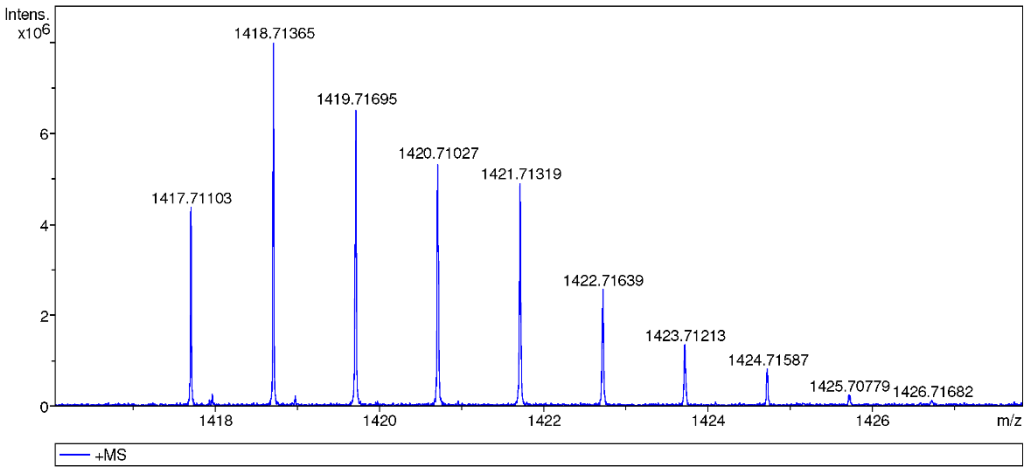

Sum Formula	Sigma	m/z	Err [ppm]	Mean Err [ppm]	Err [mDa]	rdb	N Rule	e⁻
C 78 H 110 Cl 2 N 2 Na 1 Pt 1 Si 2	0.177	1418.71246	-0.84	-0.54	-1.20	25.50	-	even

Bruker Daltonics DataAnalysis 3.4 printed: 09/06/2020 11:04:52 AM Page 1 of 1

Figure S16. Expansion of HRMS for compound **$Pt(L_{ref})_2Cl_2$**

Qualitative Compound Report

Data File	20061203.d	**Sample Name**	yh-60-1
Instrument Name	oaTOF6220	**User Name**	ami
Acquired Time	6/12/2020 3:57:14 PM	**DA Method**	ami-fia.m
Comment	Y. Hoyu, Tykwinski		

MS Spectrum

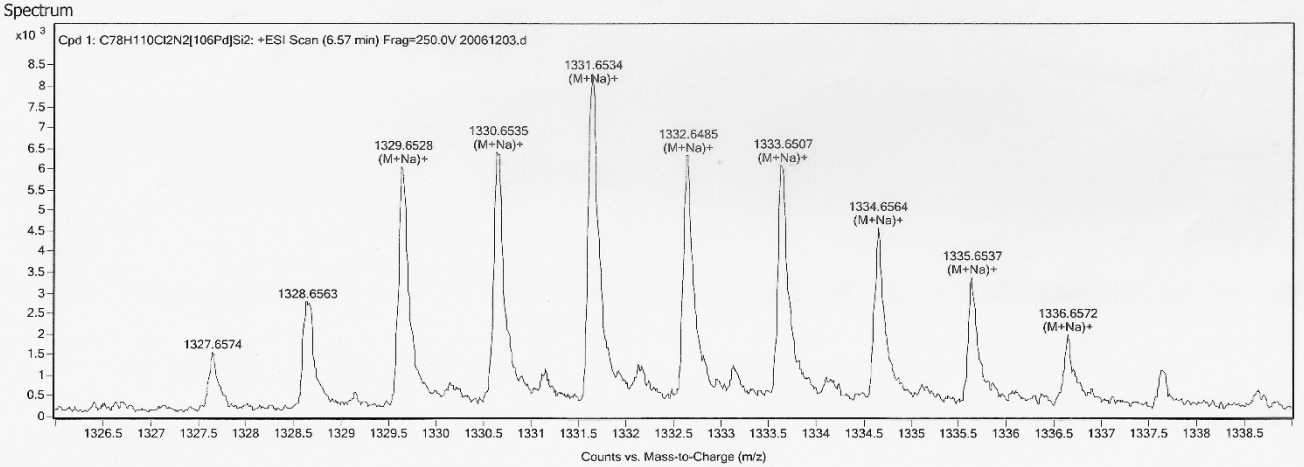

MS Spectrum Peak List

Formula	*m/z*	*Calc m/z*	Diff(ppm)	z	Ion	Abund
C78 H110 Cl2 N2 Na [106Pd] Si2	1329.6528	1329.6512	1.24	1	(M+Na)+	6009

--- End Of Report ---

Printed at: 4:20 PM on:6/12/2020

Figure S17. Expansion of HRMS for compound **Pd(L_{ref})$_2$Cl**

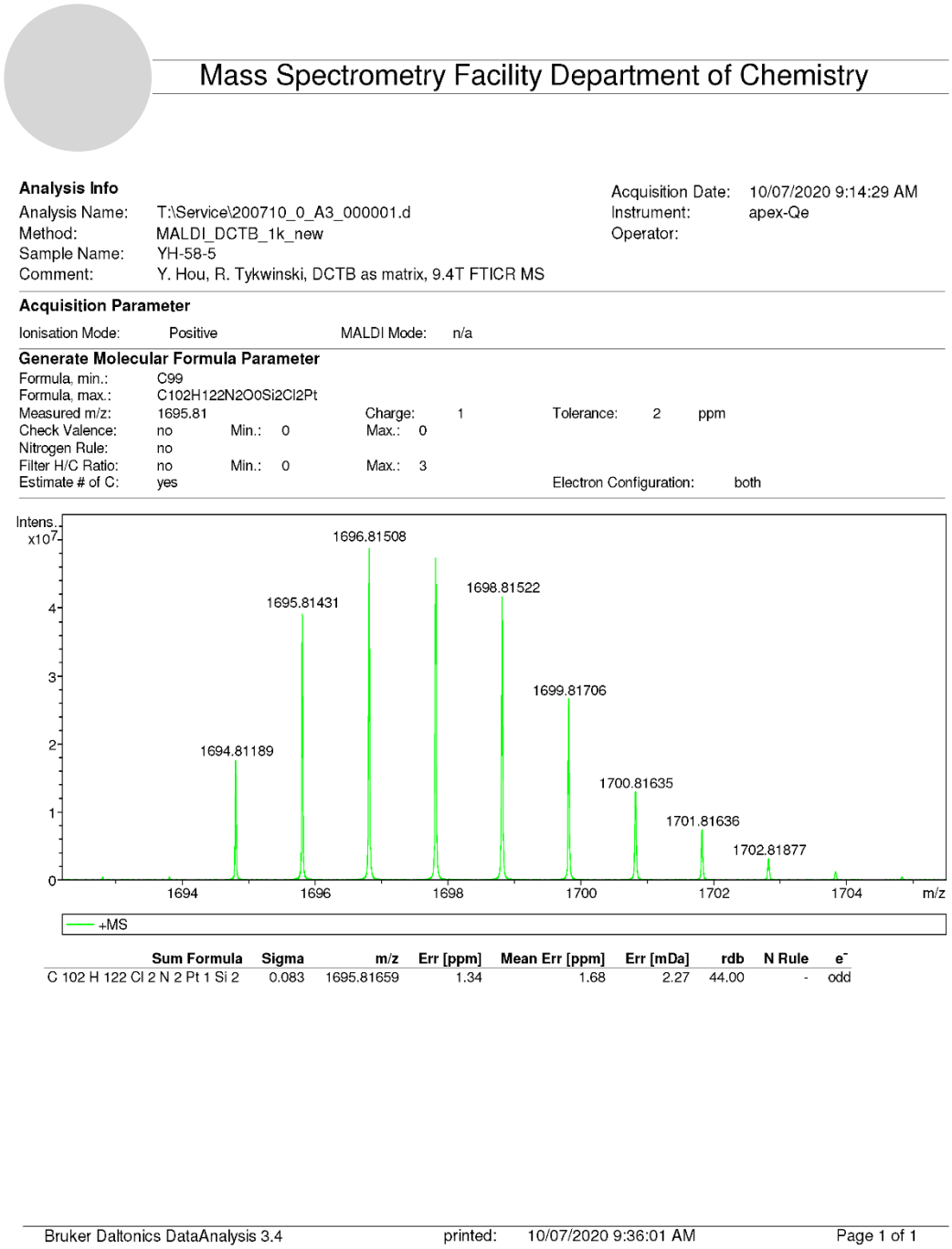

Figure S18. Expansion of HRMS for compound **Pt(L_{pc})(L_{ref})Cl_2**

Mass Spectrometry Facility Department of Chemistry

Analysis Info

Analysis Name:	U:\Service\230623_0_B5_000001.d	Acquisition Date:	6/23/2023 2:34:43 PM
Method:	MALDI_DCTB_mz600_new	Instrument:	apex-Qe
Sample Name:	YH-61	Operator:	
Comment:	Y. Hou, R. Tykwinski, DCTB as matrix, 9.4T FTICR MS		

Acquisition Parameter

Ionisation Mode: Positive MALDI Mode: n/a

Generate Molecular Formula Parameter

Formula, min.:	C89						
Formula, max.:	N2O0Si2Cl2Pd						
Measured m/z:	1606.75			Charge:	1	Tolerance: 2	mDa
Check Valence:	yes	Min.:	0	Max.:	100		
Nitrogen Rule:	no						
Filter H/C Ratio:	no	Min.:	0	Max.:	3		
Estimate # of C:	yes					Electron Configuration:	both

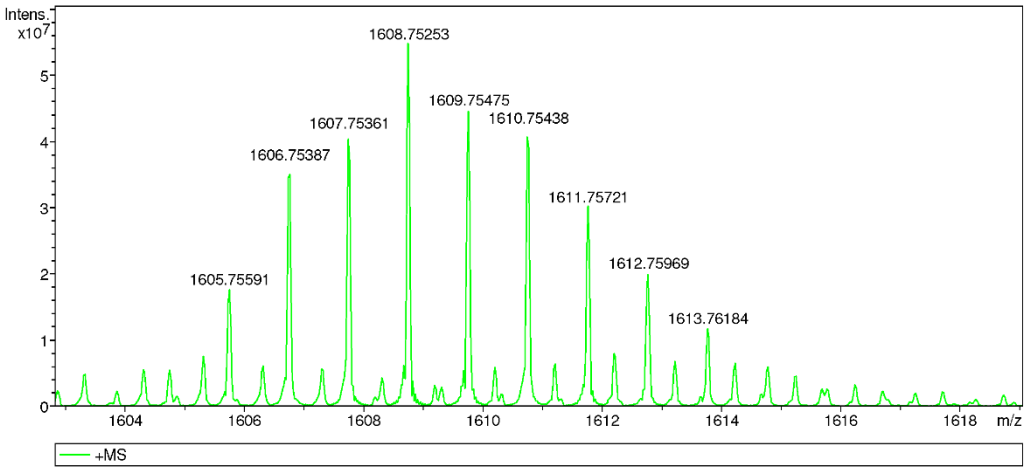

Sum Formula	Sigma	m/z	Err [ppm]	Mean Err [ppm]	Err [mDa]	rdb	N Rule	e⁻
C 102 H 122 Cl 2 N 2 Pd 1 Si 2	0.036	1606.75529	0.88	1.66	1.42	44.00	ok	odd
C 113 H 110 Cl 2 N 1 Si 2	0.147	1606.75484	0.60	1.51	0.96	60.50	ok	even

Bruker Daltonics DataAnalysis 3.4 printed: 6/23/2023 3:21:22 PM Page 1 of 1

Figure S19. Expansion of HRMS for compound **Pd(L_{pc})(L_{ref})Cl_2**

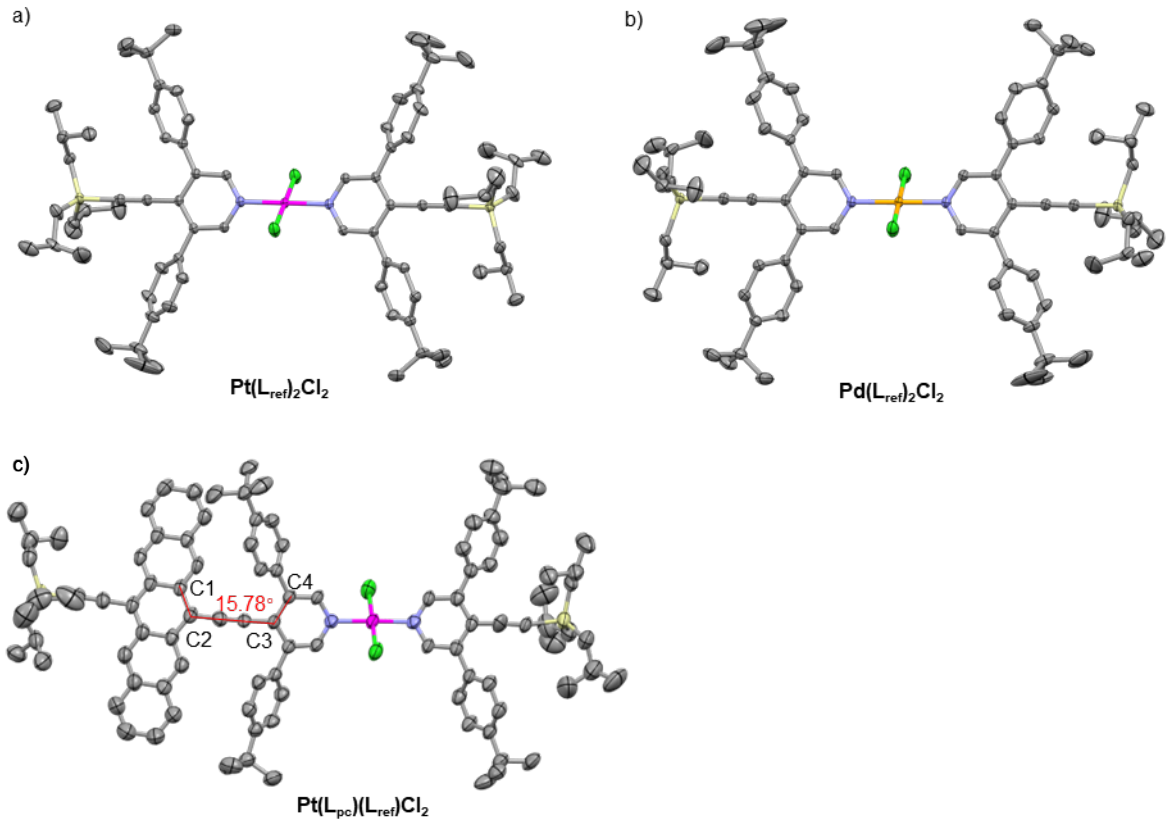

Figure S20. ORTEP drawing of a) **Pd(L$_{ref}$)$_2$Cl$_2$**, b) **Pt(L$_{ref}$)$_2$Cl$_2$**, and c) **Pt(L$_{ref}$)(L$_{pc}$)Cl$_2$** with torsion angle of C1–C2–C3–C4.

Photophysical Characterization

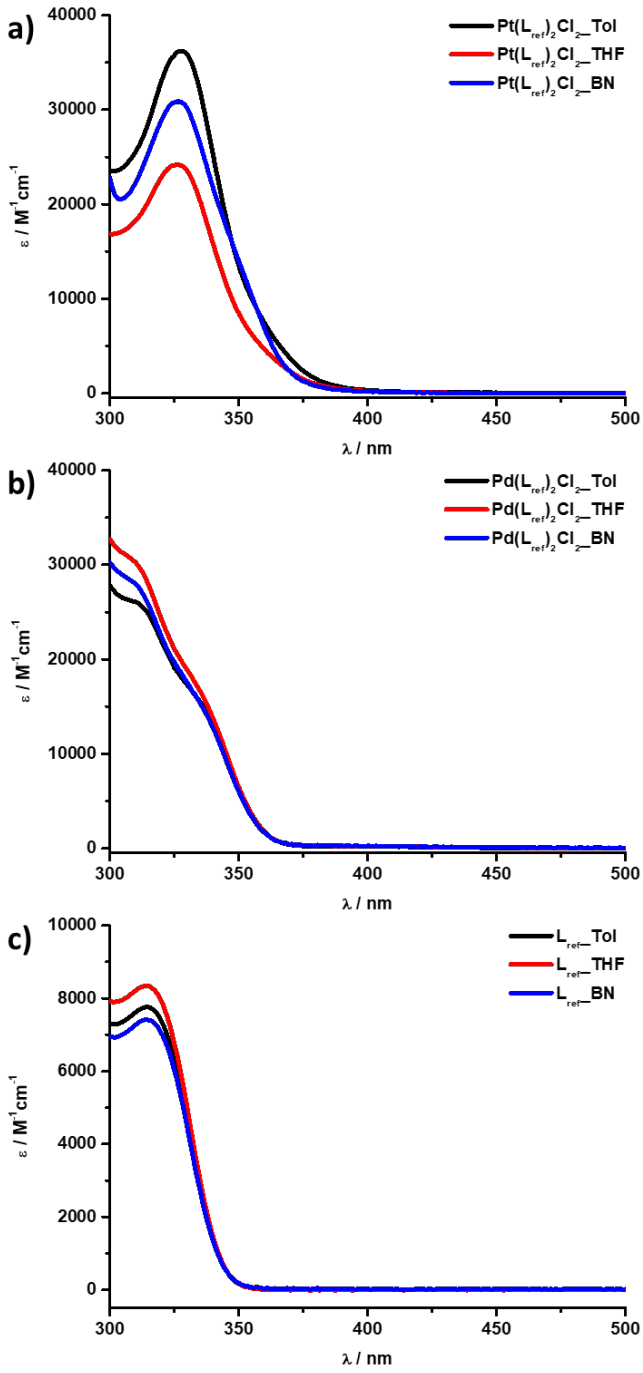

Figure S21. Steady-state absorption spectra of a) **Pt(L$_{ref}$)$_2$Cl$_2$**, b) **Pd(L$_{ref}$)$_2$Cl$_2$**, and c) **L$_{ref}$** in Tol (black), THF (red), and BN (blue).

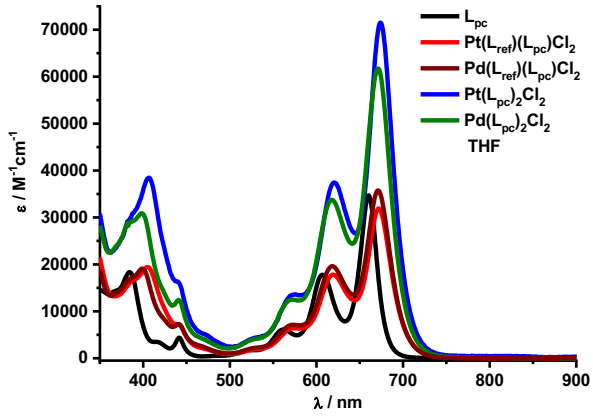

Figure S22. Steady-state absorption spectra of $\mathbf{L_{pc}}$ (black), $\mathbf{Pt(L_{pc})(L_{ref})Cl_2}$ (red), $\mathbf{Pd(L_{pc})(L_{ref})Cl_2}$ (brown), $\mathbf{Pt(L_{pc})_2Cl_2}$ (blue), and $\mathbf{Pd(L_{pc})_2Cl_2}$ (green) in THF.

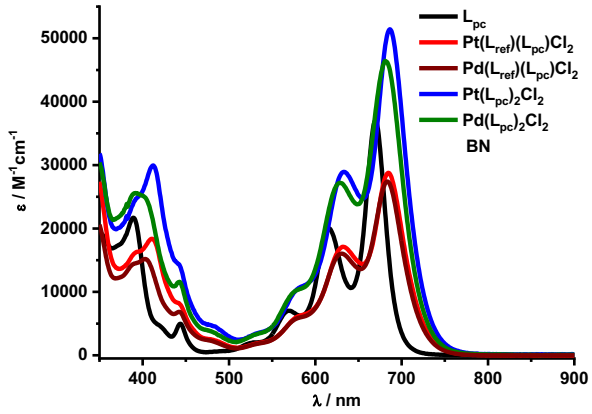

Figure S23. Steady-state absorption spectra of $\mathbf{L_{pc}}$ (black), $\mathbf{Pt(L_{pc})(L_{ref})Cl_2}$ (red), $\mathbf{Pd(L_{pc})(L_{ref})Cl_2}$ (brown), $\mathbf{Pt(L_{pc})_2Cl_2}$ (blue), and $\mathbf{Pd(L_{pc})_2Cl_2}$ (green) in BN.

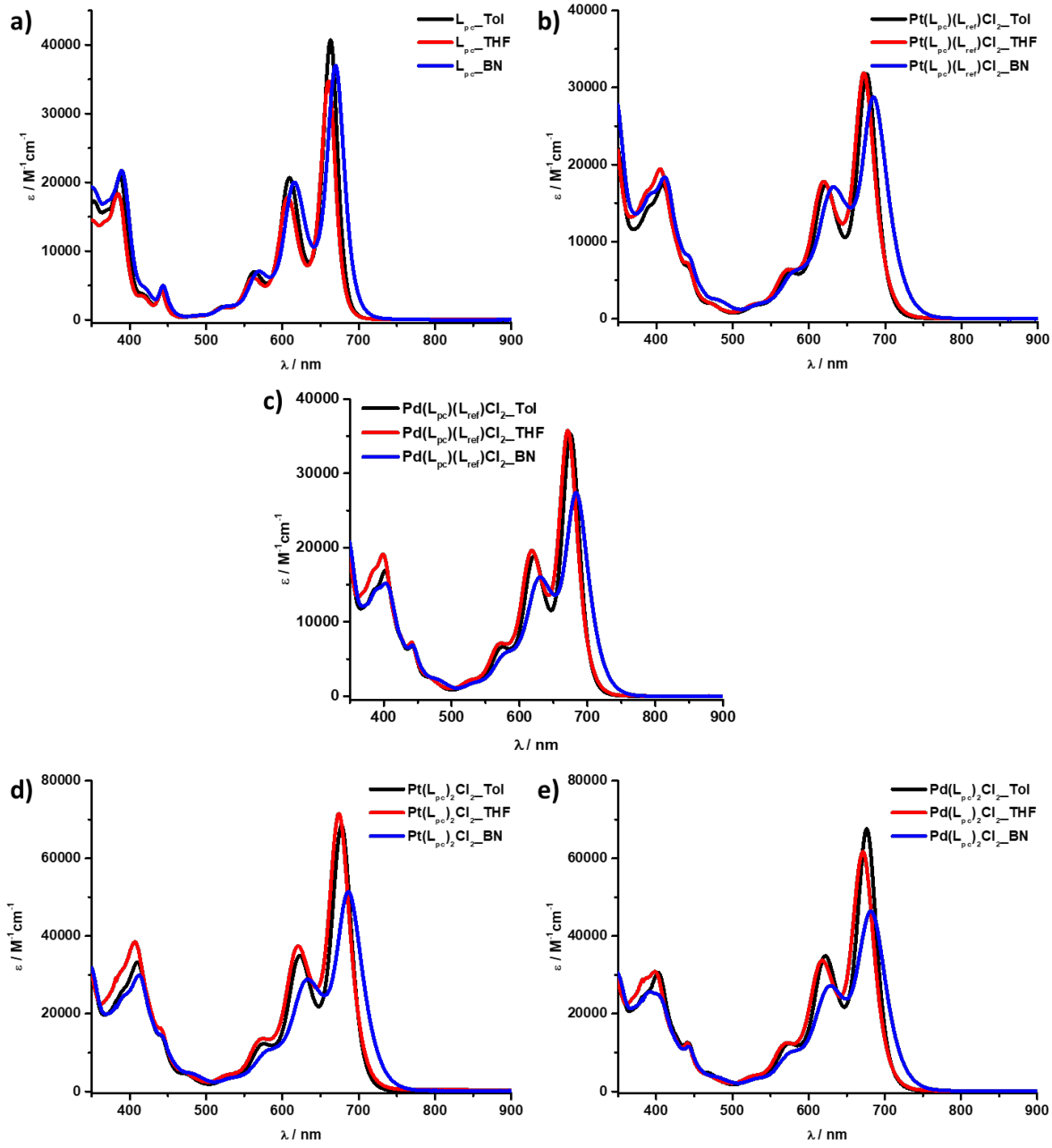

Figure S24. Steady-state absorption spectra of a) $\mathbf{L_{pc}}$, b) $\mathbf{Pt(L_{pc})(L_{ref})Cl_2}$, c) $\mathbf{Pd(L_{pc})(L_{ref})Cl_2}$, d) $\mathbf{Pt(L_{pc})_2Cl_2}$, and e) $\mathbf{Pd(L_{pc})_2Cl_2}$ in Tol (black), THF (red), and BN (blue).

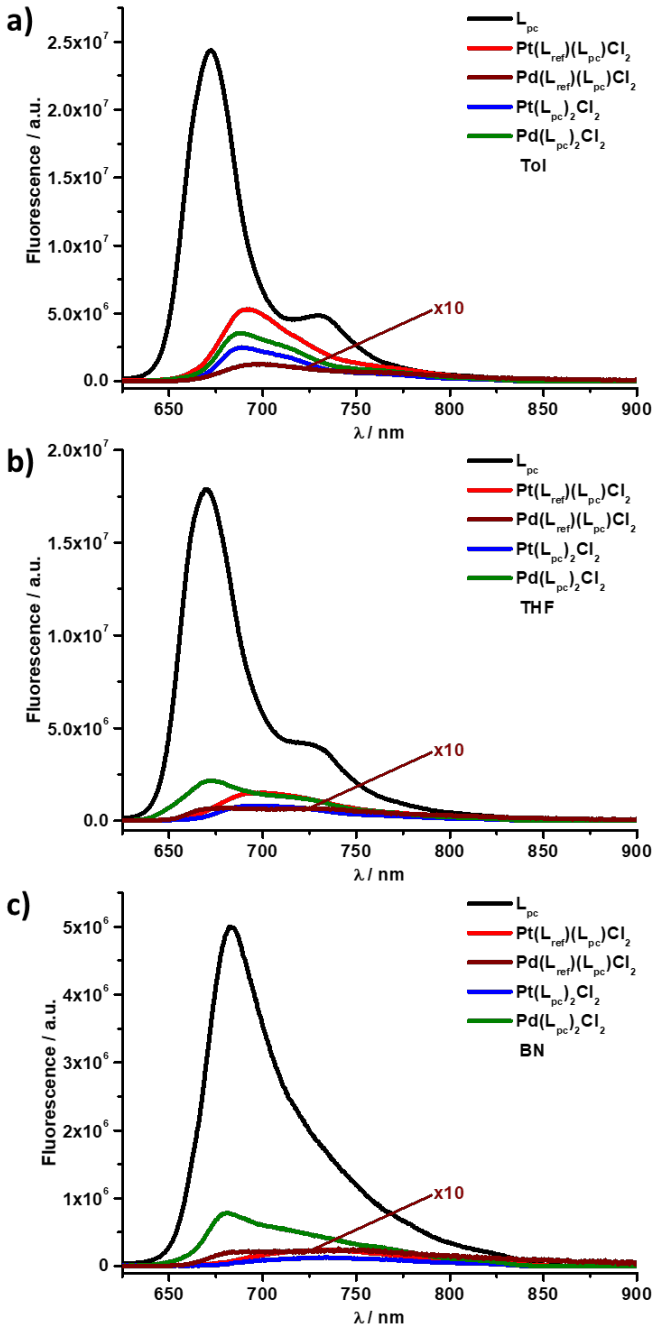

Figure S25. Steady-state fluorescence spectra of $\mathbf{L_{pc}}$ (black), $\mathbf{Pt(L_{pc})(L_{ref})Cl_2}$ (red), $\mathbf{Pd(L_{pc})(L_{ref})Cl_2}$ (brown), $\mathbf{Pt(L_{pc})_2Cl_2}$ (blue), and $\mathbf{Pd(L_{pc})_2Cl_2}$ (green) in a) Tol, b) THF, and c) BN, respectively.

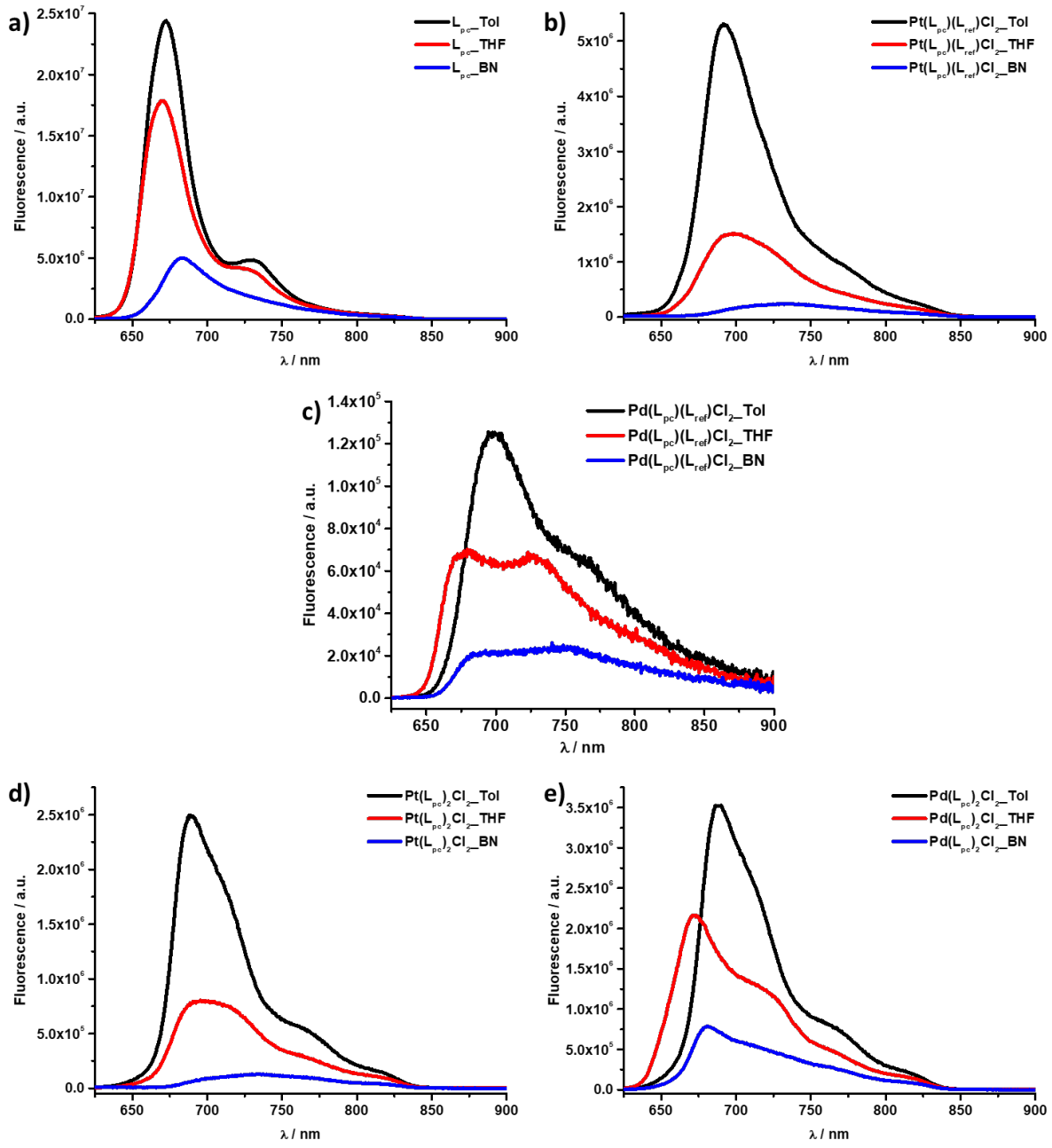

Figure S26. Steady-state fluorescence spectra of a) $\mathbf{L_{pc}}$, b) $\mathbf{Pt(L_{pc})(L_{ref})Cl_2}$, c) $\mathbf{Pd(L_{pc})(L_{ref})Cl_2}$, d) $\mathbf{Pt(L_{pc})_2Cl_2}$, and e) $\mathbf{Pd(L_{pc})_2Cl_2}$ in Tol (black), THF (red), and BN (blue), respectively.

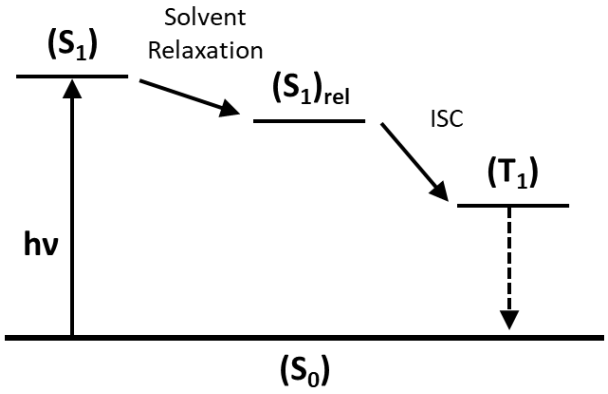

Figure S27. Applied kinetic model used for fitting the fsTAS and nsTAS raw data of L_{pc}, **Pt(L_{pc})(L_{ref})Cl_2** and **Pd(L_{pc})(L_{ref})Cl_2**.

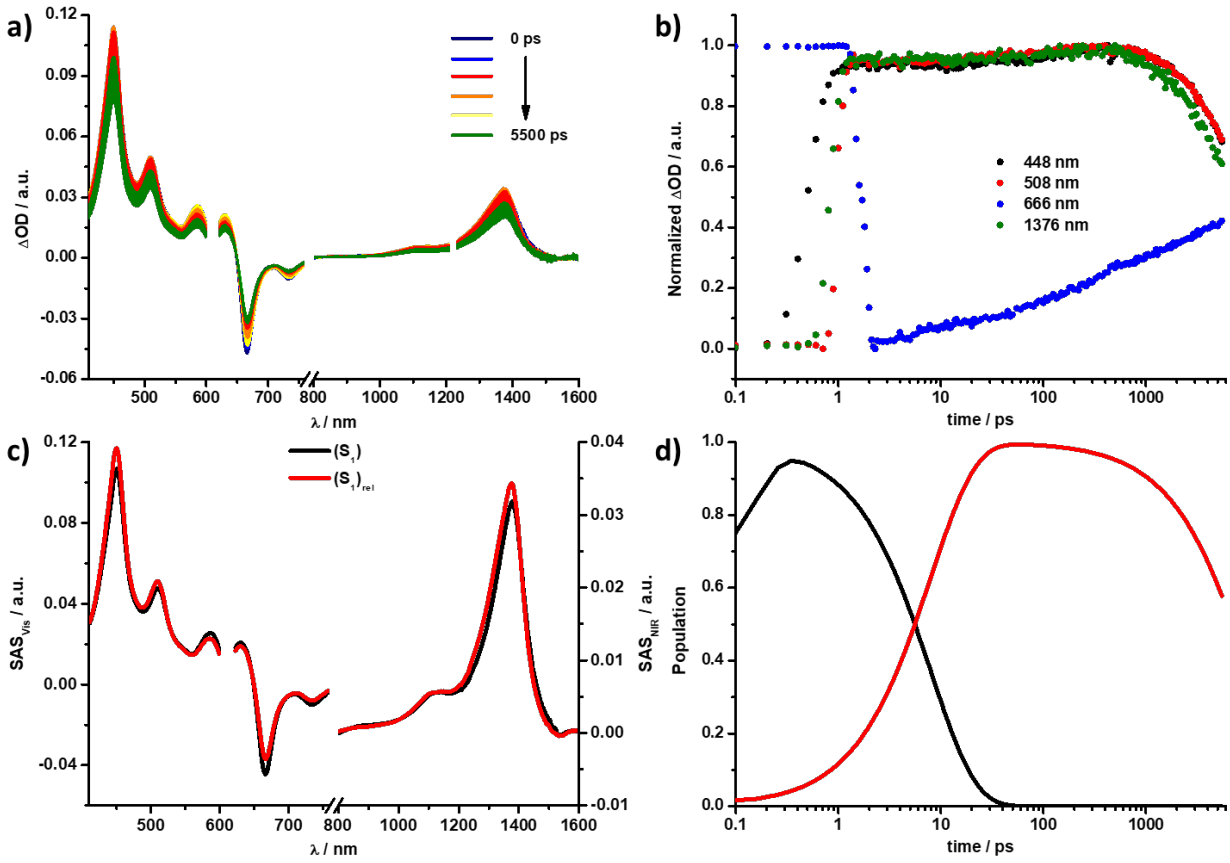

Figure S28. (a) fsTAS (λ_{ex} = 610 nm, 400 nJ) of L_{pc} in Tol with time delays between 0–5 500 ps. (b) Respective normalized time absorption profiles at the illustrated wavelengths. (c) Deconvoluted fsTAS of the singlet excited state (S_1) (black) and solvent relaxed singlet excited state $(S_1)_{rel}$ (red) of L_{pc} in Tol as obtained by target analysis. (d) Respective population kinetics.

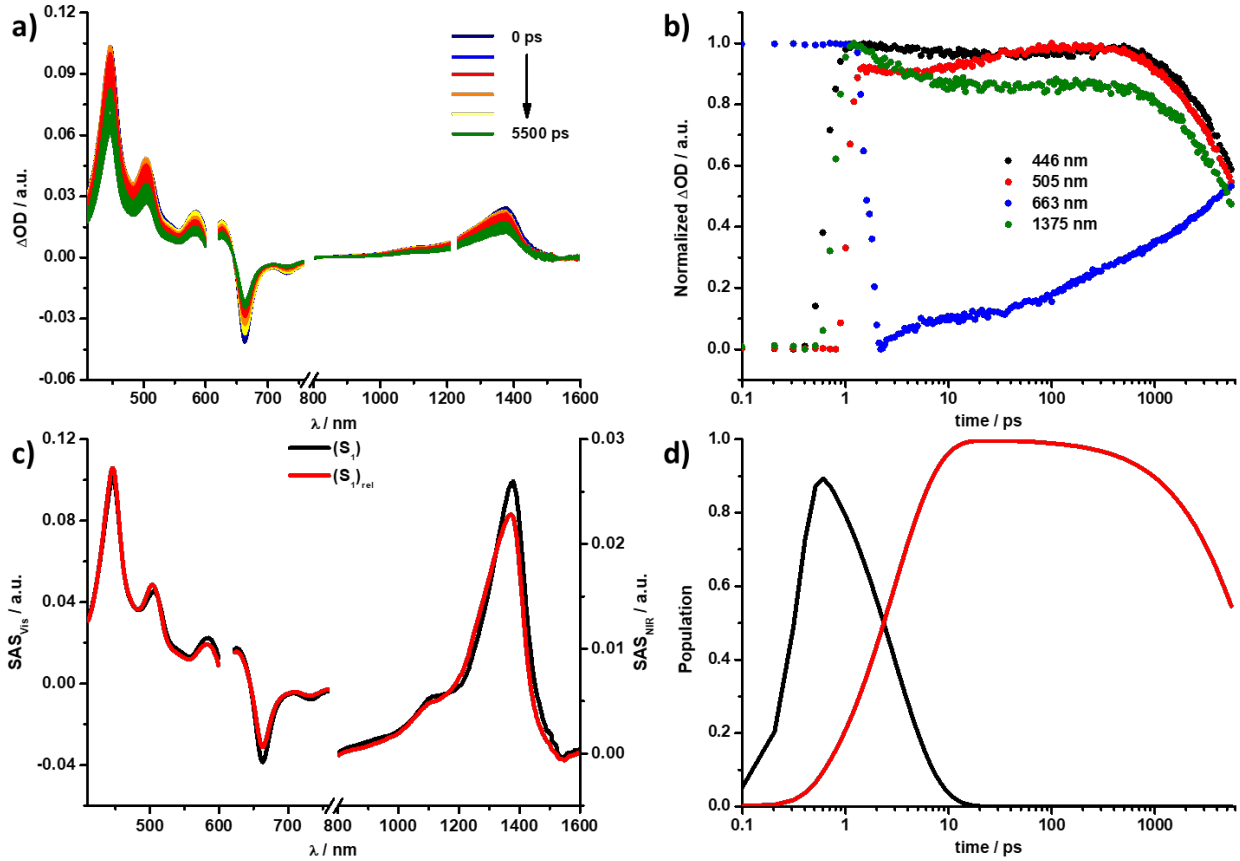

Figure S29. (a) fsTAS (λ_{ex} = 610 nm, 400 nJ) of $\mathbf{L_{pc}}$ in THF with time delays between 0–5 500 ps. (b) Respective normalized time absorption profiles at the illustrated wavelengths. (c) Deconvoluted fsTAS of the singlet excited state (S_1) (black) and solvent relaxed singlet excited state $(S_1)_{rel}$ (red) of $\mathbf{L_{pc}}$ in THF as obtained by target analysis. (d) Respective population kinetics.

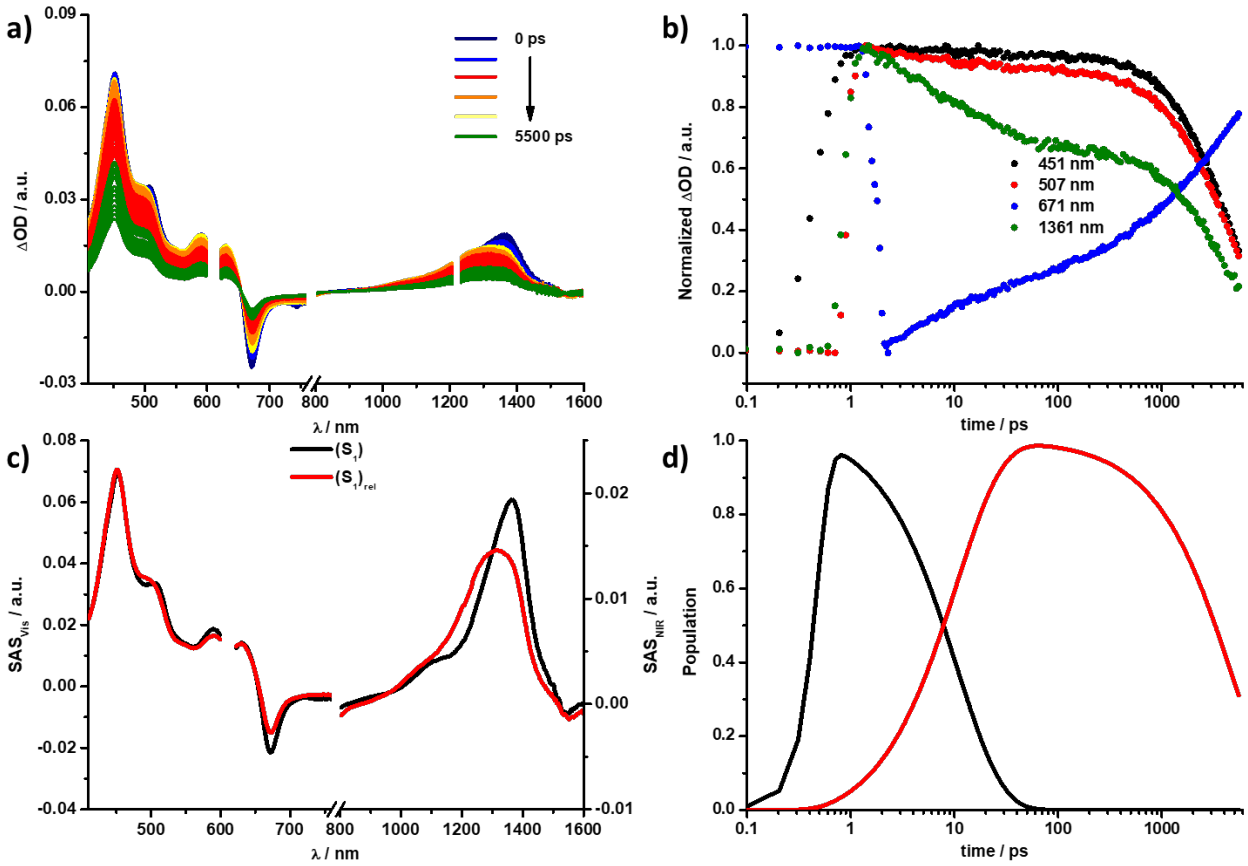

Figure S30. (a) fsTAS (λ_{ex} = 610 nm, 400 nJ) of **L$_{pc}$** in BN with time delays between 0–5 500 ps. (b) Respective normalized time absorption profiles at the illustrated wavelengths. (c) Deconvoluted fsTAS of the singlet excited state (S_1) (black) and solvent relaxed singlet excited state $(S_1)_{rel}$ (red) of **L$_{pc}$** in BN as obtained by target analysis. (d) Respective population kinetics.

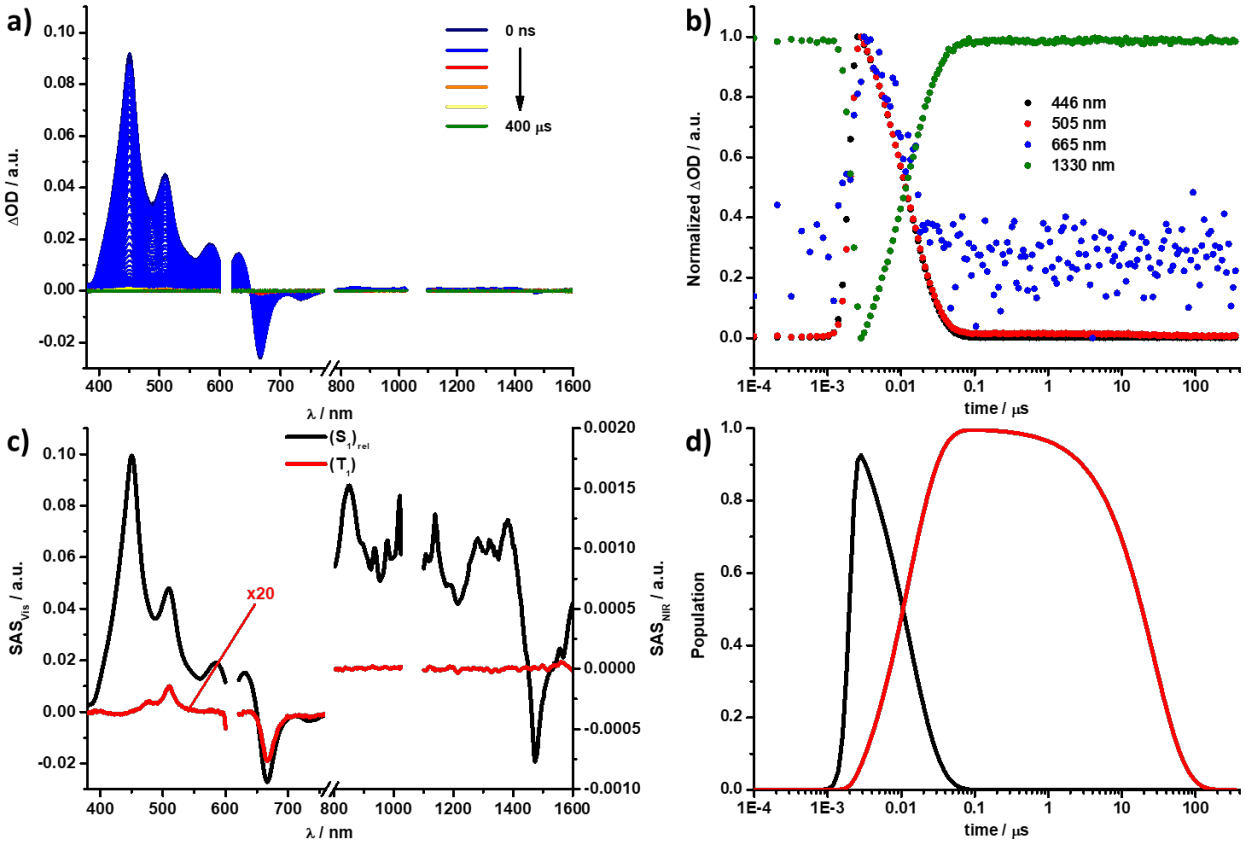

Figure S31. (a) nsTAS (λ_{ex} = 610 nm, 400 nJ) of **L_{pc}** in Tol with time delays between 0 ns – 400 µs. (b) Respective normalized time absorption profiles at the illustrated wavelengths. (c) Deconvoluted nsTAS of the solvent relaxed singlet excited state $(S_1)_{rel}$ (black) and triplet excited state (T_1) (red) of **L_{pc}** in Tol as obtained by target analysis. (d) Respective population kinetics.

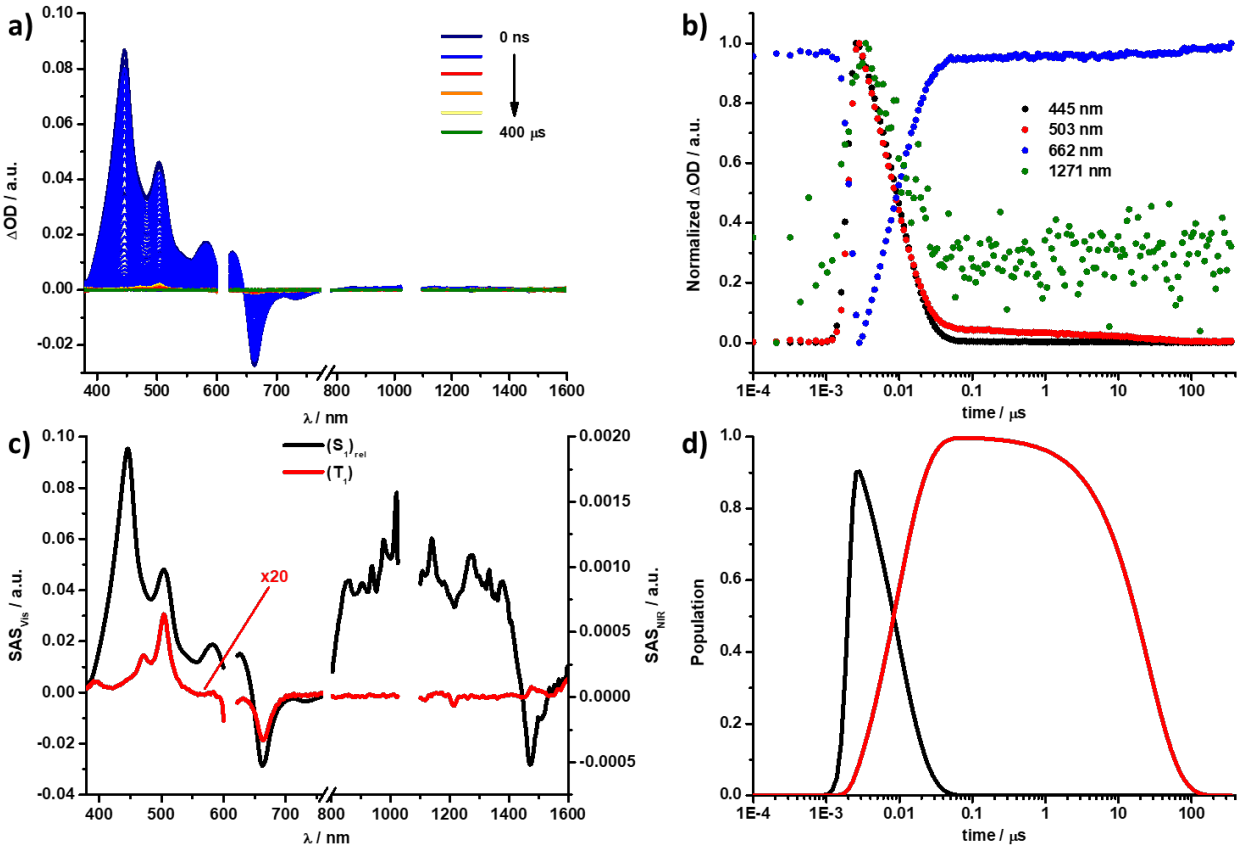

Figure S32. (a) nsTAS (λ_{ex} = 610 nm, 400 nJ) of $\mathbf{L_{pc}}$ in THF with time delays between 0 ns – 400 µs. (b) Respective normalized time absorption profiles at the illustrated wavelengths. (c) Deconvoluted nsTAS of the solvent relaxed singlet excited state $(S_1)_{rel}$ (black) and triplet excited state (T_1) (red) of $\mathbf{L_{pc}}$ in THF as obtained by target analysis. (d) Respective population kinetics.

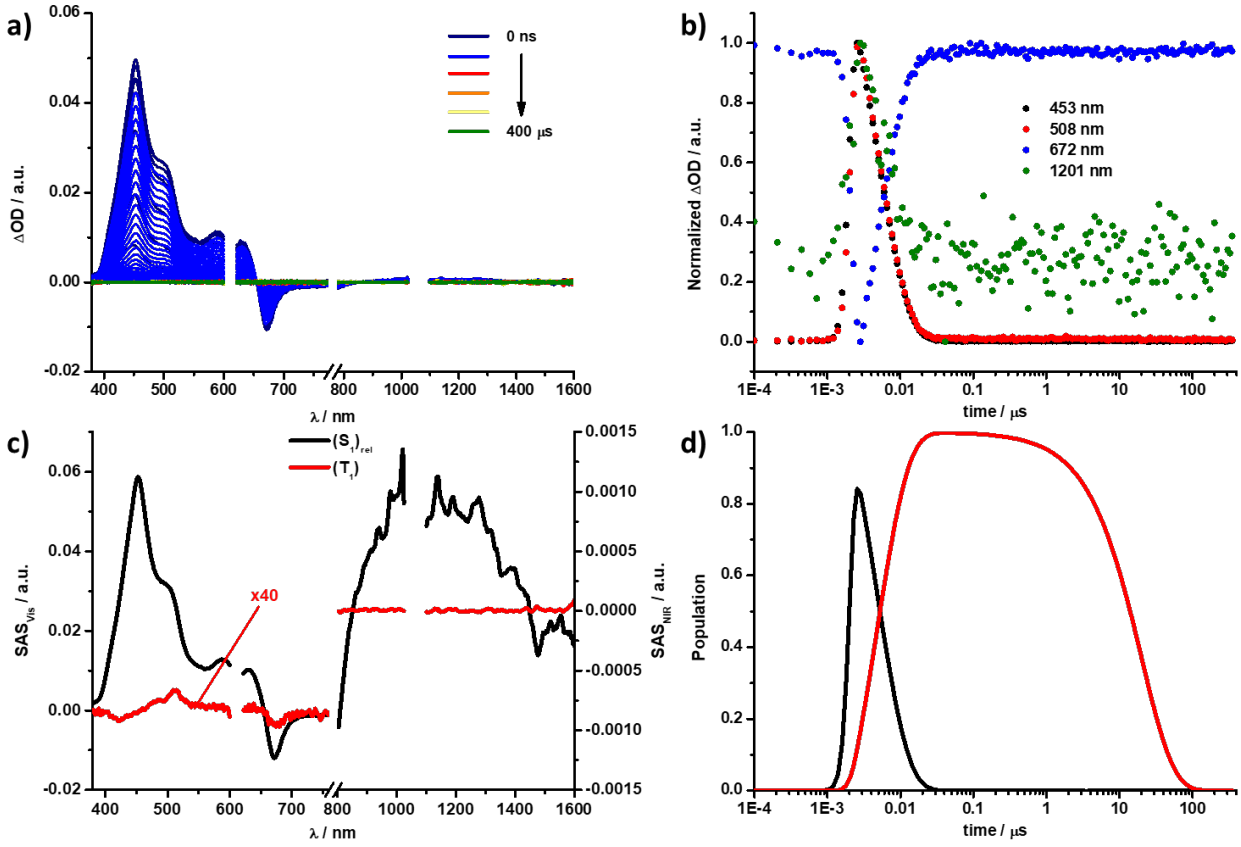

Figure S33. (a) nsTAS (λ_{ex} = 610 nm, 400 nJ) of $\mathbf{L_{pc}}$ in BN with time delays between 0 ns – 400 µs. (b) Respective normalized time absorption profiles at the illustrated wavelengths. (c) Deconvoluted nsTAS of the solvent relaxed singlet excited state $(S_1)_{rel}$ (black) and triplet excited state (T_1) (red) of $\mathbf{L_{pc}}$ in BN as obtained by target analysis. (d) Respective population kinetics.

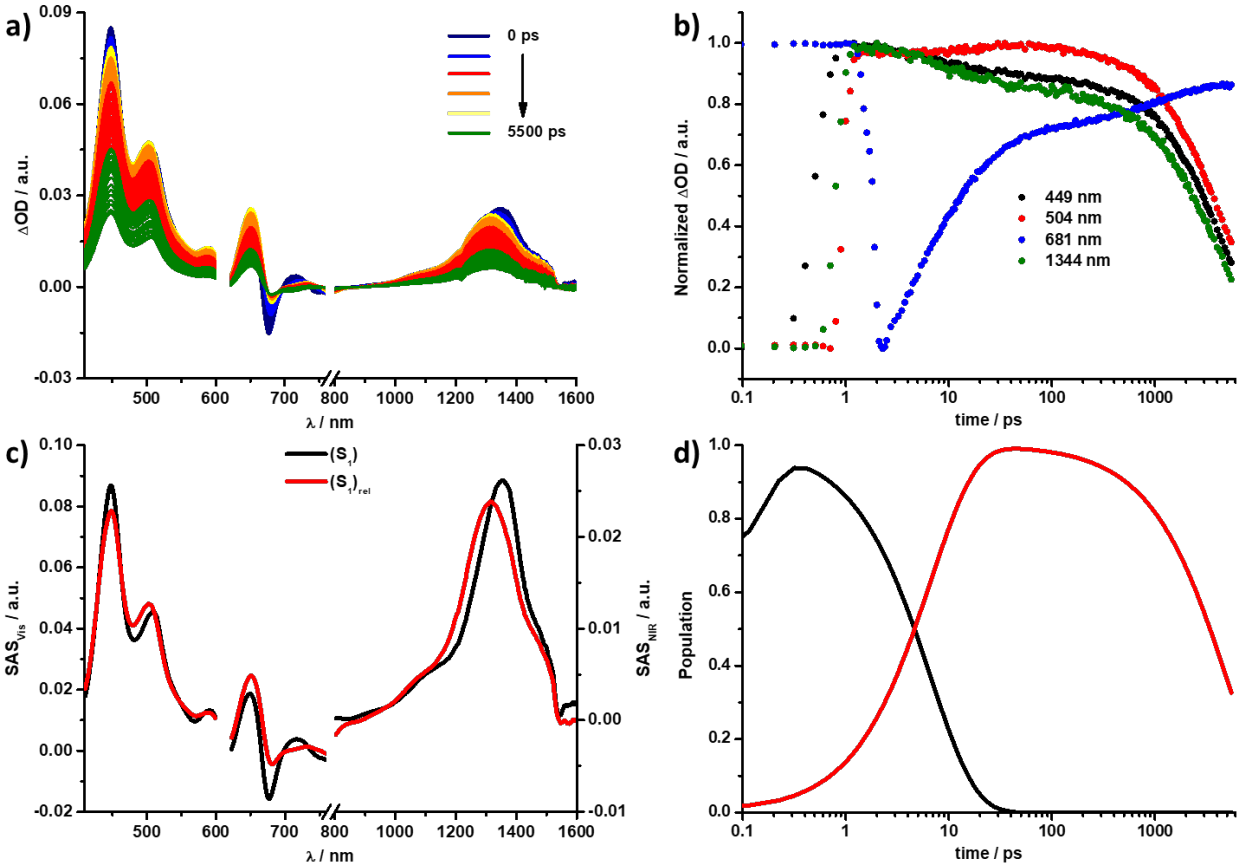

Figure S34. (a) fsTAS (λ_{ex} = 610 nm, 400 nJ) of **Pt(L_{pc})(L_{ref})Cl_2** in Tol with time delays between 0–5 500 ps. (b) Respective normalized time absorption profiles at the illustrated wavelengths. (c) Deconvoluted fsTAS of the singlet excited state (S_1) (black) and solvent relaxed singlet excited state $(S_1)_{rel}$ (red) of **Pt(L_{pc})(L_{ref})Cl_2** in Tol as obtained by target analysis. (d) Respective population kinetics.

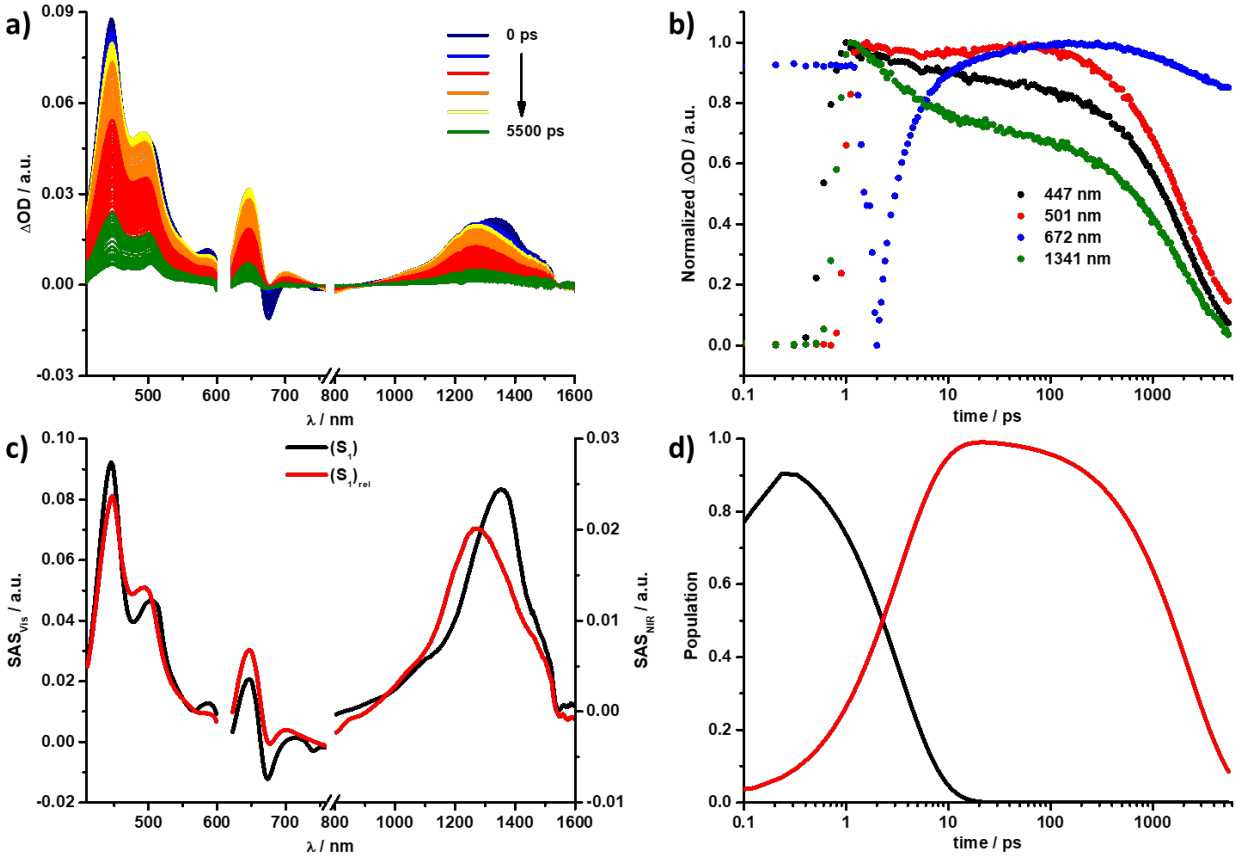

Figure S35. (a) fsTAS (λ_{ex} = 610 nm, 400 nJ) of **Pt(L_{pc})(L_{ref})Cl_2** in THF with time delays between 0–5 500 ps. (b) Respective normalized time absorption profiles at the illustrated wavelengths. (c) Deconvoluted fsTAS of the singlet excited state (S_1) (black) and solvent relaxed singlet excited state $(S_1)_{rel}$ (red) of **Pt(L_{pc})(L_{ref})Cl_2** in THF as obtained by target analysis. (d) Respective population kinetics.

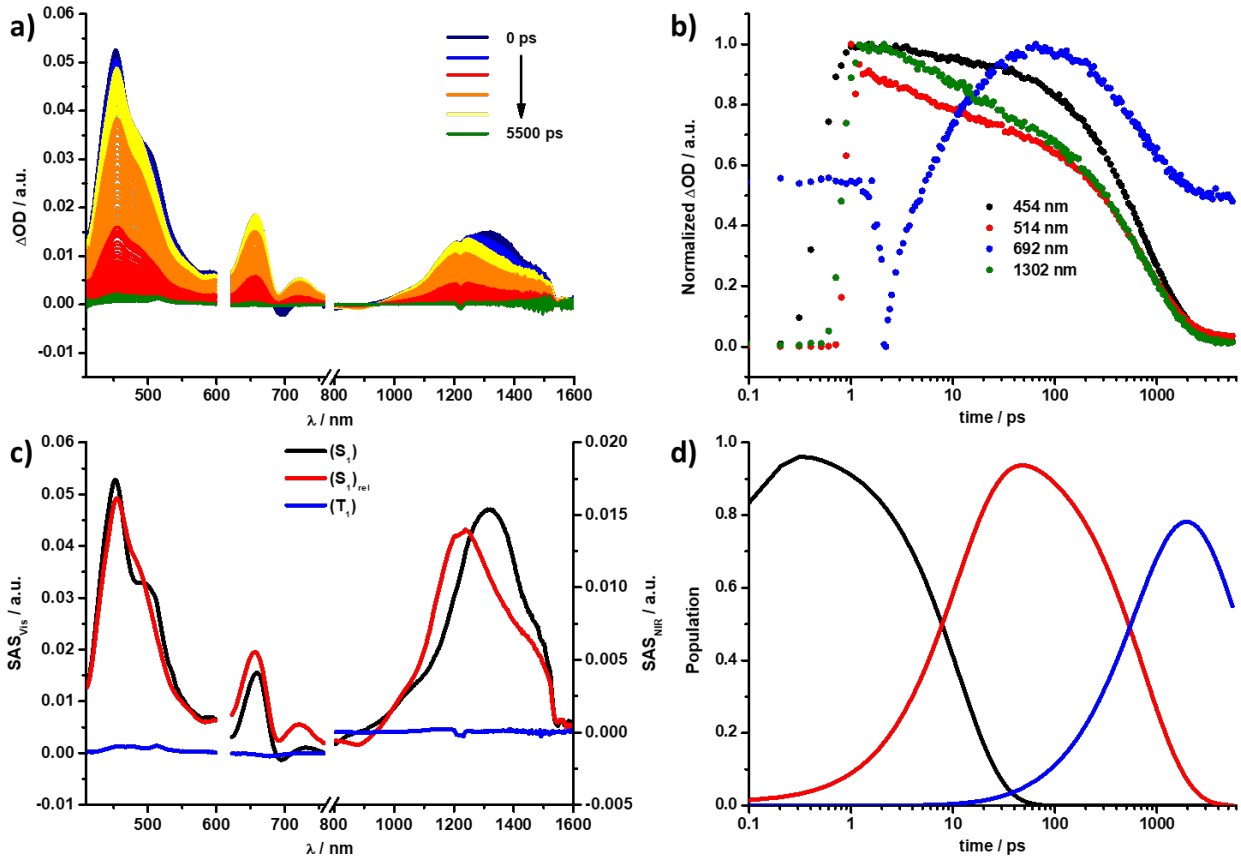

Figure S36. (a) fsTAS (λ_{ex} = 610 nm, 400 nJ) of **Pt(L_{pc})(L_{ref})Cl_2** in BN with time delays between 0–5 500 ps. (b) Respective normalized time absorption profiles at the illustrated wavelengths. (c) Deconvoluted fsTAS of the singlet excited state (S_1) (black), solvent relaxed singlet excited state $(S_1)_{rel}$ (red), and triplet excited state (T_1) of **Pt(L_{pc})(L_{ref})Cl_2** in BN as obtained by target analysis. (d) Respective population kinetics.

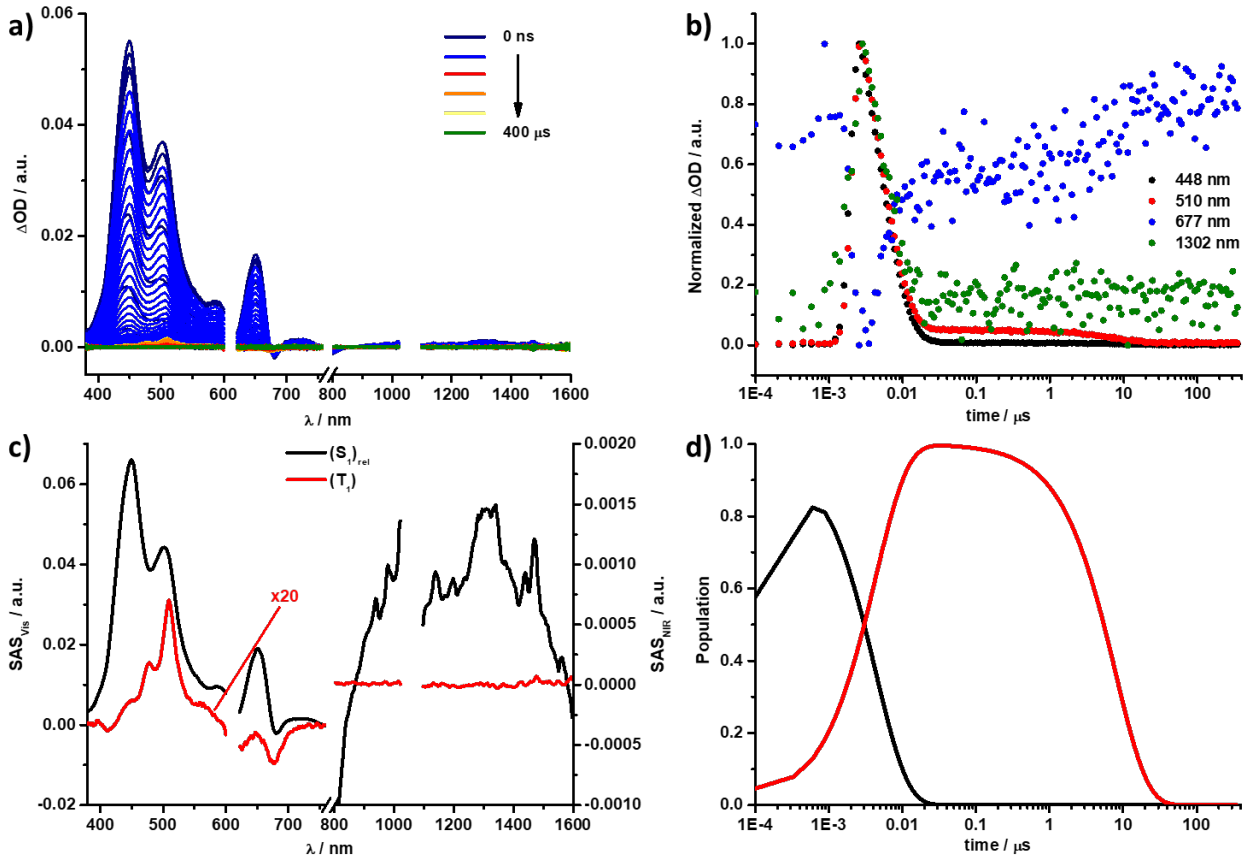

Figure S37. (a) nsTAS (λ_{ex} = 610 nm, 400 nJ) of **Pt(L_{pc})(L_{ref})Cl_2** in Tol with time delays between 0 ns – 400 µs. (b) Respective normalized time absorption profiles at the illustrated wavelengths. (c) Deconvoluted nsTAS of the solvent relaxed singlet excited state $(S_1)_{rel}$ (black) and triplet excited state (T_1) (red) of **Pt(L_{pc})(L_{ref})Cl_2** in Tol as obtained by target analysis. (d) Respective population kinetics.

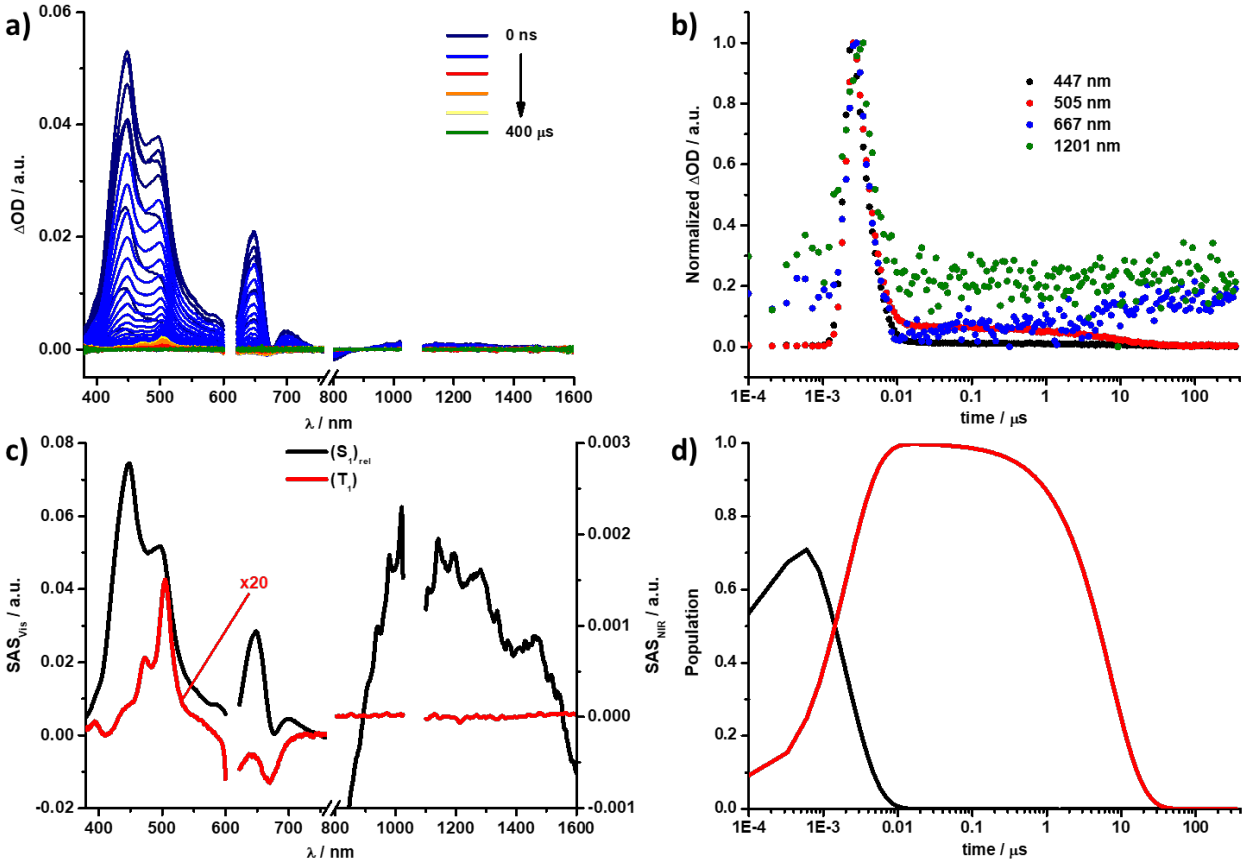

Figure S38. (a) nsTAS (λ_{ex} = 610 nm, 400 nJ) of **Pt(L_{pc})(L_{ref})Cl_2** in THF with time delays between 0 ns – 400 µs. (b) Respective normalized time absorption profiles at the illustrated wavelengths. (c) Deconvoluted nsTAS of the solvent relaxed singlet excited state $(S_1)_{rel}$ (black) and triplet excited state (T_1) (red) of **Pt(L_{pc})(L_{ref})Cl_2** in THF as obtained by target analysis. (d) Respective population kinetics.

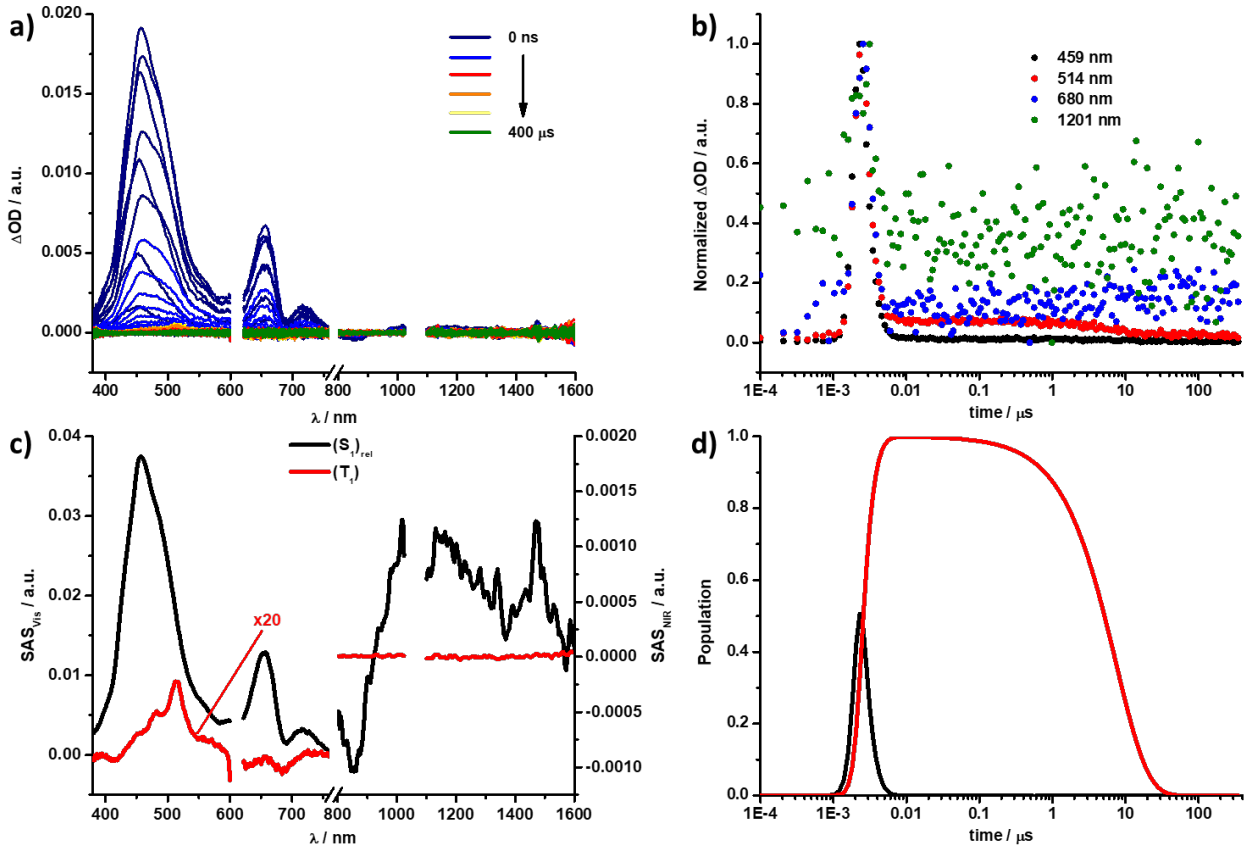

Figure S39. (a) nsTAS (λ_{ex} = 610 nm, 400 nJ) of **Pt(L_{pc})(L_{ref})Cl_2** in BN with time delays between 0 ns – 400 µs. (b) Respective normalized time absorption profiles at the illustrated wavelengths. (c) Deconvoluted nsTAS of the solvent relaxed singlet excited state $(S_1)_{rel}$ (black) and triplet excited state (T_1) (red) of **Pt(L_{pc})(L_{ref})Cl_2** in BN as obtained by target analysis. (d) Respective population kinetics.

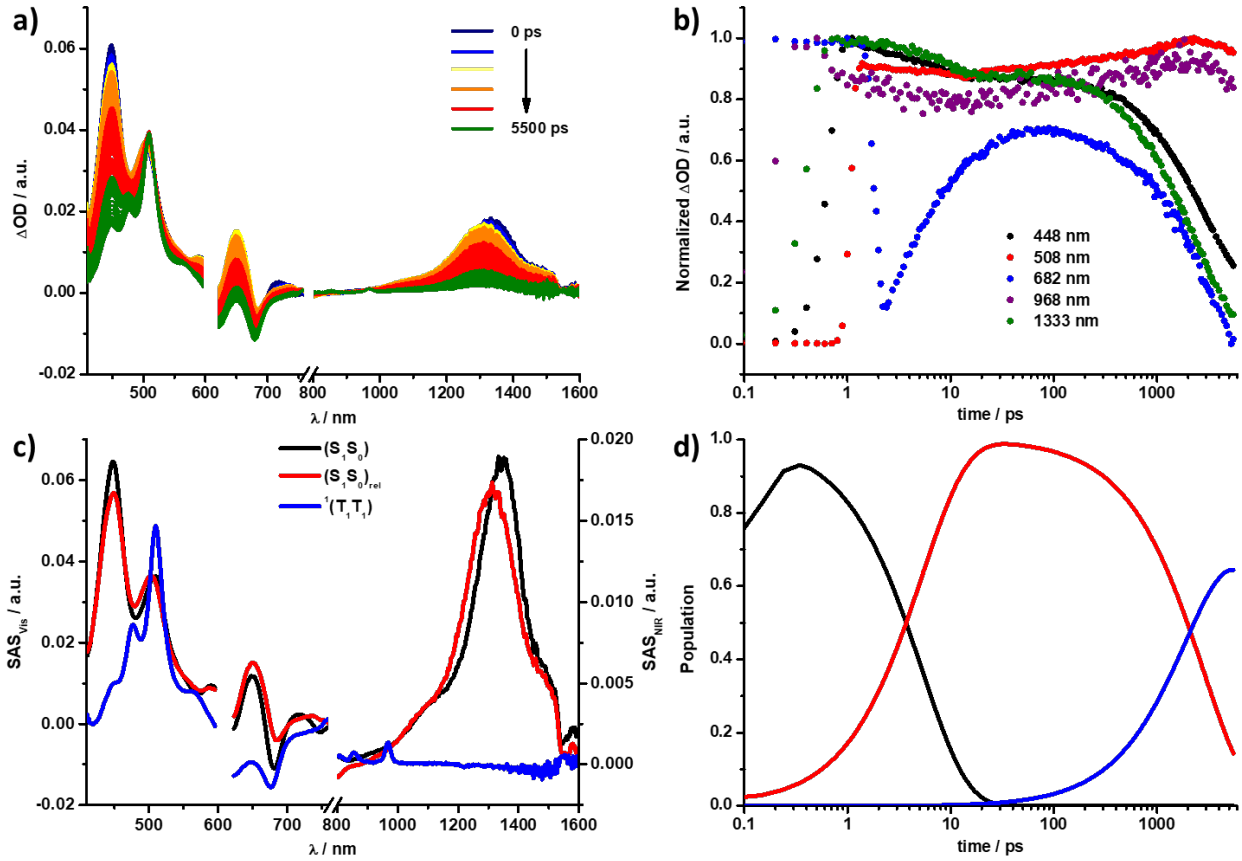

Figure S40. (a) fsTAS (λ_{ex} = 610 nm, 400 nJ) of **Pt(L$_{pc}$)$_2$Cl$_2$** in Tol with time delays between 0–5 500 ps. (b) Respective normalized time absorption profiles at the illustrated wavelengths. (c) Deconvoluted fsTAS of the singlet excited state (S_1S_0) (black), solvent relaxed singlet excited state $(S_1S_0)_{rel}$ (red), and singlet correlated triplet pair $^1(T_1T_1)$ (blue) of **Pt(L$_{pc}$)$_2$Cl$_2$** in Tol as obtained by target analysis. (d) Respective population kinetics.

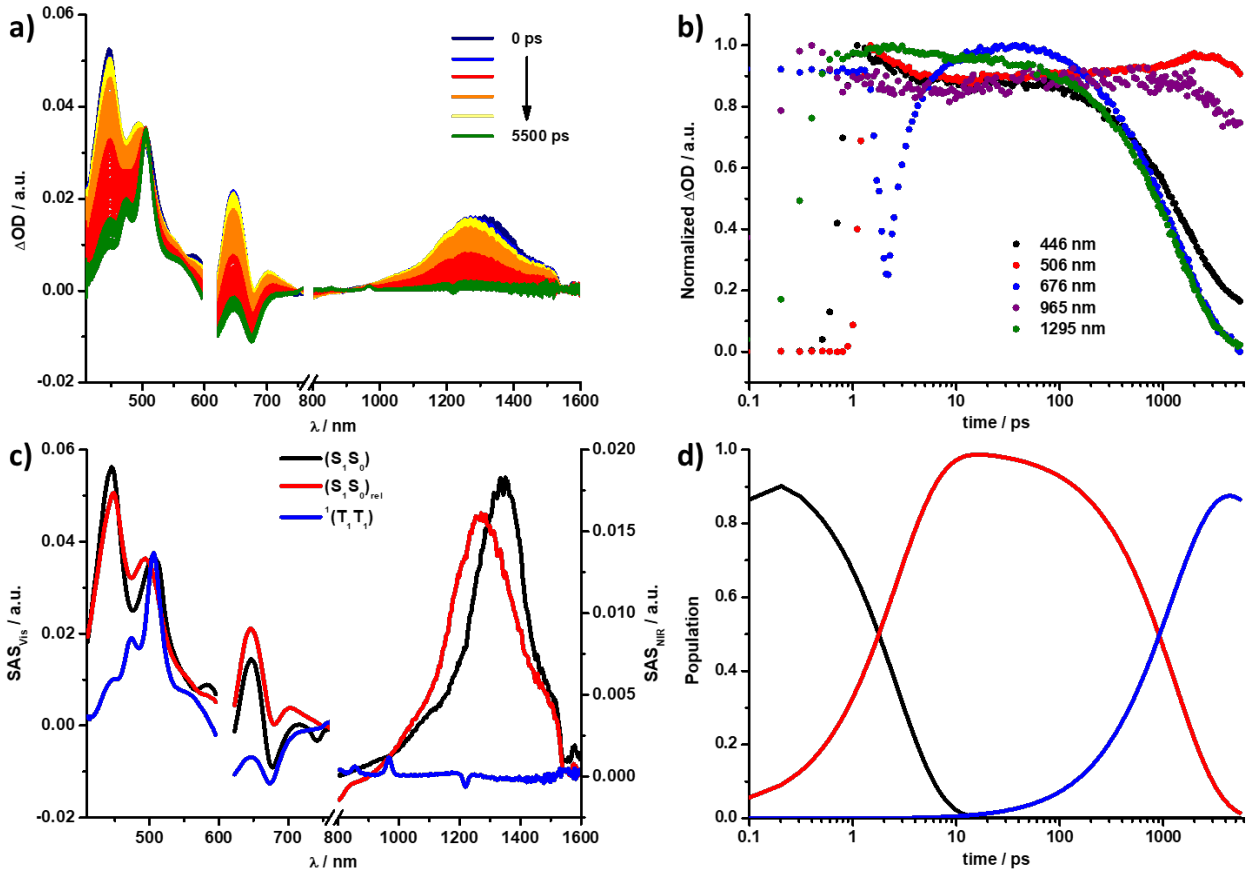

Figure S41. (a) fsTAS (λ_{ex} = 610 nm, 400 nJ) of **Pt(L$_{pc}$)$_2$Cl$_2$** in THF with time delays between 0–5 500 ps. (b) Respective normalized time absorption profiles at the illustrated wavelengths. (c) Deconvoluted fsTAS of the singlet excited state (S_1S_0) (black), solvent relaxed singlet excited state $(S_1S_0)_{rel}$ (red), and singlet correlated triplet pair $^1(T_1T_1)$ (blue) of **Pt(L$_{pc}$)$_2$Cl$_2$** in THF as obtained by target analysis. (d) Respective population kinetics.

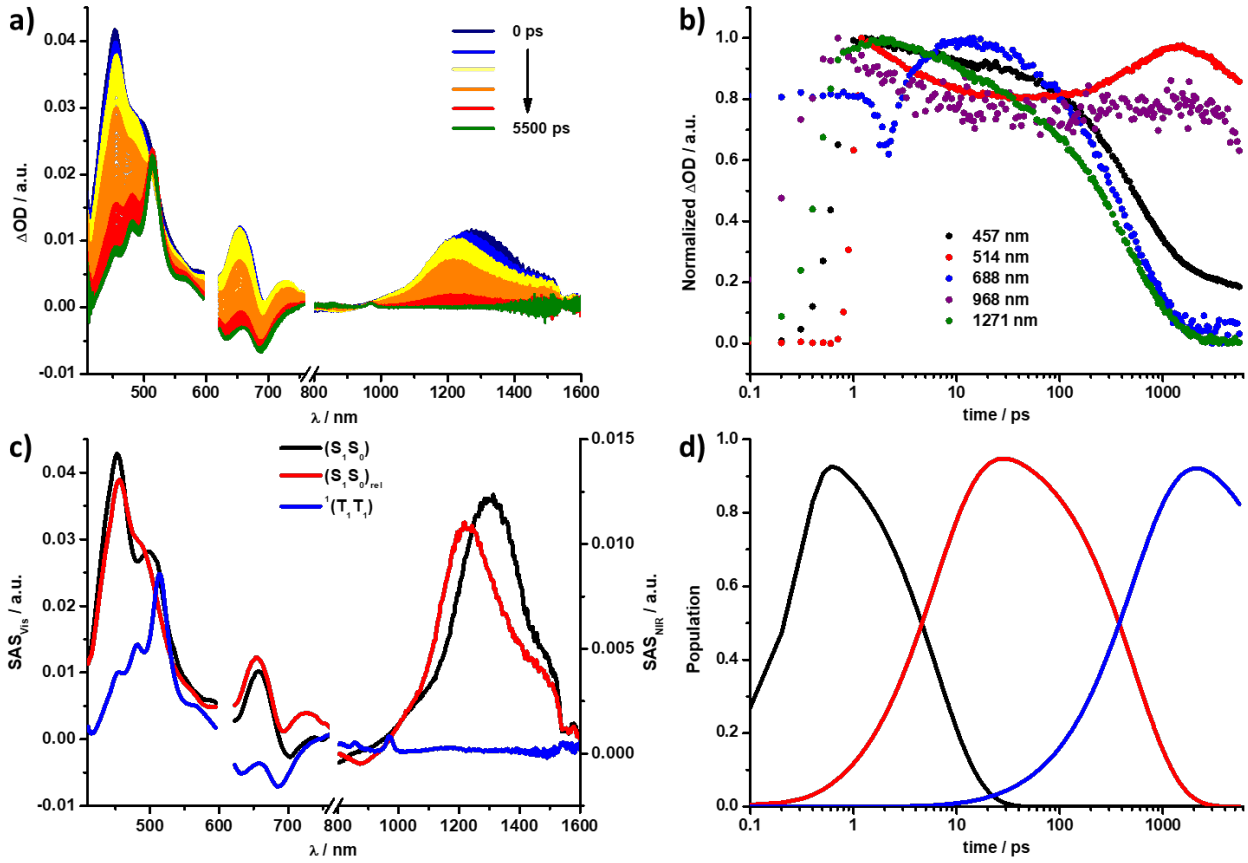

Figure S42. (a) fsTAS (λ_{ex} = 610 nm, 400 nJ) of **Pt(L$_{pc}$)$_2$Cl$_2$** in BN with time delays between 0–5 500 ps. (b) Respective normalized time absorption profiles at the illustrated wavelengths. (c) Deconvoluted fsTAS of the singlet excited state (S_1S_0) (black), solvent relaxed singlet excited state $(S_1S_0)_{rel}$ (red), and singlet correlated triplet pair $^1(T_1T_1)$ (blue) of **Pt(L$_{pc}$)$_2$Cl$_2$** in BN as obtained by target analysis. (d) Respective population kinetics.

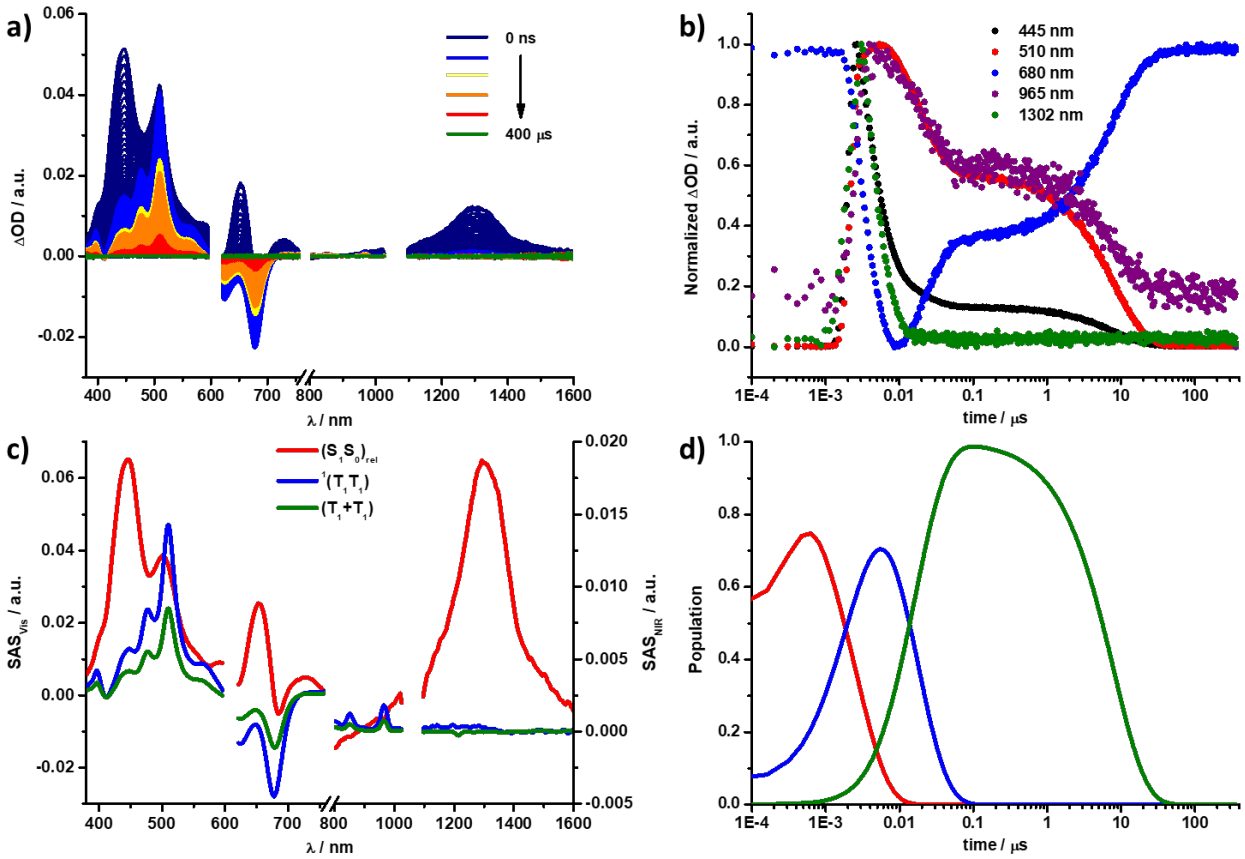

Figure S43. (a) nsTAS (λ_{ex} = 610 nm, 400 nJ) of **Pt(L$_{pc}$)$_2$Cl$_2$** in Tol with time delays between 0 ns – 400 µs. (b) Respective normalized time absorption profiles at the illustrated wavelengths. (c) Deconvoluted nsTAS of the solvent relaxed singlet excited state $(S_1S_0)_{rel}$ (red), singlet correlated triplet pair $^1(T_1T_1)$ (blue), and uncorrelated triplet excited states (T_1+T_1) (green) of **Pt(L$_{pc}$)$_2$Cl$_2$** in Tol as obtained by target analysis. (d) Respective population kinetics.

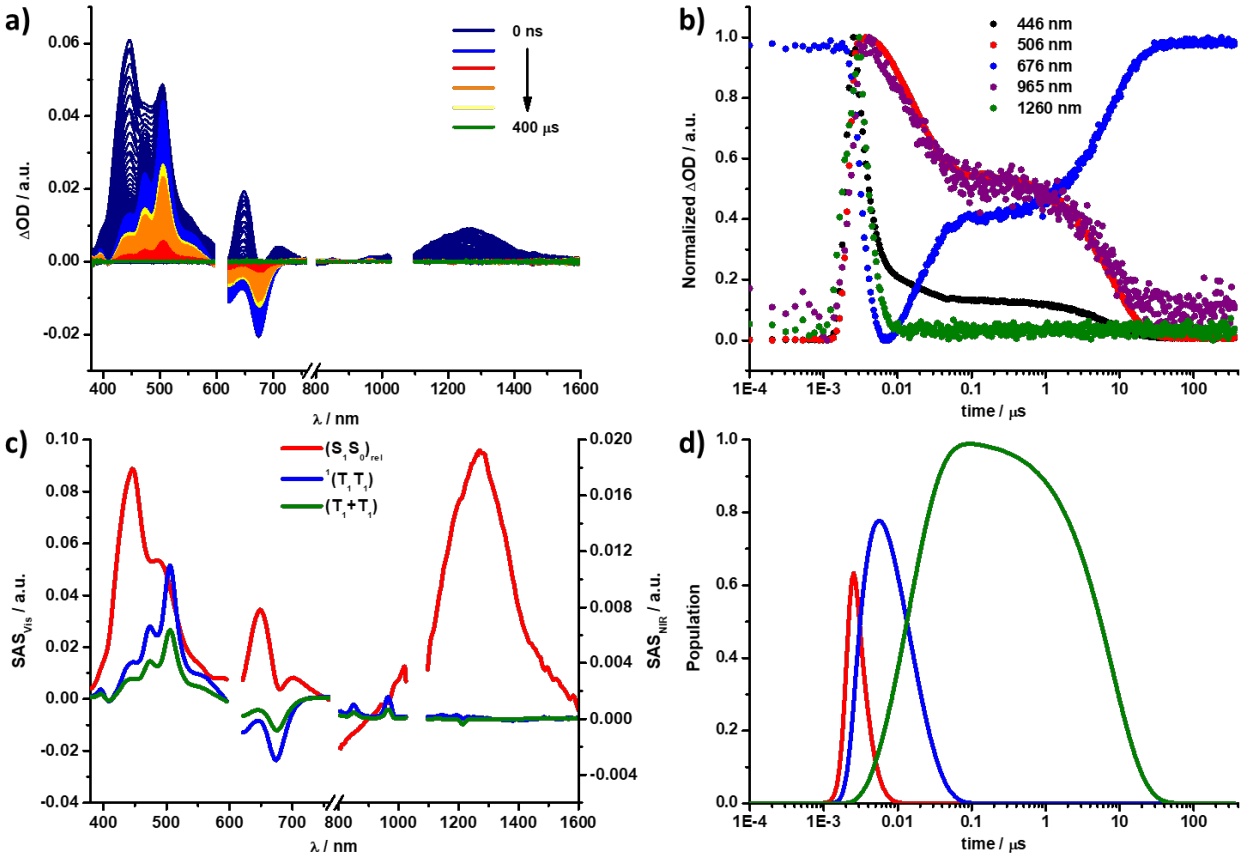

Figure S44. (a) nsTAS (λ_{ex} = 610 nm, 400 nJ) of **Pt(L$_{pc}$)$_2$Cl$_2$** in THF with time delays between 0 ns – 400 µs. (b) Respective normalized time absorption profiles at the illustrated wavelengths. (c) Deconvoluted nsTAS of the solvent relaxed singlet excited state $(S_1S_0)_{rel}$ (red), singlet correlated triplet pair $^1(T_1T_1)$ (blue), and uncorrelated triplet excited states (T_1+T_1) (green) of **Pt(L$_{pc}$)$_2$Cl$_2$** in THF as obtained by target analysis. (d) Respective population kinetics.

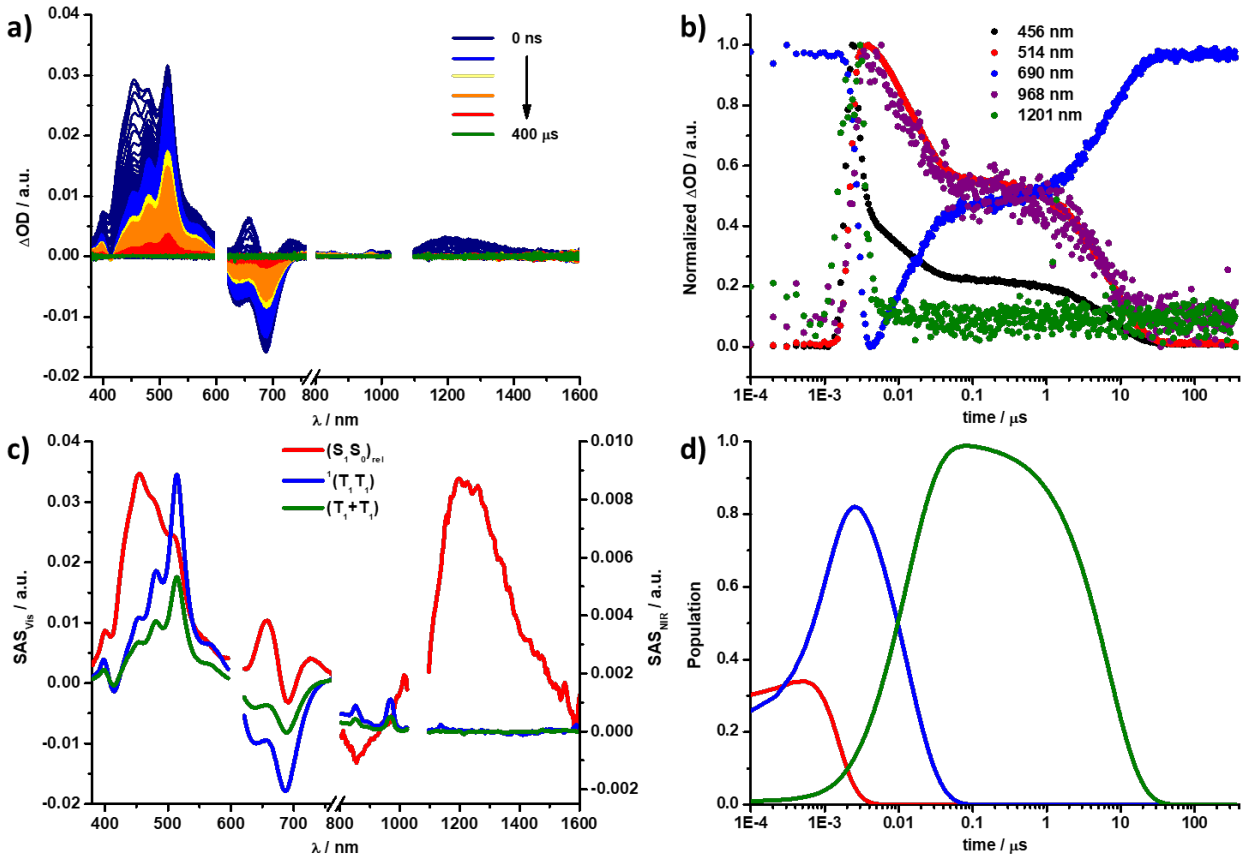

Figure S45. (a) nsTAS (λ_{ex} = 610 nm, 400 nJ) of **Pt(L$_{pc}$)$_2$Cl$_2$** in BN with time delays between 0 ns – 400 µs. (b) Respective normalized time absorption profiles at the illustrated wavelengths. (c) Deconvoluted nsTAS of the solvent relaxed singlet excited state $(S_1S_0)_{rel}$ (red), singlet correlated triplet pair $^1(T_1T_1)$ (blue), and uncorrelated triplet excited states (T_1+T_1) (green) of **Pt(L$_{pc}$)$_2$Cl$_2$** in BN as obtained by target analysis. (d) Respective population kinetics.

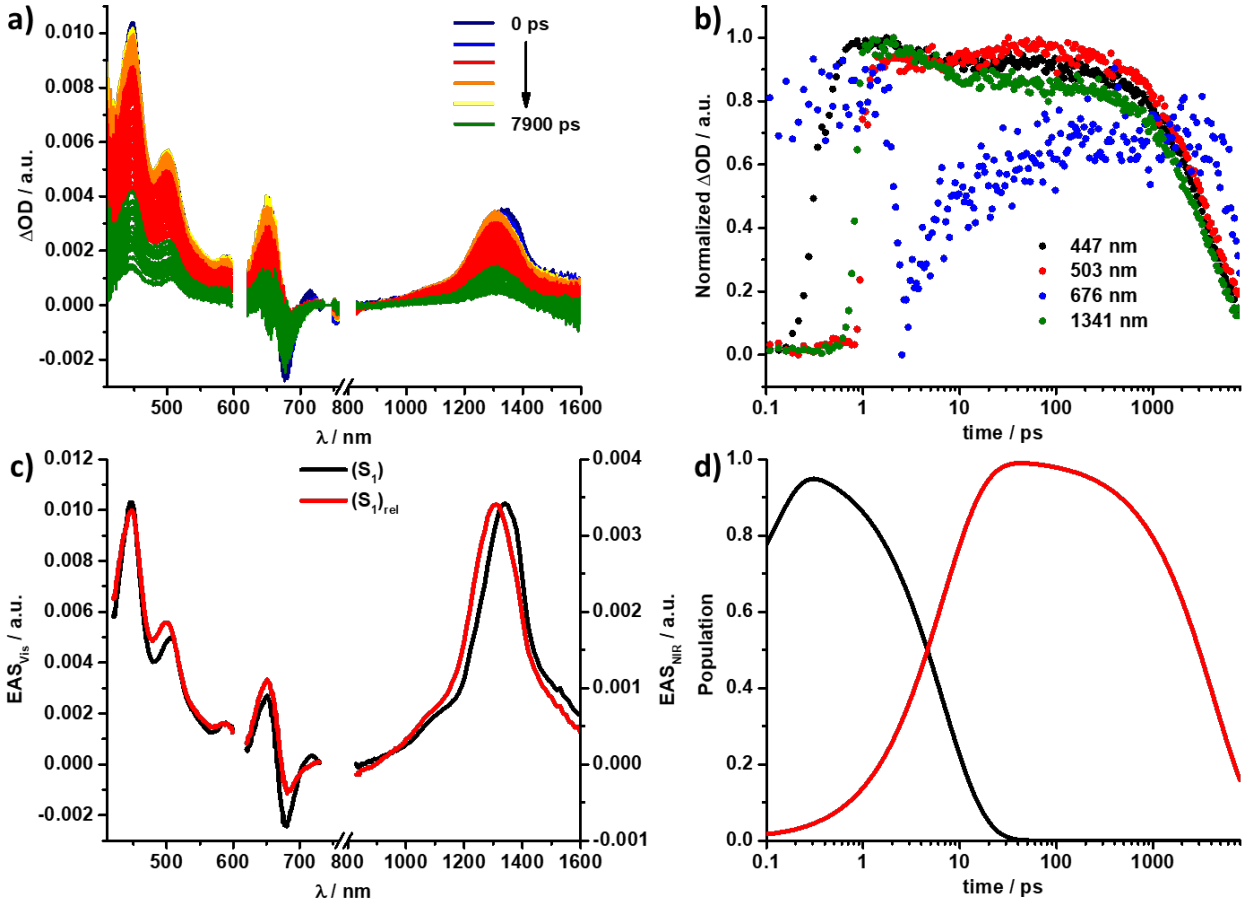

Figure S46. (a) fsTAS (λ_{ex} = 610 nm, 400 nJ) of **Pd(L_{pc})(L_{ref})Cl_2** in Tol with time delays between 0–7 900 ps. (b) Respective normalized time absorption profiles at the illustrated wavelengths. (c) Deconvoluted fsTAS of the singlet excited state (S_1) (black) and solvent relaxed singlet excited state $(S_1)_{rel}$ (red) of **Pd(L_{pc})(L_{ref})Cl_2** in Tol as obtained by global analysis. (d) Respective population kinetics.

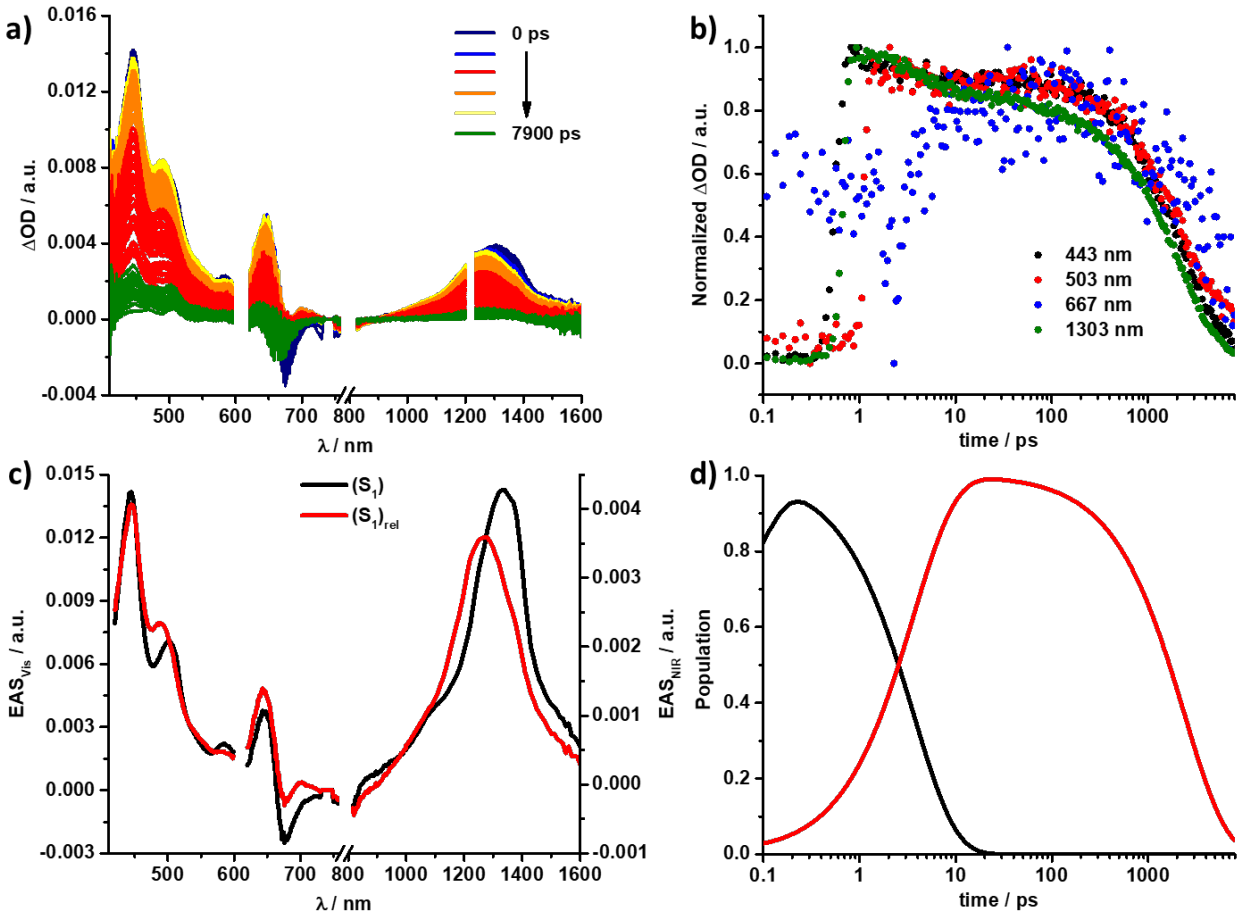

Figure S47. (a) fsTAS (λ_{ex} = 610 nm, 400 nJ) of **Pd(L_{pc})(L_{ref})Cl_2** in THF with time delays between 0–7 900 ps. (b) Respective normalized time absorption profiles at the illustrated wavelengths. (c) Deconvoluted fsTAS of the singlet excited state (S_1) (black) and solvent relaxed singlet excited state $(S_1)_{rel}$ (red) of **Pd(L_{pc})(L_{ref})Cl_2** in THF as obtained by global analysis. (d) Respective population kinetics.

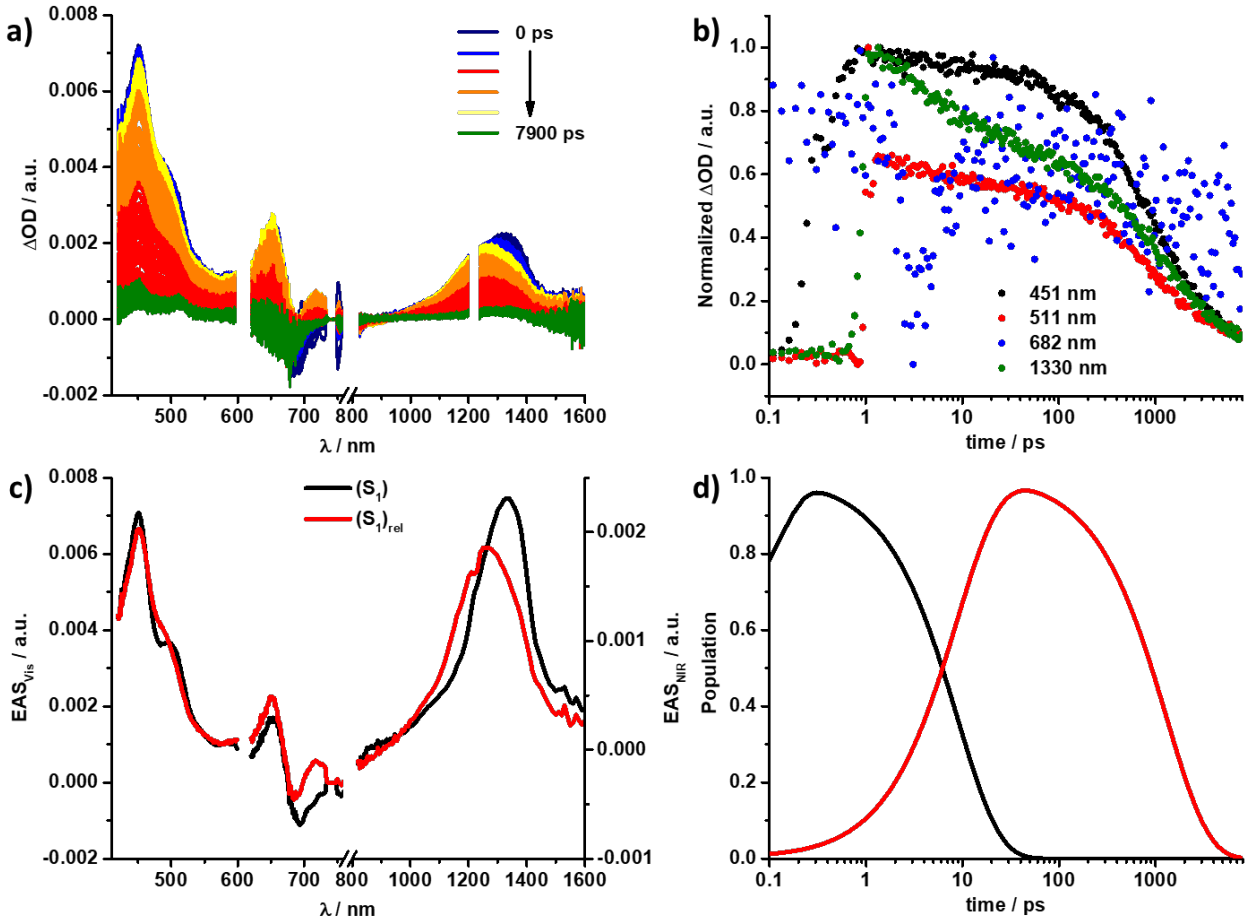

Figure S48. (a) fsTAS (λ_{ex} = 610 nm, 400 nJ) of **Pd(L_{pc})(L_{ref})Cl_2** in BN with time delays between 0–7 900 ps. (b) Respective normalized time absorption profiles at the illustrated wavelengths. (c) Deconvoluted fsTAS of the singlet excited state (S_1) (black) and solvent relaxed singlet excited state $(S_1)_{rel}$ (red) of **Pd(L_{pc})(L_{ref})Cl_2** in BN as obtained by global analysis. (d) Respective population kinetics.

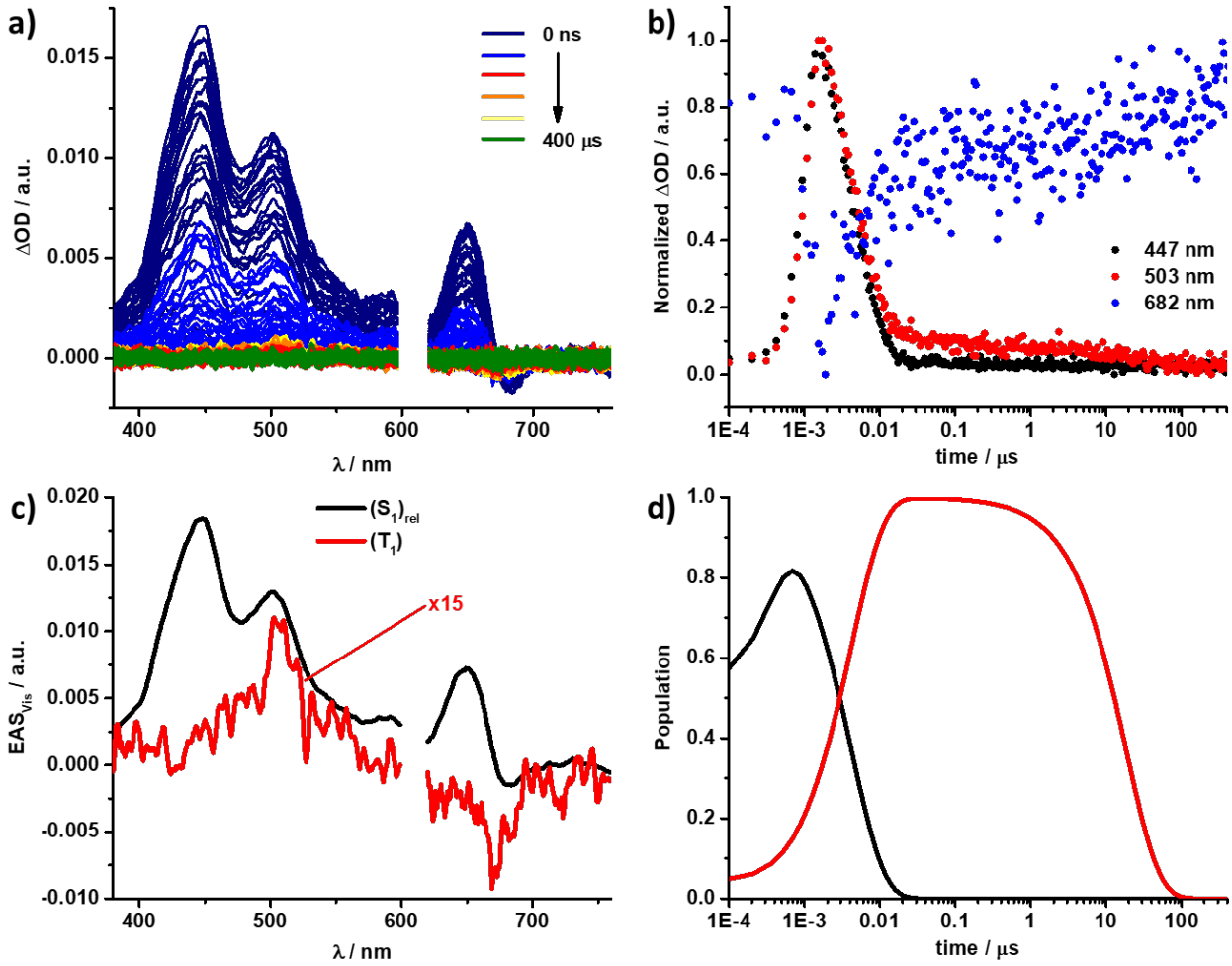

Figure S49. (a) nsTAS (λ_{ex} = 610 nm, 400 nJ) of **Pd(L_{pc})(L_{ref})Cl_2** in Tol with time delays between 0 ns – 400 µs. (b) Respective normalized time absorption profiles at the illustrated wavelengths. (c) Deconvoluted nsTAS of the solvent relaxed singlet excited state $(S_1)_{rel}$ (black) and triplet excited state (T_1) (red) of **Pd(L_{pc})(L_{ref})Cl_2** in Tol as obtained by global analysis. (d) Respective population kinetics. Intensities of the NIR were too weak and are thus not shown.

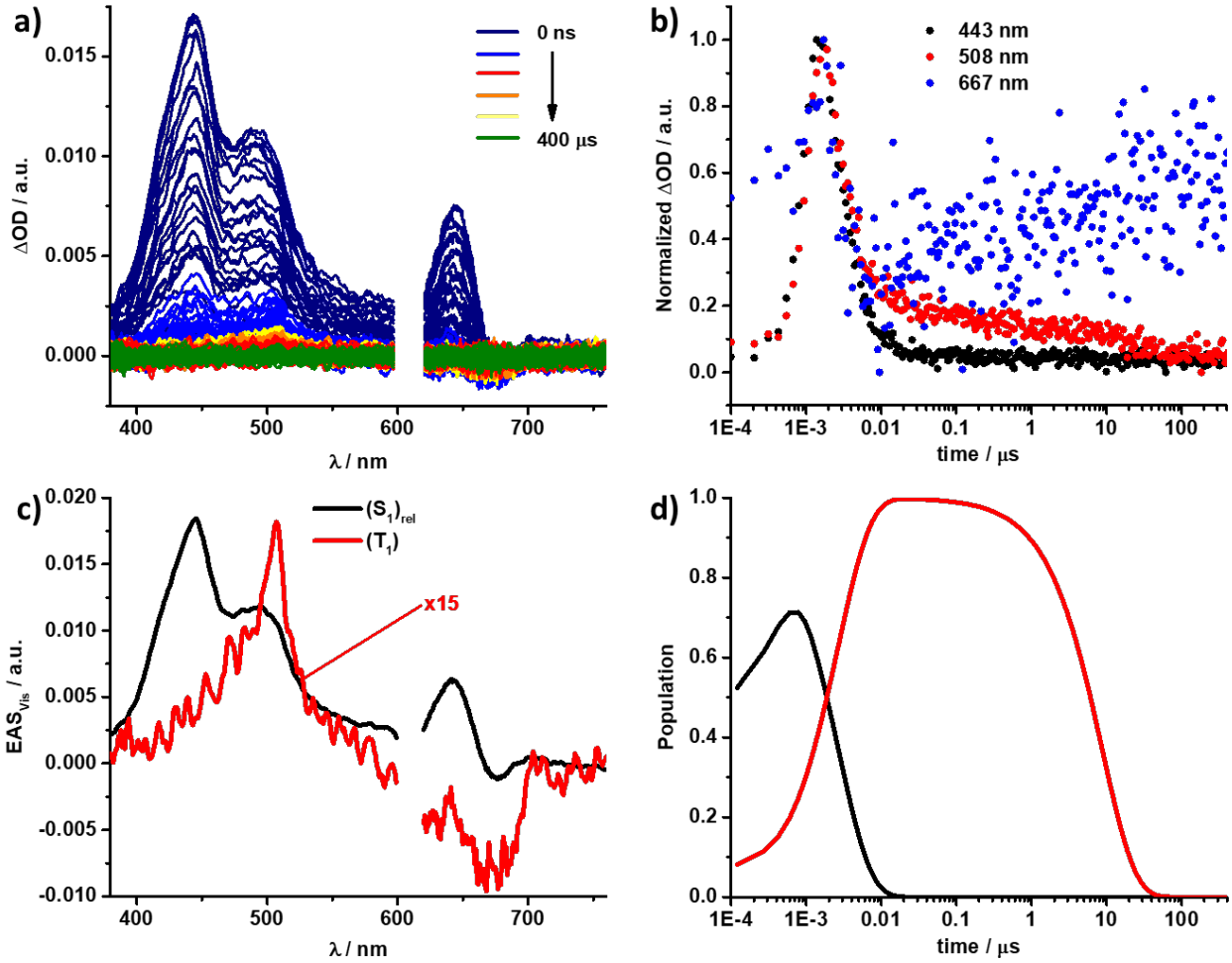

Figure S50. (a) nsTAS (λ_{ex} = 610 nm, 400 nJ) of **Pd(L_{pc})(L_{ref})Cl_2** in THF with time delays between 0 ns – 400 µs. (b) Respective normalized time absorption profiles at the illustrated wavelengths. (c) Deconvoluted nsTAS of the solvent relaxed singlet excited state $(S_1)_{rel}$ (black) and triplet excited state (T_1) (red) of **Pd(L_{pc})(L_{ref})Cl_2** in THF as obtained by global analysis. (d) Respective population kinetics. Intensities of the NIR were too weak and are thus not shown.

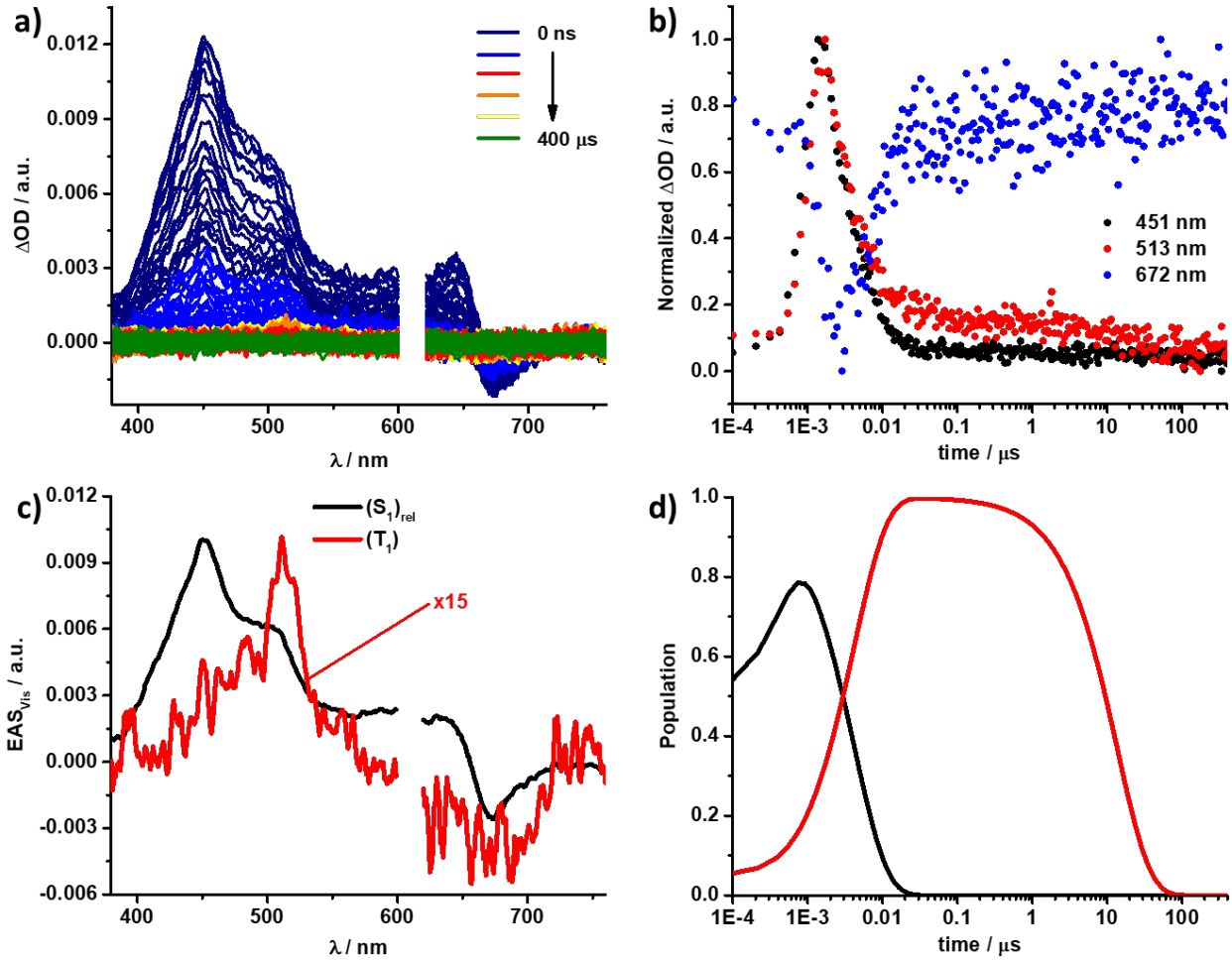

Figure S51. (a) nsTAS (λ_{ex} = 610 nm, 400 nJ) of **Pd(L_{pc})(L_{ref})Cl_2** in BN with time delays between 0 ns – 400 µs. (b) Respective normalized time absorption profiles at the illustrated wavelengths. (c) Deconvoluted nsTAS of the solvent relaxed singlet excited state $(S_1)_{rel}$ (black) and triplet excited state (T_1) (red) of **Pd(L_{pc})(L_{ref})Cl_2** in BN as obtained by global analysis. (d) Respective population kinetics. Intensities of the NIR were too weak and are thus not shown.

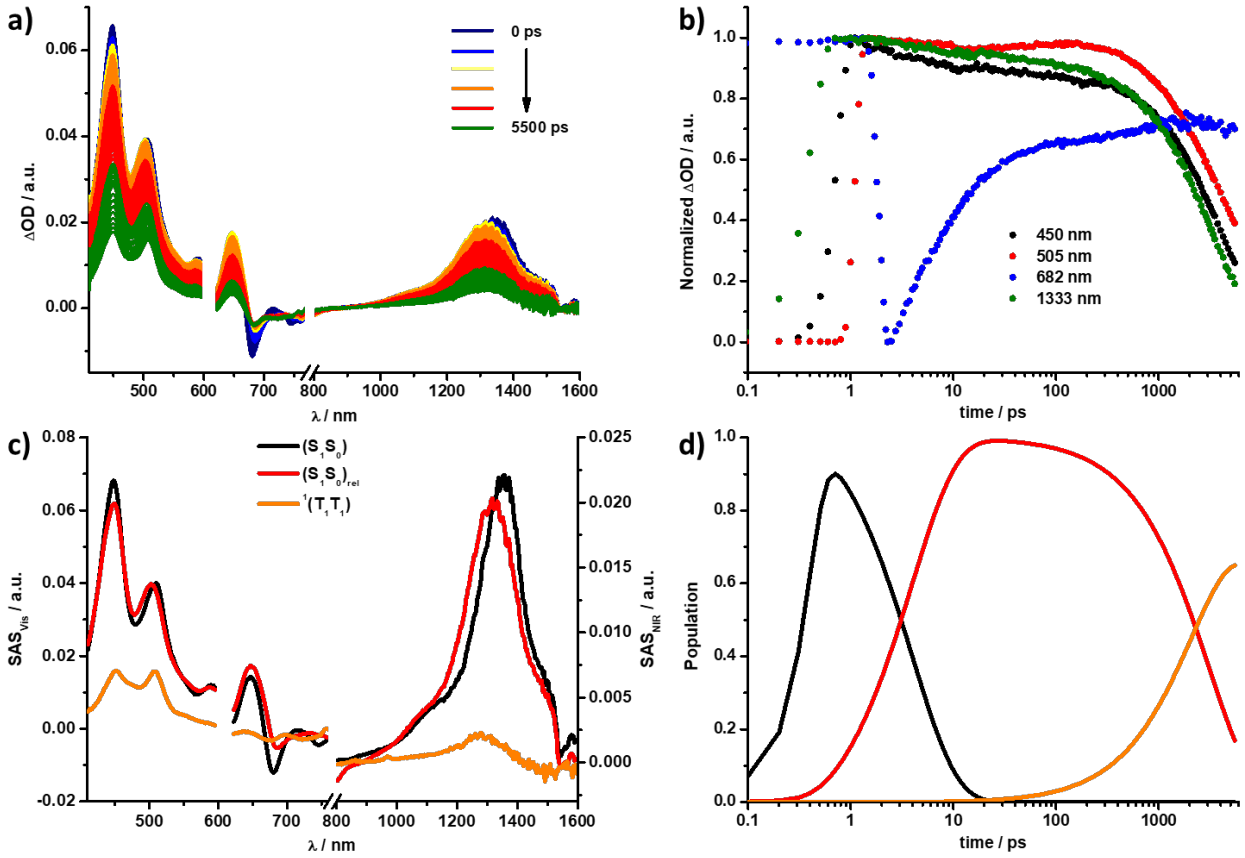

Figure S52. (a) fsTAS (λ_{ex} = 610 nm, 400 nJ) of **Pd(L$_{pc}$)$_2$Cl$_2$** in Tol with time delays between 0–5 500 ps. (b) Respective normalized time absorption profiles at the illustrated wavelengths. (c) Deconvoluted fsTAS of the singlet excited state (S_1S_0) (black), solvent relaxed singlet excited state $(S_1S_0)_{rel}$ (red), and singlet correlated triplet pair $^1(T_1T_1)$ (orange) of **Pd(L$_{pc}$)$_2$Cl$_2$** in Tol as obtained by target analysis. (d) Respective population kinetics.

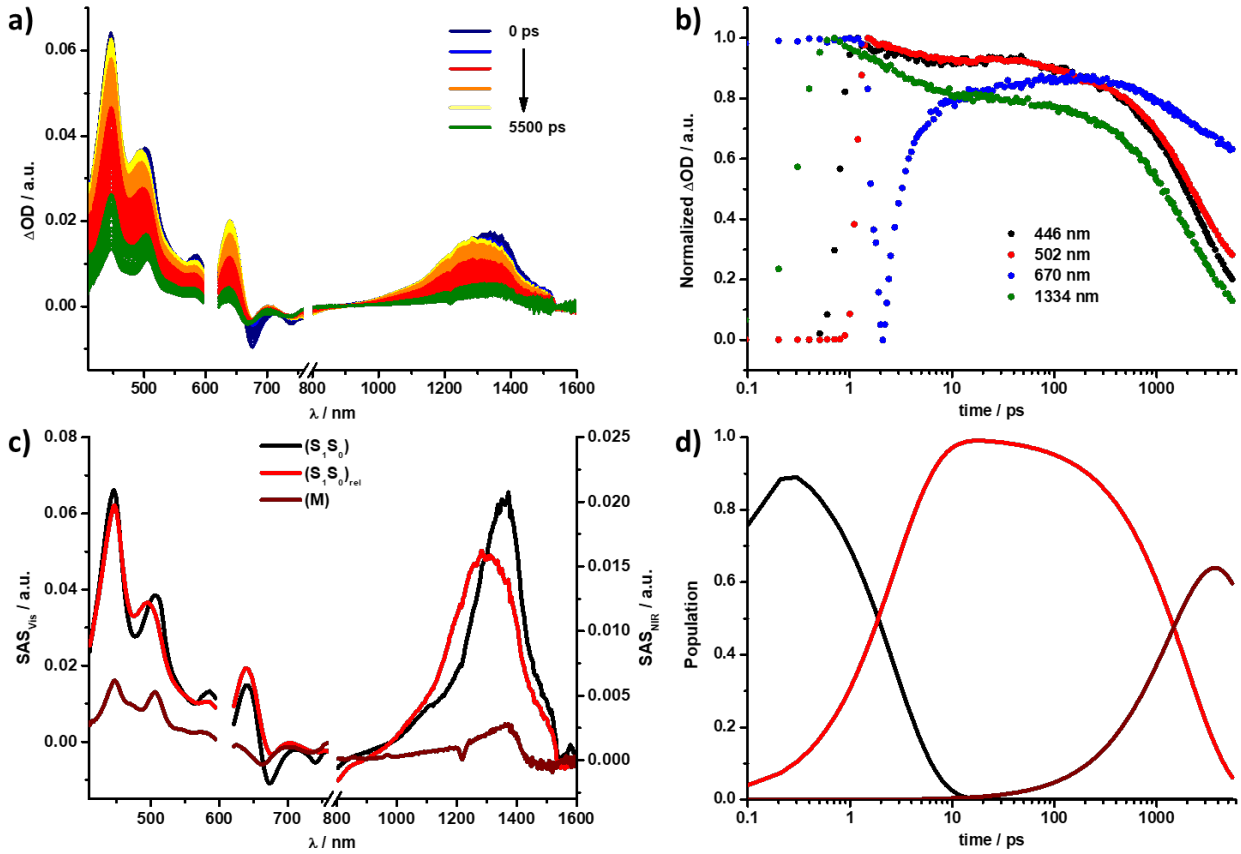

Figure S53. (a) fsTAS (λ_{ex} = 610 nm, 400 nJ) of **Pd(L$_{pc}$)$_2$Cl$_2$** in THF with time delays between 0–5 500 ps. (b) Respective normalized time absorption profiles at the illustrated wavelengths. (c) Deconvoluted fsTAS of the singlet excited state (S_1S_0) (black), solvent relaxed singlet excited state $(S_1S_0)_{rel}$ (red), and mixed singlet / triplet / charge transfer intermediate state (M) (brown) of **Pd(L$_{pc}$)$_2$Cl$_2$** in THF as obtained by target analysis. (d) Respective population kinetics.

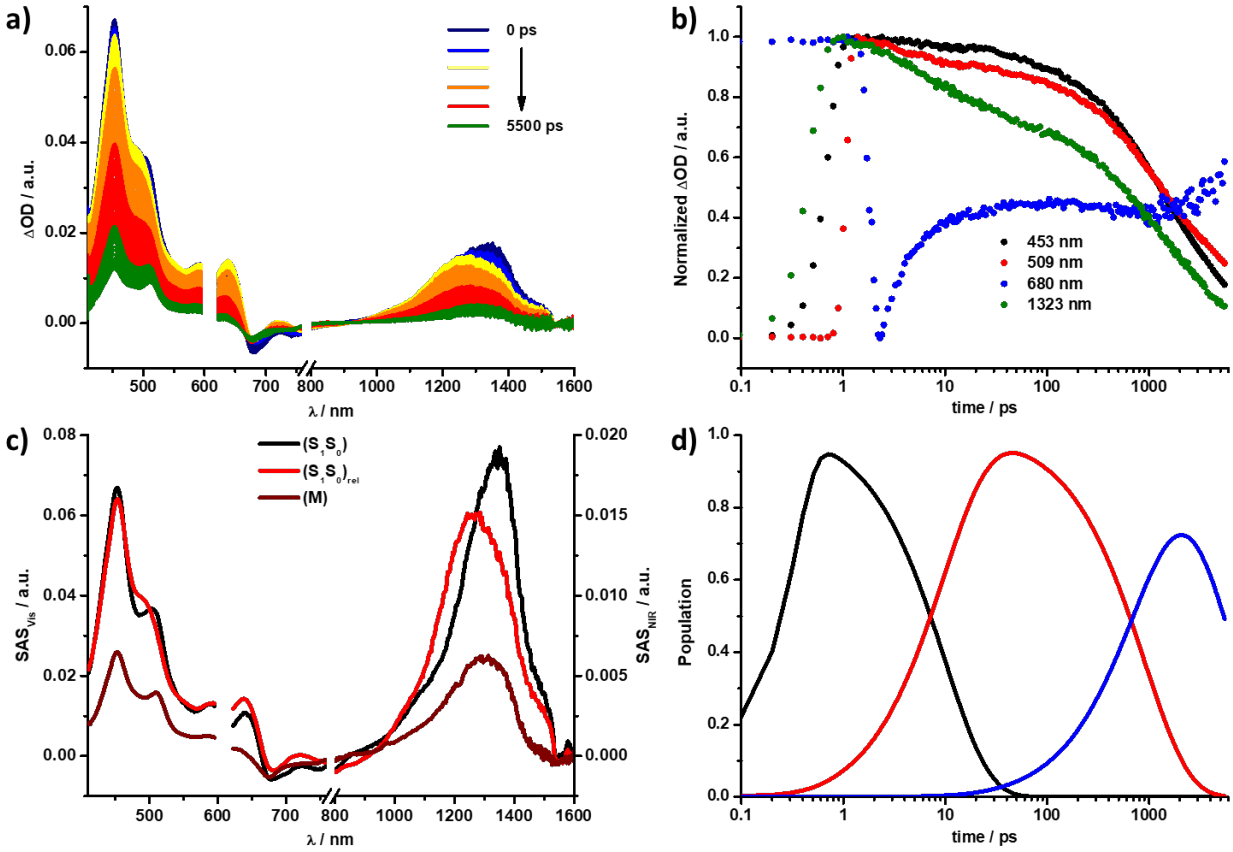

Figure S54. (a) fsTAS (λ_{ex} = 610 nm, 400 nJ) of **Pd(L$_{pc}$)$_2$Cl$_2$** in BN with time delays between 0–5 500 ps. (b) Respective normalized time absorption profiles at the illustrated wavelengths. (c) Deconvoluted fsTAS of the singlet excited state (S_1S_0) (black), solvent relaxed singlet excited state $(S_1S_0)_{rel}$ (red), and mixed singlet / triplet / charge transfer intermediate state (M) (brown) of **Pd(L$_{pc}$)$_2$Cl$_2$** in BN as obtained by target analysis. (d) Respective population kinetics.

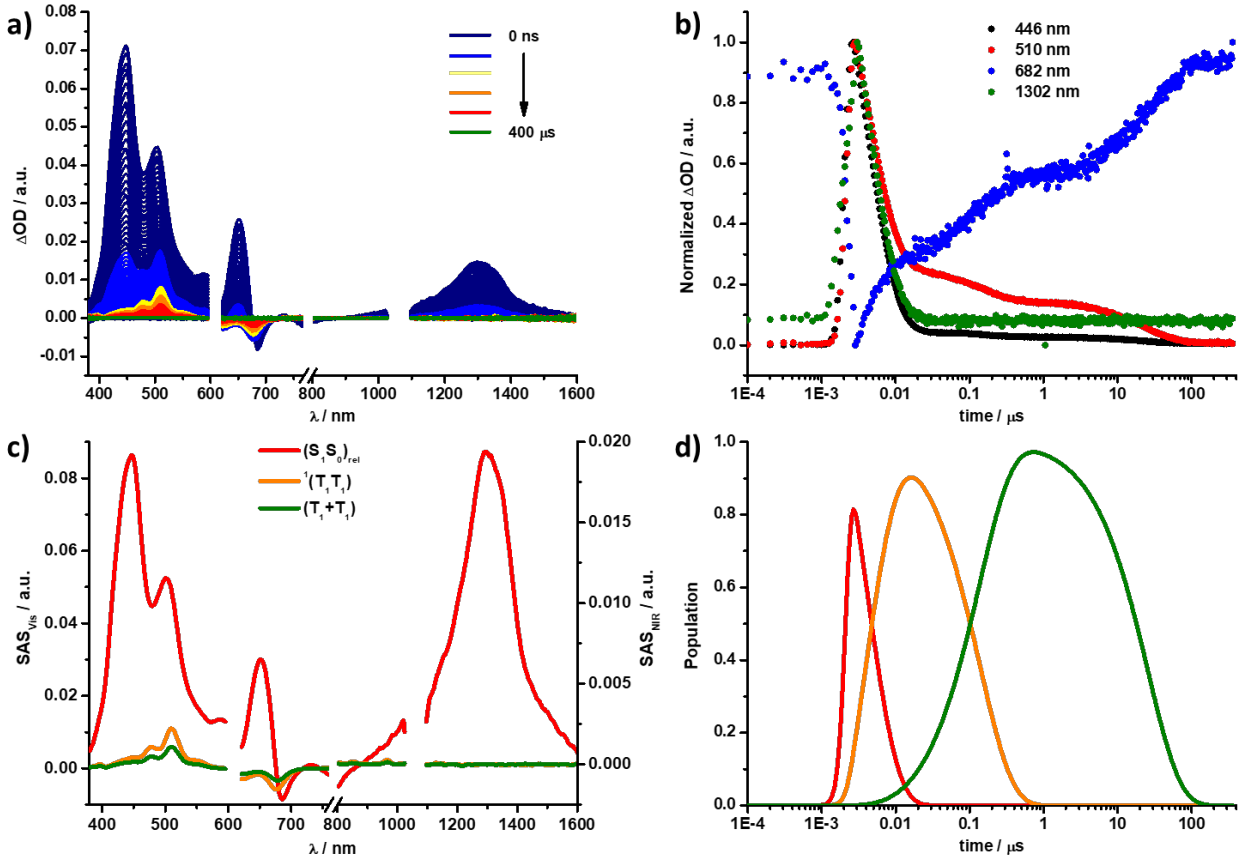

Figure S55. (a) nsTAS (λ_{ex} = 610 nm, 400 nJ) of **Pd(L$_{pc}$)$_2$Cl$_2$** in Tol with time delays between 0 ns – 400 µs. (b) Respective normalized time absorption profiles at the illustrated wavelengths. (c) Deconvoluted nsTAS of the solvent relaxed singlet excited state $(S_1S_0)_{rel}$ (red), singlet correlated triplet pair $^1(T_1T_1)$ (orange), and uncorrelated triplet excited states (T_1+T_1) (green) of **Pd(L$_{pc}$)$_2$Cl$_2$** in Tol as obtained by target analysis. (d) Respective population kinetics.

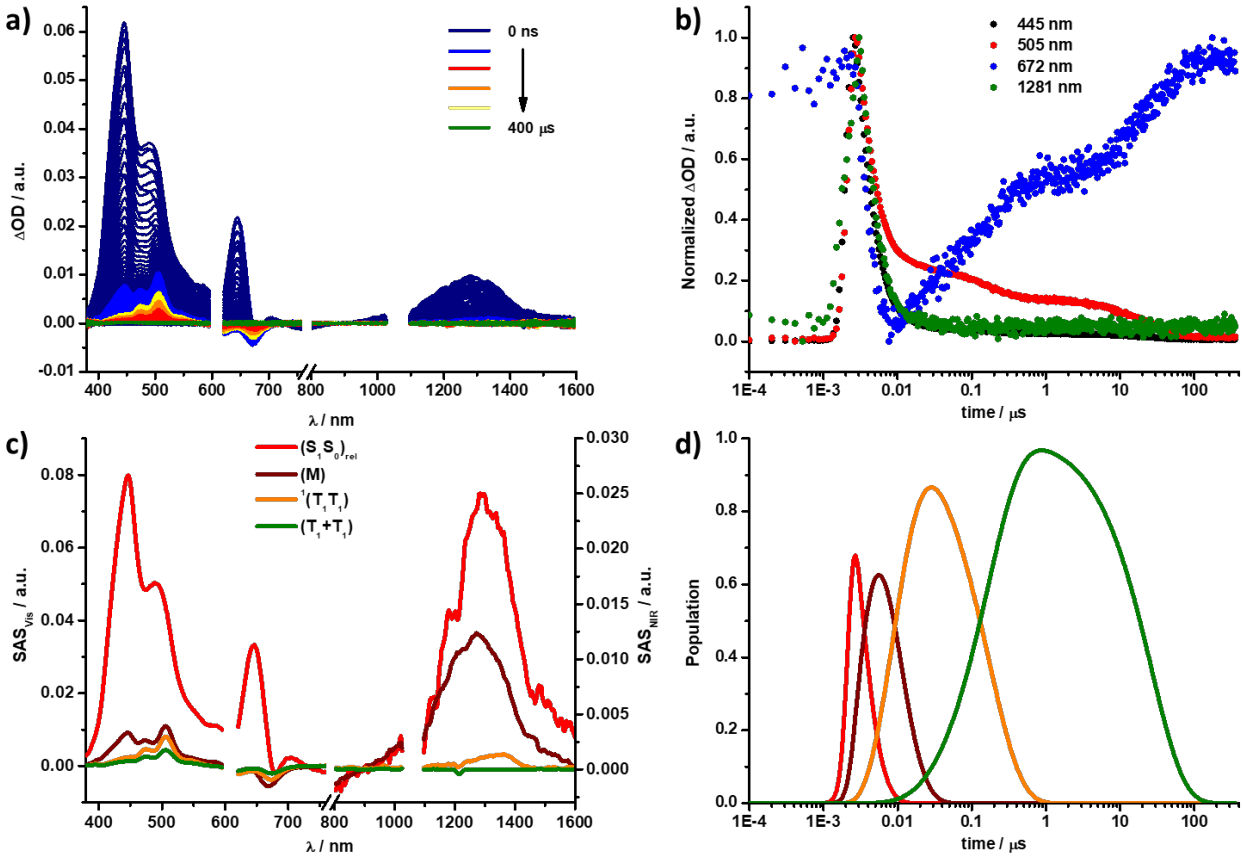

Figure S56. (a) nsTAS (λ_{ex} = 610 nm, 400 nJ) of **Pd(L$_{pc}$)$_2$Cl$_2$** in THF with time delays between 0 ns – 400 µs. (b) Respective normalized time absorption profiles at the illustrated wavelengths. (c) Deconvoluted nsTAS of the solvent relaxed singlet excited state $(S_1S_0)_{rel}$ (red), mixed singlet / triplet / charge transfer intermediate state (M) (brown), singlet correlated triplet pair $^1(T_1T_1)$ (orange), and uncorrelated triplet excited states (T_1+T_1) (green) of **Pd(L$_{pc}$)$_2$Cl$_2$** in THF as obtained by target analysis. (d) Respective population kinetics.

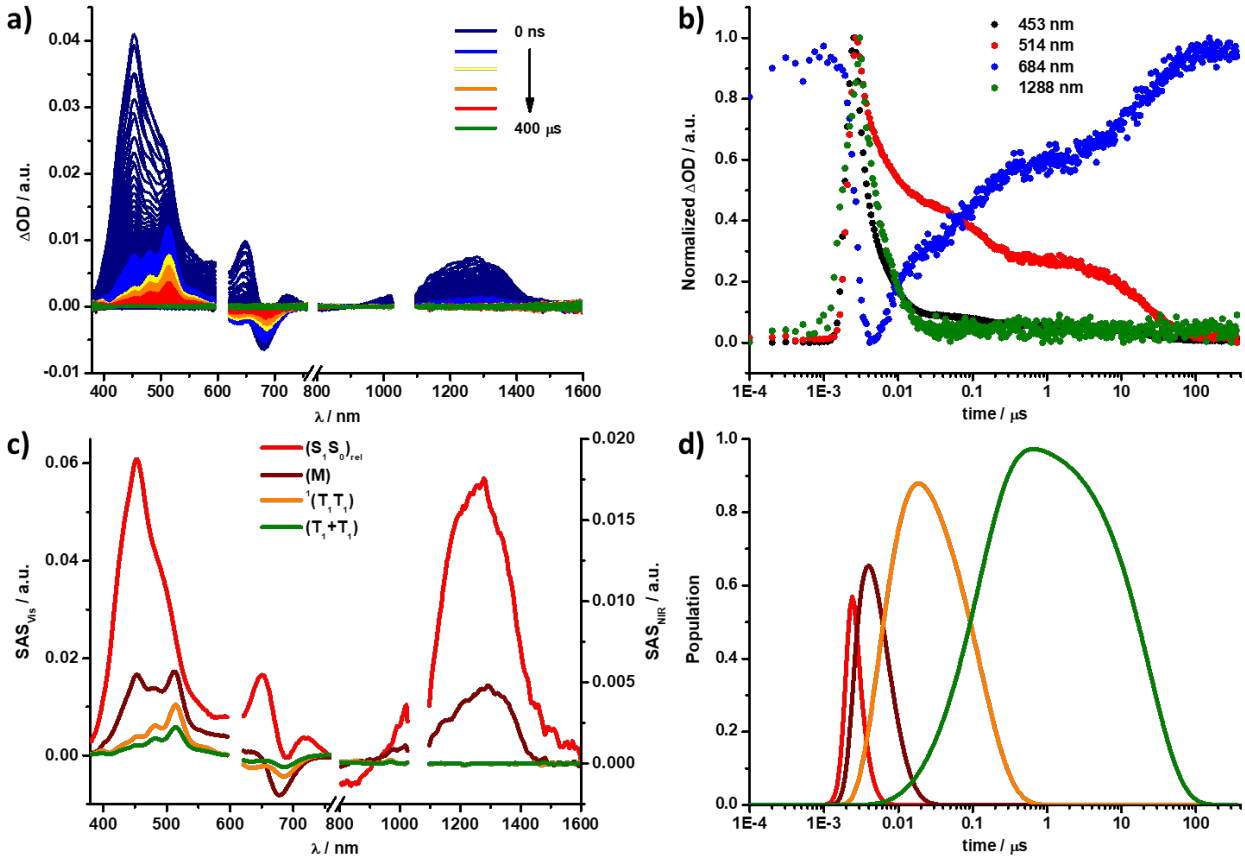

Figure S57. (a) nsTAS (λ_{ex} = 610 nm, 400 nJ) of **Pd(L$_{pc}$)$_2$Cl$_2$** in BN with time delays between 0 ns – 400 µs. (b) Respective normalized time absorption profiles at the illustrated wavelengths. (c) Deconvoluted nsTAS of the solvent relaxed singlet excited state $(S_1S_0)_{rel}$ (red), mixed singlet / triplet / charge transfer intermediate state (M) (brown), singlet correlated triplet pair $^1(T_1T_1)$ (orange), and uncorrelated triplet excited states (T_1+T_1) (green) of **Pd(L$_{pc}$)$_2$Cl$_2$** in BN as obtained by target analysis. (d) Respective population kinetics.

Supplementary Reference

1. Hou, Y.; Papadopoulos, I.; Ferguson, M. J.; Jax, N.; Tykwinski, R. R.; Guldi, D. M. Photophysical Characterization of a Ruthenium-based Tetrameric Pentacene Complex. *J. Porphyrins Phthalocyanines* **2023**, *27*, 686–693; https://doi.org/10.1142/S1088424623500645
2. Imperiale, C. J.; Green, P. B.; Miller, E. G.; Damrauer, N. H.; Wilson, M. W. B. Triplet-Fusion Upconversion Using a Rigid Tetracene Homodimer. *J. Phys. Chem. Lett.* **2019**, *10*, 7463–7469; https://doi.org/10.1021/acs.jpclett.9b03115.
3. Wu, L. P.; Suenaga, Y.; Kuroda-Sowa, T.; Maekawa, M.; Furuichi, K.; Munakata, M. Syntheses, Structures and Properties of Palladium (II) Complexes with Photochromic 4-Methoxyazobenzene. *Inorganica Chim. Acta* **1996**, *248*, 147–152; https://doi.org/10.1016/0020-1693(95)04995-9.